Beyond Standard Model phenomenology with or without a light Higgs

Alberto Filipuzzi
IFIC (CSIC-UVEG), Departamento de Física Teórica
Universitat de València

Tesis doctoral, 2012
Director de tesis: Jorge Portolés Ibáñez

JORGE PORTOLÉS IBÁÑEZ,
científico titular del Instituto de Física Corpuscular (IFIC),

CERTIFICA:

Que la presente memoria "Beyond Standard Model phenomenology with or without a light Higgs" ha sido realizada bajo su dirección en el Instituto de Física Corpuscular, centro mixto de la Universitat de València y del CSIC, por ALBERTO FILIPUZZI y constituye su Tesis para optar al grado de Doctor en Física.

Y para que así conste, en cumplimiento de la legislación vigente, presenta en el Departamento de Física Teórica de la Universitat de València la referida Tesis Doctoral, y firma el presente certificado.

Valencia, a 4 de Octubre de 2012.

Jorge Portolés Ibáñez

Contents

Resumen de la tesis

El Modelo Estándar (ME) es una teoría que describe en manera sorprendentemente precisa la gran mayoría de los datos experimentales que han sido producidos hasta la fecha [1]. No obstante hay algunas indicaciones, entre las cuales la evidencia experimental de que los neutrinos tienen una masa finita, de que la teoría no es completa y que probablemente hay que considerarla sólo una descripción de baja energía de una teoría más completa de las fuerzas naturales. La búsqueda de una posible extensión del ME puede recorrer diferentes caminos y basarse en datos experimentales que incluyan medidas de precisión de los parámetros de la teoría electrodébil, búsqueda directa en aceleradores de alta energía y estudio de procesos raros o no permitidos en el ME.

El trabajo presentado en esta tesis se ha centrado en el análisis de distintos problemas teóricos y fenomenológicos, relacionados con la estructura de sabor del ME y de sus posibles extensiones, con posibles violaciones de la universalidad leptónica debidas a efectos de Nueva Física y también con escenarios en los que la ruptura de la simetría electrodébil está generada por Nueva Física que interactúa de manera fuerte. Para enfrentarse a este tipo de problemas ha sido muy eficaz utilizar el marco de trabajo que proporcionan las Teorías Efectivas, un método independiente de modelos específicos, es decir una descripción general a través de parámetros no fijados, de las posibles interacciones resultantes de la integración de los nuevos grados de libertad que la teoría que extiende el ME tiene que describir. Este método, que incluye un análisis fenomenológico y que se basa en la gran precisión que los datos experimentales han alcanzado, permite obtener informaciones muy valiosas sobre la estructura de la nueva teoría y descartar de esta manera algunos de los modelos que han sido construidos en los últimos años.

La primera parte de la tesis presenta tres análisis basados en teorías efectivas en las que se supone que el ME está realizado en la naturaleza, con particular referencia al sector de Higgs. Tras una breve introducción al ME, en los Capítulos 1 y 2 se explica la teoría efectiva con Higgs del ME,

analizando sus principales características e incluyendo la base de operadores efectivos de dimensión seis [2, 3].

El primer estudio de esta primera parte, presentado en el Capítulo 3, ha sido dedicado al análisis de posibles efectos de violación de la simetría de sabor leptónico inducidos por física más allá de ME. En este análisis hemos utilizado una teoría efectiva basada en el principio de violación minima del sabor leptónico [4]. Dentro de este contexto hemos estudiado las desintegraciones leptónicas de los mesones pseudoescalares y los relativos cocientes de universalidad, que, gracias a una predicción teórica y medidas experimentales muy precisas, son observables perfectos para encontrar señales de Nueva Física.

Las desviaciones respecto al ME que hemos encontrado analizando el escenario de MFV son demasiado pequeñas para que los futuros experimentos las puedan medir [5]. No obstante, si se considera modelos de Gran Unificación [6], algunos efectos se podrían medir en la desintegraciones leptónicas de mesones pesados, que están siendo estudiadas con creciente precisión en las factorías de B. Por otro lado, si los experimentos midieran desviaciones en las desintegraciones de piones y kaones, habría que suponer que nuevas estructuras de sabor, distintas de las que aparecen en el ME, tienen que aparecer al extender del ME. Nuestro análisis es un útil instrumento para evaluar modelos específicos y podrá ser desarrollado para incluir nuevas medidas experimentales, especialmente en el sector de los mesones pesados B, D y D_S.

El Capítulo 4 está dedicado a un estudio sobre la violación de la universalidad leptónica en desintegraciones leptónicas del W, observada experimentalmente en los datos de LEP2 [7, 8, 9, 10, 11]. El objetivo del análisis, en el que hemos utilizado los instrumentos de las teorías efectivas para estudiar el problema de manera lo más posible independiente de modelos, ha sido verificar la posibilidad de que la desviación observada experimentalmente sea un efecto de Física más allá del Modelo Estándar. A través de un fit global de resultados experimentales de múltiples procesos de tipo electrodébil, hemos podido verificar que la anomalía en los datos no puede ser descrita en términos del tipo de Nueva Física asumida al principio del trabajo [12]. De hecho en ambos escenarios considerados, en los que dos distintas simetrías de sabor han sido supuestas, las restricciones impuestas por los observables electrodébiles son demasiado fuertes para que sea posible incluir la desviación de la universalidad en las desintegraciones del W como un verdadero efecto de Nueva Física. Para explicar los resultados experimentales asociados a la violación de la universalidad leptónica considerados en este estudio hay probablemente que asumir un tipo de física más allá del ME que incluya nuevos tipos de partículas de baja energía [13, 14] o un sector de sabor con una

estructura muy peculiar. El método desarrollado en nuestro trabajo podrá ser utilizado para analizar otras medidas experimentales no explicadas por el ME, como por ejemplo la desviación de la universalidad observada en las desintegraciones del mesón B [15].

El tercer estudio, que concluye la primera parte de la tesis y está presentado en el Capítulo 5, tiene como objetivo el comparar las cotas que distintos experimentos de baja y alta energía podrían poner en los próximos años sobre posibles acoplamientos escalares y tensoriales inducidos por Nueva Física. En particular el análisis se ha centrado en la precisión que alcanzarán los futuros experimentos que miden la desintegración beta del neutrón [16, 17], en comparación con la que se supone alcanzará el LHC. Para analizar al mismo tiempo procesos de energía tan diferente se ha utilizado una teoría efectiva y se ha calculado la evolución con la escala de sus parámetros.

El análisis incluye una reseña de todas las actuales cotas sobre las interacciones escalares y tensoriales y un estudio detallado del papel jugado en este contexto por los experimentos sobre la desintegración beta del neutrón. Se ha discutido el impacto del error teórico asociado a los factores de forma hadrónicos sobre las cotas experimentales que se pueden obtener de los experimentos con neutrones, llegando a predecir la precisión teórica mínima necesaria para aprovechar al máximo las futuras mejorías experimentales. Analizando las potencialidades del LHC, se ha concluido que la planeada precisión en los futuros experimentos de baja energía podrá ser suficiente para competir con la que se alcanzará en los procesos de alta energía. Este estudio es una referencia muy importante para el desarrollo de los distintos experimentos. En particular ha sido relevante relacionar entre si experimentos tan diferentes como los que se están llevando a cabo en el LHC y los que han sido planeados sobre desintegraciones beta del neutrón [18].

La segunda parte de la tesis analiza la posibilidad de que el Higgs del ME sea muy pesado o no exista en absoluto y que la ruptura de la simetría electrodébil esté relacionada con un nuevo sector fuerte a las escala del Tera electronvoltio (TeV). La teoría efectiva quiral electrodébil que describe este escenario se describe en el Capítulo 6, donde se introduce también el Lagrangiano de $\mathcal{O}(p^4)$ [19, 20, 21]. Asociadas al nuevo sector fuerte podrían existir resonancias de tipo vectorial que se han estudiado en el último capítulo de la tesis. El método utilizado para el análisis ha sido desarrollado anteriormente [22] en el contexto de la Teoría de Perturbaciones Quiral (ChPT), un límite de baja energía de QCD, y en nuestro trabajo hemos aprovechado las similitudes existentes entre ChPT y la teoría efectiva electrodébil quiral. A través de nuestro método ha sido posible obtener valiosa información sobre

las resonancias vectoriales analizando los ceros de la amplitud de scattering de las componentes longitudinales de los bosones de gauge W y Z.

Para demonstrar las potencialidades del método utilizado, se ha analizado el caso bien conocido de la resonancia $\rho(770)$. El estudio ha sido desarrollado usando el lagrangiano quiral a $\mathcal{O}(p^4)$ y se ha analizado también el impacto del siguiente orden perturbativo. En el caso electrodébil, a través del análisis de los ceros de la amplitud de scattering $W_L Z_L \to W_L Z_L$ y suponiendo que la principal contribución a las constantes de baja energía sea debida a las resonancias vectoriales, ha sido posible explorar el espacio de los parámetros de las dos constantes efectivas que contribuyen la amplitud estudiada. De esta forma se han encontrado las zonas del espacio de parámetros donde las resonancias dominan la amplitud de scattering y se ha podido estimar su masa [23]. El análisis, basado en una teoría efectiva independiente de modelos, puede ser utilizado para excluir algunas clases de modelos sin bosón de Higgs y predecir hasta qué punto los experimentos del LHC podrán estudiar este tipo de resonancias vectoriales.

Introduction

In this exciting summer of 2012 the particle physics scenario has been dramatically changed by the July 4$^{\text{th}}$ LHC announcement of the discovery of a new boson, compatible with the Standard Model (SM) Higgs. Only few months ago we would have written that "the next months will be undoubtedly a special moment for the particle physics community" and that "we are approaching an important crossroad in the development of particle physics, but it is not yet obvious which is the right way". Now a big step toward the confirmation of the last piece of the SM has been done and the work we have been doing in the last years has to be revisited in the light of this new situation. First, though, we will explain the context in which this thesis has been developed and how some still experimentally unanswered questions played an important role in shaping its structure.

On one side during the last months we were waiting for big news that could change the course of physics history and, on the other side, recent experimental data already had suggested that an important twist could appear also in supposedly well established sectors. In a so exciting, but at the same time unclear situation the work of theoretical physicists needed to address a wide range of possibilities, with the goal of giving to existing data a coherent explanation and driving the development of future experimental tests. Following this line of thought the thesis we present in these pages embrace very different subjects, in an attempt of analyzing aspects of the physical scenarios that should be tested by near future experiments.

The big news at which we hinted before were, of course, the results of the LHC search for the SM Higgs boson. The LHC was in fact narrowing down the SM Higgs hunting to the low-mass region, pointing at a mass scale compatible with the results of the global fit to precision electroweak data. Then it made sense to think that there were good chances that the SM picture would be confirmed in a short range of time. On the other hand the window unexplored by the LHC was becoming smaller and smaller and still no clear sign of a SM Higgs boson had been found. We had then to recognize that a Higgsless world was still a viable possibility and certainly a very interesting

theoretical framework to analyze.

In our work we present analyses based on both Higgs scenarios. The first one assumes that the SM symmetry breaking sector is realized in Nature and then that the low-energy SM particle spectrum contains a Higgs boson. In this case our attention has been focused in particular on the structure of the SM flavor sector and the possibility that effects related to tensor and scalar interactions will arise due to physics beyond the SM. The second scenario considers the case in which no light Higgs is associated to the spontaneous electroweak symmetry breaking, leaving the door open for non-standard descriptions of the dynamics responsible for the known symmetry breaking pattern. Working in this framework, we developed a method that allowed us to extract, from processes at the electroweak scale, information about the possible strong dynamics responsible for the symmetry breaking. We will comment in Chapter 7 on the implications of the new LHC data on this specific framework.

Even though the studies we develop throughout this thesis face very different physical issues, they are united by the working method we use to address them. In fact each of our analyses is based on a specific implementation of the effective field theory (EFT) method. They share the philosophy and tools of the EFT framework, in particular the model independence of the results and the possibility of relating in a simple and efficient way experimental data coming from processes at very different energies.

The two main EFT implementations we will use in this thesis are directly related to the two Higgs scenarios we commented above. After presenting in Chapter 1 a brief introduction to the SM and the main questions that are still unanswered within this theory, in Chapter 2 we will describe an effective theory based on the hypothesis that the symmetry breaking sector is the one of the SM and, consequently, the low energy spectrum contain an explicit Higgs boson. Special flavor symmetries will then be considered in Chapters 3 and 4 as a tool to analyze particular physical hypothesis in a more and systematic way. Chapter 6, on the other hand, will be devoted to an introduction to the Higgsless EFT scenario and to its main features, that will become the fundamental instruments to develop the analysis of Chapter 7.

The structure of the SM flavor sector is certainly one of the most interesting puzzles of particle physics and great efforts have been done, both on experimental and theoretical side, to understand the dynamics driving its peculiar features. In our work, published in [5], we focus on the issues related to the lepton flavor sector, developing first an analysis of the possible violation of the lepton flavor symmetry in the context of the Minimal Flavor Violation framework, in which only a minimal set of flavor violating sources is allowed even if beyond SM physics effects are taken into account.

Working within this framework, in Chapter 3 we will study the possibility of measuring flavor violating effects in leptonic decays of pseudoscalar mesons, focusing on the very precisely measured π and K decays and then expanding our study to heavy meson decays, that can become a very powerful probe in the near future with the fast development of the super-B factories.

Another important aspect of the leptonic flavor sector will be examined in Chapter 4, based on the published paper [12]. Starting from the well established LEP2 results that show a departure from lepton universality in the tau channel of leptonic W decays, we will analyze the interplay of this anomaly with other very precise electroweak measurements, testing the possibility that beyond SM effects could explain it. Thanks to the features of our EFT framework, our results can be applied to a broad range of models and our analysis can be easily extended to include future experimental results or different theoretical flavor-symmetries ansätze. In particular, when more precise data will be made available, could be interesting to test one of the recent experimental results we were referring to at the beginning: the excess found in the $B \to D^{(*)}\tau\nu_\tau$ channel by the Babar collaboration [15], that can be a new indication of lepton flavor violation.

With the aim of assessing the present and future sensitivity of neutron beta decays to beyond SM effects, we will present in Chapter 5 a very broad comparative analysis of different constraints on new scalar and tensor interactions, published also in [18]. We will compare different bounds coming from low- and high-energy processes, showing at what level and in which theoretical scenarios neutron-decay experiments planned for the near future can compete with next runs at LHC. Making use of the most recent Lattice-QCD estimates of the scalar and tensor form-factors, we will study the impact of the theoretical uncertainties of these parameters on the precision achievable in the extraction of beyond SM constraints.

The last chapter of this thesis will be devoted to investigate the possible existence of vector resonances associated to a strongly interacting sector that can produce the spontaneous breaking of the electroweak symmetry in a Higgsless world. Exploiting the analogies, arising in this scenario, between the electroweak theory and low-energy QCD cases, we will analyze the scattering of longitudinally polarized W and Z gauge bosons, finding valuable information about the vector resonances and the possibility left for LHC to disentangle their presence. The work has been published in [23].

Chapter 1

The Standard Model

1.1. Standard Model: an overview

The SM is the reference theory for the description of particle physics phenomena. This chapter will introduce the main features of the SM, focusing on the aspects that will be the theoretical background of the work presented in this thesis. Some basic notation and concepts will be developed and we will also describe some of the open questions of this theory, that constitute the theoretical motivations of our work, setting in this way the stage for the analysis that we will present in the following chapters. We will conclude discussing briefly the motivations of looking beyond the SM and sketching the effective field theory method we will use throughout the thesis to analyze the phenomenology of possible extension of the SM.

1.1.1. The gauge sector

The SM is a local gauge theory based on the symmetry group $SU(3)_C \times SU(2)_L \times U(1)_Y$, where $SU(3)_C$ is the group of strong interactions [24, 25, 26] and the electroweak (EW) part of the theory can be described by the $SU(2)_L \times U(1)_Y$ group [27, 28, 29]. As the main focus of the thesis is on the electroweak phenomena, we will reduce our discussion to this sector. An introduction to the strong sector can be found for example in [30].

The basic features of the EW sector are finely summarized by the minimal Lagrangian:

$$\mathcal{L}_{\rm SM} = \overline{f} i \not{D} f - \frac{1}{4} W^I_{\mu\nu} W^{\mu\nu, I} - \frac{1}{4} B_{\mu\nu} B^{\mu\nu} \ , \tag{1.1}$$

where f indicates generically a fermionic matter field, $I = 1, 2, 3$ are $SU(2)_L$ indices and $W^{\mu\nu}$ and $B^{\mu\nu}$ are the strength tensors associated to the gauge

	fermions					scalars
field	ℓ_L	e_R	q_L	u_R	d_R	h
hypercharge Y	$-\frac{1}{2}$	-1	$\frac{1}{6}$	$\frac{2}{3}$	$-\frac{1}{3}$	$\frac{1}{2}$

Table 1.1: The hypercharge assigned to the SM matter content and to the SM Higgs.

bosons:

$$\begin{aligned} W^I_{\mu\nu} &= \partial_\mu W^I_\nu - \partial_\nu W^I_\mu + g\,\epsilon^{IJK} W^J_\mu W^K_\nu \ , \\ B_{\mu\nu} &= \partial_\mu B_\nu - \partial_\nu B_\mu \end{aligned} \tag{1.2}$$

and D_μ is the covariant derivative that reads:

$$D_\mu = \partial_\mu - igS^I W^I_\mu - ig'Y B_\mu \ . \tag{1.3}$$

Here we indicated with $S^I = \tau^I/2$ the $SU(2)_L$ generators, where τ^I are the Pauli matrices, and with Y the hypercharge of the field the covariant derivative is applied on (see Table 1.1). Once we choose the matter fields (quarks and leptons), the only free parameter of the EW sector of the SM at this stage are the dimensionless constants associated to the two gauge groups: g and g' for $SU(2)_L$ and $U(1)_Y$ respectively.

The observed matter fields are classified in the SM in five different representation of the gauge group:

- quark sector: we have one left-handed doublet q_L and two right-handed singlets for up and down quarks, u_R and d_R respectively;
- lepton sector: we introduce one left-handed doublet ℓ_L and one right-handed singlet e_R for the charged leptons (the right-handed singlet for the neutrinos doesn't interact with any other particle in the SM context, so it is neglected).

Each of these fermion fields is then multiplicated in three families, with the mass being the only difference between the different generations. It is then useful to consider each fermion field as a vector in the generation space (called, in some contexts, also flavor space). The quark fields read now:

$$\begin{aligned} q_L &= \left(\begin{pmatrix} u_L \\ d_L \end{pmatrix}, \begin{pmatrix} c_L \\ s_L \end{pmatrix}, \begin{pmatrix} t_L \\ b_L \end{pmatrix} \right) \ , \\ u_R &= (u_R,\ c_R,\ t_R) \ , \qquad d_R = (d_R,\ s_R,\ b_R) \ . \end{aligned} \tag{1.4}$$

The lepton sector becomes:

$$\ell_L = \left(\begin{pmatrix} \nu_L^{(e)} \\ e_L \end{pmatrix}, \begin{pmatrix} \nu_L^{(\mu)} \\ \mu_L \end{pmatrix}, \begin{pmatrix} \nu_L^{(\tau)} \\ \tau_L \end{pmatrix} \right) \ , \quad e_R = (e_R,\ \mu_R,\ \tau_R) \ . \tag{1.5}$$

The multiplication of the fermion fields in different generations is introduced in the SM in order to describe adequately the phenomenology. Why there exist in nature almost identical copies of each fermion and why they are exactly three, are questions that are not addressed in the SM and are still waiting for a complete answer. The SM Lagrangian in Eq. (1.1) becomes explicitly:

$$\mathcal{L}_{\rm SM} = \sum_f \sum_i \overline{f}_i i \not{D} f_i - \frac{1}{4} W^I_{\mu\nu} W^{\mu\nu, I} - \frac{1}{4} B_{\mu\nu} B^{\mu\nu} \ , \tag{1.6}$$

where $f = q_L, u_R, d_R, \ell_L, e_R$ and i is a flavor index running over the three generations of fermions. It is then clear that at this stage, i.e. with only massless particles in the theory, no interaction between fermions of different generations is allowed. We will see in Section 1.1.3 how mass terms will change this picture. It is also interesting to note that the coupling of the gauge bosons to fermions is flavor independent: this is the so called *universality* of the gauge coupling constants. In Chapter 4 we will test, through a global analysis based on all the precise electroweak observables, the possibility that effects of beyond SM physics induce a violation of universality in the interaction between the W boson and the leptons.

1.1.2. The Yukawa and Higgs sector

In the minimal formulation given by the Lagrangian in Eq. (1.1) all the particles in the SM are massless. In order to reproduce the phenomenological observations, we then need to introduce mass terms for the different fields, without spoiling the gauge symmetry that provides the renormalizability of the theory. This is achieved through the Higgs mechanism [31, 32]: we introduce a new scalar doublet h that, after spontaneous symmetry breaking (SSB), acquire a non-zero vacuum expectation value (vev) v:

$$h(x) = \begin{pmatrix} h^{(+)}(x) \\ h^{(0)}(x) \end{pmatrix} \ , \qquad \langle 0 |\, h \,| 0 \rangle \ \equiv \begin{pmatrix} 0 \\ v \end{pmatrix} \ . \tag{1.7}$$

The particular choice of the vev breaks the EW gauge symmetry group down to the electromagnetic group $U(1)_{em}$:

$$SU(2)_L \otimes U(1)_Y \qquad \stackrel{SSB}{\Longrightarrow} \qquad U(1)_{em} \, . \tag{1.8}$$

In this way we obtain massive W and Z gauge bosons and a massless photon, as required by the experimental data. The physical gauge boson fields are:

- charged W_μ bosons defined by:

$$W_\mu^\pm = \frac{W_\mu^1 \mp i W_\mu^2}{\sqrt{2}} \tag{1.9}$$

  with a tree level mass given by $M_W = gv/\sqrt{2}$;

- the A_μ photon and the neutral Z_μ boson defined by:

$$\begin{aligned} Z_\mu &= \cos\theta_W W_\mu^3 - \sin\theta_W B_\mu \\ A_\mu &= \sin\theta_W W_\mu^3 + \cos\theta_W B_\mu \ , \end{aligned} \tag{1.10}$$

  where $\tan\theta_W \equiv g'/g$ defines the weak angle θ_W. The mass of the Z boson, at first order, is given by $M_Z = M_W/\cos\theta_W$.

We want to stress that, using the experimental value of the Fermi constant G_F, we can obtain the value of the Higgs vev:

$$G_F = \frac{1}{2\sqrt{2}v^2} \simeq 1.17 \times 10^{-5}\ \text{GeV}^{-2} \quad \Rightarrow \quad v \simeq 174\ \text{GeV} \tag{1.11}$$

On the other hand the Higgs mass is a free parameter of the SM and can be inferred only through the loop effects on precise electroweak observables or a direct search like the one LHC is currently performing.

The fermion masses are introduced through Yukawa-type interactions:

$$\mathcal{L}_Y = -q'_L\, \lambda_u\, u'_R\, \tilde{h} - \ q'_L\, \lambda_d\, d'_R\, h - \ell'_L\, \lambda_e\, e'_R\, h + \text{h.c.}\ . \tag{1.12}$$

where $\tilde{h} = i\tau^2 h^*$, the flavor indices have been neglected for simplicity and the fermion fields $q'_L, u'_R, d'_R, \ell'_L, e'_R$ are gauge eigenstates. Eq. (1.12) is the most general renormalizable Lagrangian involving fermions and the Higgs field, once we impose gauge symmetry and we take into account the values for the hypercharge of each field (see Table 1.1). The three coefficients of Eq. (1.12) λ_X, with $X = u, d, e$, are the Yukawa matrices and are 3×3 matrices in flavor space. The elements of these matrices are free parameters of the theory and are chosen in order to correctly describe the phenomenology. The special pattern of the Yukawas, characterized by a strong hierarchy between the different generations, is again one of the open questions of the SM.

1.1.3. Flavor mixing

In the Yukawa Lagrangian of Eq. (1.12) we used the gauge eigenstates for the fermion fields. It is instructive to see what happens when we express the same Lagrangian in terms of the mass eigenstates. We study first the case of the quark sector, being the case of leptons trivial, at least in the context of the SM with massless neutrinos. The Yukawa Lagrangian for the quarks reads:

$$\begin{aligned}\mathcal{L}_{Y_q} &= -q'_L\,\lambda_u\,u'_R\,\tilde{h} - q'_L\,\lambda_d\,d'_R\,h + \text{h.c.} \\ &\overset{SSB}{\Longrightarrow} -u'_L\,Y_u\,u'_R - u'_L\,Y_d\,d'_R + \text{h.c.}\ ,\end{aligned} \tag{1.13}$$

The second line is the Lagrangian we get after SSB and keeping only the mass terms, where the new matrices are simply $Y_X \equiv v\lambda_X$. We can then diagonalize the two Yukawas using unitary matrices:

$$\begin{aligned}Y_u &= U_{u_L}\,\bar{Y}_u\,U^\dagger_{u_R}\ , \\ Y_d &= U_{d_L}\,\bar{Y}_d\,U^\dagger_{d_R}\ ,\end{aligned} \tag{1.14}$$

where $\bar{Y}_X$ are diagonal matrices with real and positive elements. In this way we defined the field transformations from gauge to mass eigenstates:

$$\begin{aligned}u'_L &= U_{u_L}u_L\ , & u'_R &= U_{u_R}u_R\ , \\ d'_L &= U_{d_L}d_L\ , & d'_R &= U_{d_R}d_R\ .\end{aligned} \tag{1.15}$$

Let's consider now the quark charged current coupled to the charged W boson:

$$\bar{u}'_L\gamma_\mu d'_L = \bar{u}_L U^\dagger_{u_L}\gamma_\mu U_{d_L}d_L = \bar{u}_L\gamma_\mu V_{\text{CKM}}d_L\ . \tag{1.16}$$

In the last step we defined the Cabibbo-Kobayashi-Maskawa (CKM) matrix [33, 34] that parameterizes the mixing between the different generations of quarks. We want to stress that there is no such a mixing matrix related to neutral currents and then there are no Flavor Changing Neutral Currents (FCNC) at tree level in the SM. On the other hand the CKM matrix controls all the possible flavor changing processes. It can be written in a convenient way through the Wolfestein parametrization [35]:

$$\begin{aligned}V_{\text{CKM}} &\equiv \begin{pmatrix} V_{ud} & V_{us} & V_{ub} \\ V_{cd} & V_{cs} & V_{cb} \\ V_{td} & V_{ts} & V_{tb} \end{pmatrix} \\ &= \begin{pmatrix} 1-\frac{\lambda^2}{2} & \lambda & A\lambda^3(\varrho - i\eta) \\ -\lambda & 1-\frac{\lambda^2}{2} & A\lambda^2 \\ A\lambda^3(1-\varrho-i\eta) & -A\lambda^2 & 1 \end{pmatrix} + O(\lambda^4)\ ,\end{aligned} \tag{1.17}$$

where the expansion parameter is $\lambda = |V_{us}| \sim 0.22$ and the other parameters are of $\mathcal{O}(1)$. Even if the expansion in λ is only an approximation, it is useful to understand the main features of the CKM matrix:

- The diagonal elements, that control the mixing between quarks of the same generation, have a value very close to one. This kind of transitions are then completely allowed in the SM;

- The off-diagonal elements are instead small parameters, working then as suppression factors for the transitions between different quark generations;

- There is one physical phase in the CKM mixing matrix (to see it at first glance, the "standard parametrization" is the one we should use) that controls the CP violating processes in the SM. It is interesting to note that with less than three generations there is no physical phase remaining in the theory (all the phases can be absorbed in a field redefinition). Consequently, in order to describe the CP violation observed for example in the kaon sector, we need to introduce at least three quark generations in the theory.

The flavor sector for the leptons is, as we said, very simple in the minimal version of the SM. Being the neutrinos massless, we can diagonalize directly the charged leptons mass matrix $\bar{Y}_e$ (the bar indicates that the matrix is diagonal):

$$\mathcal{L}_{Y_\ell} = -\lambda_e \, \ell'_L e'_R \, h + \text{h.c.} \quad \stackrel{SSB}{\Longrightarrow} \quad -\bar{Y}_e \, \ell_L e_R + \text{h.c.} \, . \tag{1.18}$$

When dealing with extensions of the SM that include massive neutrinos, it is useful to introduce a leptonic version of the CKM mixing matrix, called the Pontecorvo-Maki-Nakagawa-Sakata mixing matrix [36, 37]. We define it as the matrix that generates the neutrino mass eigenstates starting from the gauge eigenstates:

$$|\, \nu_\alpha \rangle \; = \sum_i U^*_{\alpha i} \, |\, \nu_i \rangle \;\; . \tag{1.19}$$

The neutrino mass eigenstate can be defined as the state produced in the decay $W \to \ell_\alpha \nu_\alpha$. The standard parametrization of lepton mixing matrix

reads [38]:

$$U_{\text{PMNS}} = \begin{pmatrix} c_{12}c_{13} & s_{12}c_{13} & s_{13}e^{-i\delta} \\ -s_{12}c_{23} - c_{12}s_{23}s_{13}e^{i\delta} & c_{12}c_{23} - s_{12}s_{23}s_{13}e^{i\delta} & s_{23}c_{13} \\ s_{12}s_{23} - c_{12}c_{23}s_{13}e^{i\delta} & -s_{23}c_{12} - s_{12}c_{23}s_{13}e^{i\delta} & c_{23}c_{13} \end{pmatrix} \times \text{diag}(1, e^{i\alpha_{21}/2}, e^{i\alpha_{31}/2}) \quad . \tag{1.20}$$

The phases α_{ij} can be absorbed in the field definition if the neutrinos are not Majorana particles. In that case the U_{PMNS} has the same form of the CKM mixing matrix, but with different values of the elements.

1.1.4. Accidental symmetries

We conclude this brief review on the Standard Model noting that the theory possesses some so called "accidental symmetries". The name derives from the fact that these symmetries are not imposed in the construction of the theory, but are a bonus feature of the SM structure. Looking at the Lagrangian in Eq. (1.12) it is easy to see that total lepton (L) and baryon (B) numbers are conserved. In addition also the generation number is conserved in the lepton sector, i.e. we have three lepton numbers (L_e, L_μ and L_τ) conserved separately. The consequence is that in the SM context no lepton flavor violating processes are allowed at any order. Introducing Dirac masses for the neutrinos breaks the generation numbers, but keeps the total lepton number, whereas Majorana terms break also this last symmetry.

In order to introduce a proper description for the observed non-vanishing neutrino masses, most of the SM extensions are actually allowing lepton flavor violating processes at a level that in most cases is already excluded by experimental data. A possible solution to this problem is to constrain the structure of the flavor sector of the high energy theory through convenient flavor symmetries. We will analyze one of these scenarios in Chapter 3, where we will study the consequences of a minimal violation of the lepton flavor symmetry on the leptonic meson decays.

1.2. Standard Model as an Effective Theory

The Standard Model as we sketched it in the previous sections has been tested with impressive precision in past experiments (for a review see for example [1]) and it is still the reference theory to interpret the results of

LHC and other current experiments. However there are clear evidences for the need of a completion of SM. As we already noted we do not understand yet why fermions are replicated in three (and apparently only three) nearly identical copies or what is the origin of the SM flavor structure. Moreover we need a consistent description for the neutrino masses and mixing and to understand the gauge symmetry breaking mechanism, confirming the Higgs picture or developing a new scenario.

Irrespective of the specific high-energy features of the new theory, the SM will certainly represent its low-energy limit. The high-energy theory should then satisfy some requirements:

- Its gauge group should contain the SM gauge group $SU(3)_C \times SU(2)_L \times U(1)_Y$;
- Its particle content should include the SM fields, either as fundamental or composite degrees of freedom. As we will see in the following, the linear realization of the Higgs sector used in the SM context is not a fundamental ingredient in the gauge symmetry breaking mechanism, at least from a theoretical point of view. Although, the recent LHC announcement of the discovery of a new scalar particle in the 125 GeV range is certainly a strong indication that the SM symmetry breaking picture could be actually realized in Nature;
- Neglecting undiscovered weakly-coupled light particles, like axions or sterile neutrinos, the new theory should reduce at low energy to the SM.

In order to extend the present theoretical framework, one way to proceed is to build up a full theory that respects these requirements, as has been done for example with supersymmetric theories. In this thesis we will use a different and complementary approach, in which we considered the SM as an effective theory valid up to a certain energy scale Λ at which new degrees of freedom will show up. At energies below this cut-off, we can then integrate out these new particles generating a series of higher-dimensional operators O_i built with only low-energy fields. Short-distance physics will be described by effective coefficients that multiply the operators that, in a bottom-up approach like the one we will follow, are free parameters of the effective theory.

In order to build a proper effective theory, we need to specify a number of features that have to be satisfied. While we know that the gauge group has to be the SM one and the SM fermions and gauge bosons must be included in the particle content of the low energy theory, the gauge symmetry breaking

sector is not clearly defined. What we really know is that there has to exist a system coupled to the SM displaying a symmetry breaking pattern from a group G (that has to include the SM gauge group $SU(2)_L \times U(1)_Y$) to a subgroup H. It can be shown (see for example [39]) that there is only one possible choice, i.e. $G = SU(2)_L \times SU(2)_R$ and $H = SU(2)_{L+R}$. Starting from this basic hypothesis different symmetry breaking sectors can be build, being the SM one the simplest choice.

As anticipated, the LHC discovery of a new scalar particle represents a big step toward the confirmation of the SM and its symmetry breaking mechanism. On the other hand, in these years various alternative options to the SM Higgs mechanism have been developed on the market, from an enlarged Higgs sector to a composite Higgs. These possibilities are certainly very interesting from a theoretical point of view and could be reconsidered if experiments will not fully confirm the SM picture. In this thesis we will focus on the standard scenario with the SM Higgs sector and on a framework based on a dynamical electroweak symmetry breaking mechanism without a Higgs boson, on the wake of what happens in QCD with chiral symmetry.

In Chapter 2 we will analyze a general effective field theory based on the assumption that the scalar sector is the one introduced in the SM and the gauge symmetry is linearly realized. We will then develop different analysis based on this scenario, focusing on a special flavor symmetry in Chapter 3, studying in Chapter 5 the impact of future experiments on neutron decay in constraining new scalar and tensor interactions and testing in Chapter 4 a possible departure from lepton universality in W decays through a global fit on the most precise electroweak observables. A different scenario will be developed in Chapter 6 where we will start from the hypothesis that the electroweak symmetry breaking is due to a new strongly interacting sector standing at the TeV scale. The possible existence of resonances, consequence of this strong sector, will be studied in Chapter 7.

Chapter 2

EFT: The SM Higgs scenario

The first EFT scenario we are going to analyze is maybe the most popular in the literature and its phenomenology has been studied in a number of papers. The basic hypothesis are:

- The existence of a gap between the SM electroweak scale v and the New Physics scale Λ;
- The assumption that the SM extension is weakly coupled at the weak scale, so the EW symmetry can be linearly realized and the low-energy theory can contain a SM-like symmetry breaking sector. Consequently the effective field theory, defined at the weak scale, will contain the Higgs doublet as an explicit field.
- The conservation of lepton and baryon total numbers. This is by no means a compulsory hypothesis, but, as we are not interested in the breaking of these two symmetries, it is a simplifying assumption. Only in Chapter 3 we will need to introduce an explicit breaking of the total lepton number in order to generate neutrino masses.

The first two assumptions result in the decoupling of heavy particles with masses of order Λ or larger and the possibility of integrating them out, describing their effects at low energy through a series of higher-dimensional operators O_i built with only low-energy fields and suppressed by inverse powers of the scale Λ:

$$\mathcal{L}_{\text{EFT}} = \mathcal{L}_{\text{SM}} + \frac{1}{\Lambda}\sum_i \alpha_i^{(5)} O_i^{(5)} + \frac{1}{\Lambda^2}\sum_i \alpha_i^{(6)} O_i^{(6)} + \mathcal{O}\left(\frac{1}{\Lambda^3}\right), \tag{2.1}$$

where $\mathcal{L}_{\text{SM}}$ is the SM Lagrangian and α_i are dimensionless effective coefficients containing all the short-distance physics. If the underlying high-energy

theory is fully specified, all these coefficients can be determined by integrating out the heavy fields. On the other hand, in a bottom-up approach like the one we will follow, they are free parameters of the effective theory. Phenomenology will be the guide to constrain these parameters and then to define the features of the theory valid at energies above the scale Λ.

This chapter will be devoted to the analysis of the complete set of operators of dimension 5 and 6, that represent the first orders of approximation in the expansion of Eq. (2.1). Terms of higher dimension are supposed to be too suppressed to give sizable contributions to any observable, at least with the current experimental precision.

2.1. Effective operator basis

2.1.1. Basic notation

We collect in this section the notation we will use in developing the effective operator basis and then in the phenomenological analyses of the following chapters. The notation will be consistent with the one introduced in Chapter 1 for the SM case. However some changes will be made with the aim of simplifying the formulas. We will drop the chirality indices L, R: the fermion fields will be always understood as chiral fields, with quantum numbers given in Table 1.1, and we will use the following convention:

$$\begin{aligned} &\text{Left-handed doublets:} \quad q, \ell \\ &\text{Right-handed singlets:} \quad u, d, e \end{aligned} \tag{2.2}$$

Our definition for the chiral projectors is $P_L = (1-\gamma_5)/2$ and $P_R = (1+\gamma_5)/2$. Besides special cases we will drop also the flavor indices $i, j, k, l = 1, 2, 3$. $SU(2)_L$ indices, indicated with Greek letters $\alpha, \beta = 1, 2$, if not explicitly written, are always contracted inside the bilinear or between the only two $SU(2)_L$ doublets present in the operator. When needed we will use the total antisymmetric tensor $\epsilon = i\tau_2$ ($\epsilon_{12} = +1$) to contract the $SU(2)_L$ indices. For $SU(3)_C$ color indices we will use latin letters $a, b, c = 1, 2, 3$.

We will follow the sign convention for covariant derivatives exemplified by:

$$(D_\mu q)^{a\alpha} = \left(\delta_{\alpha\beta}\delta_{ab}\partial_\mu - ig_s\delta_{\alpha\beta}T^A_{ab}G^A_\mu - igS^I_{\alpha\beta}\delta_{ab}W^I_\mu - ig'\delta_{\alpha\beta}\delta_{ab}Y_q B_\mu\right) q^{b\beta}. \tag{2.3}$$

Here, $T^A = \frac{1}{2}\lambda^A$ (A = 1,..8) and $S^I = \frac{1}{2}\tau^I$ (I = 1,2,3) are the $SU(3)_C$ and $SU(2)_L$ generators, while λ^A and τ^I are the Gell-Mann and Pauli matrices,

respectively. The gauge field strength tensors read:

$$\begin{aligned} G^A_{\mu\nu} &= \partial_\mu G^A_\nu - \partial_\nu G^A_\mu + g_s f^{ABC} G^B_\mu G^C_\nu \ , \\ W^I_{\mu\nu} &= \partial_\mu W^I_\nu - \partial_\nu W^I_\mu + g\epsilon^{IJK} W^J_\mu W^K_\nu \ , \\ B_{\mu\nu} &= \partial_\mu B_\nu - \partial_\nu B_\mu \ , \end{aligned} \tag{2.4}$$

and their covariant derivatives are:

$$\begin{aligned} (D_\rho G_{\mu\nu})^A &= \partial_\rho G^A_{\mu\nu} + g_s f^{ABC} G^B_\rho G^C_{\mu\nu} \ , \\ (D_\rho W_{\mu\nu})^I &= \partial_\rho W^I_{\mu\nu} + g\epsilon^{IJK} W^J_\rho W^K_{\mu\nu} \ , \\ D_\rho B_{\mu\nu} &= \partial_\rho B_{\mu\nu}. \end{aligned} \tag{2.5}$$

Dual tensors are defined by $\widetilde{X}_{\mu\nu} = \frac{1}{2}\epsilon_{\mu\nu\rho\sigma} X^{\rho\sigma}$ ($\epsilon_{0123} = +1$), where X stands for G^A, W^I or B.

2.1.2. Operator definition

The complete effective operator basis up to dimension six terms was first developed in [2, 3] and afterwards has been corrected and completed in various papers during the years. Our notation is based mainly on the conventions introduced in [2], but we will take into account the results discussed in the complete revision published in [40]. The details on the construction of effective basis and on the use of the equations of motion and Fierz identities to identify linearly dependent terms can be found in the original papers.

At dimension there is only one dimension-5 operator respecting the SM gauge symmetry:

$$Q_{\nu\nu} = (\tilde{h}^\dagger \ell)^T C (\tilde{h}^\dagger \ell) \ , \tag{2.6}$$

where C is the charge conjugation matrix, that in the Dirac representation reads $C = i\gamma^2\gamma^0$, with Bjorken and Drell [41] phase convention. This operator violates total lepton number and will be neglected in most of this thesis. However it is important to note that it generates, after spontaneous symmetry breaking, neutrino masses and mixing and then will be an important ingredient when we will discuss a lepton flavor symmetry violating scenario.

We can divide the operators depending on the kind of fields they contain:

Fermions only

The operators containing only fermion fields can be categorized in four classes, depending on the chirality of the fields involved: LLLL, RRRR, LRRL and LRLR. There are 25 independent operators of this type.

$\bar{\mathbf{L}}\mathbf{L}\bar{\mathbf{L}}\mathbf{L}$

$$O_{\ell\ell}^{(1)} = \frac{1}{2}(\bar{\ell}\gamma_\mu\ell)(\bar{\ell}\gamma^\mu\ell) \tag{2.7a}$$

$$O_{qq}^{(1,1)} = \frac{1}{2}(\bar{q}\gamma_\mu q)(\bar{q}\gamma^\mu q) \tag{2.7b}$$

$$O_{qq}^{(1,3)} = \frac{1}{2}(\bar{q}\gamma_\mu\tau^I q)(\bar{q}\gamma^\mu\tau^I q) \tag{2.7c}$$

$$O_{\ell q}^{(1)} = (\bar{\ell}\gamma_\mu\ell)(\bar{q}\gamma^\mu q) \tag{2.7d}$$

$$O_{\ell q}^{(3)} = (\bar{\ell}\gamma_\mu\tau^I\ell)(\bar{q}\gamma^\mu\tau^I q) \tag{2.7e}$$

$\bar{\mathbf{R}}\mathbf{R}\bar{\mathbf{R}}\mathbf{R}$

$$O_{ee} = \frac{1}{2}(\bar{e}\gamma_\mu e)(\bar{e}\gamma^\mu e) \tag{2.8a}$$

$$O_{uu}^{(1)} = \frac{1}{2}(\bar{u}\gamma_\mu u)(\bar{u}\gamma^\mu u) \tag{2.8b}$$

$$O_{dd}^{(1)} = \frac{1}{2}(\bar{d}\gamma_\mu d)(\bar{d}\gamma^\mu d) \tag{2.8c}$$

$$O_{eu} = (\bar{e}\gamma_\mu e)(\bar{u}\gamma^\mu u) \tag{2.8d}$$

$$O_{ed} = (\bar{e}\gamma_\mu e)(\bar{d}\gamma^\mu d) \tag{2.8e}$$

$$O_{ud}^{(1)} = (\bar{u}\gamma_\mu u)(\bar{d}\gamma^\mu d) \tag{2.8f}$$

$$O_{ud}^{(8)} = (\bar{u}\gamma_\mu\lambda^A u)(\bar{d}\gamma^\mu\lambda^A d) \tag{2.8g}$$

$\bar{\mathbf{L}}\mathbf{R}\bar{\mathbf{R}}\mathbf{L}$

$$O_{\ell e} = (\bar{\ell}e)(\bar{e}\ell) \tag{2.9a}$$

$$O_{\ell u} = (\bar{\ell}u)(\bar{u}\ell) \tag{2.9b}$$

$$O_{\ell d} = (\bar{\ell}d)(\bar{d}\ell) \tag{2.9c}$$

$$O_{qe} = (\bar{q}e)(\bar{e}q) \tag{2.9d}$$

$$O_{qu}^{(1)} = (\bar{q}u)(\bar{u}q) \tag{2.9e}$$

$$O_{qu}^{(8)} = (\bar{q}\lambda^A u)(\bar{u}\lambda^A q) \tag{2.9f}$$

$$O_{qd}^{(1)} = (\bar{q}d)(\bar{d}q) \tag{2.9g}$$

$$O_{qd}^{(8)} = (\bar{q}\lambda^A d)(\bar{d}\lambda^A q) \tag{2.9h}$$

$$O_{qde} = (\bar{\ell}e)(\bar{d}q) \tag{2.9i}$$

$\bar{\mathbf{L}}\mathbf{R}\bar{\mathbf{L}}\mathbf{R}$

$$O_{qq}^{(1)} = \epsilon^{\alpha\beta}(\bar{q}_\alpha u)(\bar{q}_\beta d) \tag{2.10a}$$

$$O_{qq}^{(8)} = \epsilon^{\alpha\beta}(\bar{q}_\alpha\lambda^A u)(\bar{q}_\beta\lambda^A d) \tag{2.10b}$$

$$O_{\ell q} = \epsilon^{\alpha\beta}(\bar{\ell}_\alpha e)(\bar{q}_\beta u) \tag{2.10c}$$

$$O_{\ell q}^{t} = \epsilon^{\alpha\beta}(\bar{\ell}_\alpha\sigma_{\mu\nu}e)(\bar{q}_\beta\sigma^{\mu\nu}u) \tag{2.10d}$$

The operators of the first three classes (LLLL, RRRR and LRRL), a part from operator O_{qde}, are Hermitian (i.e. the Hermitian conjugation is equivalent to the transposition of flavor indices. See the note at the end of this

section). The Hermitian conjugates of the LRLR operators are not listed explicitly.

Vectors only

$$O_G = f_{ABC} G_\mu^{A\nu} G_\nu^{B\lambda} G_\lambda^{C\mu} \quad (2.11a)$$
$$O_{\tilde{G}} = f_{ABC} \tilde{G}_\mu^{A\nu} G_\nu^{B\lambda} G_\lambda^{C\mu} \quad (2.11b)$$
$$O_W = \epsilon_{IJK} W_\mu^{I\nu} W_\nu^{J\lambda} W_\lambda^{K\mu} \quad (2.12a)$$
$$O_{\tilde{W}} = \epsilon_{IJK} \tilde{W}_\mu^{I\nu} W_\nu^{J\lambda} W_\lambda^{K\mu} \quad (2.12b)$$

Scalars only

$$O_h = \frac{1}{3}(h^\dagger h)^3 \quad (2.13a)$$
$$O_{h\Box} = (h^\dagger h)\Box(h^\dagger h) \quad (2.13b)$$

Scalars and vectors

$$O_{hG} = \frac{1}{2}(h^\dagger h) G_{\mu\nu}^A G^{A\mu\nu} \quad (2.14a)$$
$$O_{h\tilde{G}} = (h^\dagger h) \tilde{G}_{\mu\nu}^A G^{A\mu\nu} \quad (2.14b)$$
$$O_{hW} = \frac{1}{2}(h^\dagger h) W_{\mu\nu}^I W^{I\mu\nu} \quad (2.14c)$$
$$O_{h\tilde{W}} = (h^\dagger h) \tilde{W}_{\mu\nu}^I W^{I\mu\nu} \quad (2.14d)$$
$$O_{hB} = \frac{1}{2}(h^\dagger h) B_{\mu\nu} B^{\mu\nu} \quad (2.14e)$$
$$O_{h\tilde{B}} = (h^\dagger h) \tilde{B}_{\mu\nu} B^{\mu\nu} \quad (2.15a)$$
$$O_{WB} = (h^\dagger \tau^I h) W_{\mu\nu}^I B^{\mu\nu} \quad (2.15b)$$
$$O_{\tilde{W}B} = (h^\dagger \tau^I h) \tilde{W}_{\mu\nu}^I B^{\mu\nu} \quad (2.15c)$$
$$O_{hD} = \left(h^\dagger D^\mu h\right)^* \left(h^\dagger D_\mu h\right) \quad (2.15d)$$

All the operators of the last three sections are Hermitian. The ones involving $\tilde{X}$ are CP-odd, the others are CP-even.

Fermions and scalars

$$O_{eh} = (h^\dagger h)(\bar{\ell} e h) \quad (2.16a)$$
$$O_{uh} = (h^\dagger h)(\bar{q} u \tilde{h}) \quad (2.16b)$$
$$O_{dh} = (h^\dagger h)(\bar{q} d h) \quad (2.16c)$$

Vectors, fermions and scalars

$$O_{h\ell}^{(1)} = (h^\dagger i D_\mu h)(\bar{\ell}\gamma^\mu \ell) \quad (2.17a)$$
$$O_{h\ell}^{(3)} = (h^\dagger i \tau^I D_\mu h)(\bar{\ell}\gamma^\mu \tau^I \ell) \quad (2.17b)$$
$$O_{he} = (h^\dagger i D_\mu h)(\bar{e}\gamma^\mu e) \quad (2.17c)$$
$$O_{hq}^{(1)} = (h^\dagger i D_\mu h)(\bar{q}\gamma^\mu q) \quad (2.17d)$$
$$O_{hq}^{(3)} = (h^\dagger i \tau^I D_\mu h)(\bar{q}\gamma^\mu \tau^I q) \quad (2.17e)$$
$$O_{hu} = (h^\dagger i D_\mu h)(\bar{u}\gamma^\mu u) \quad (2.17f)$$
$$O_{hd} = (h^\dagger i D_\mu h)(\bar{d}\gamma^\mu d) \quad (2.17g)$$
$$O_{hh} = \epsilon^{\alpha\beta}(h_\alpha^* i D_\mu h_\beta)(\bar{u}\gamma^\mu d) \quad (2.17h)$$

$$O^t_{eW} = (\bar{\ell}\sigma^{\mu\nu}\tau^I e)hW^I_{\mu\nu} \quad (2.17\text{i})$$
$$O^t_{eB} = (\bar{\ell}\sigma^{\mu\nu} e)hB_{\mu\nu} \quad (2.17\text{j})$$
$$O^t_{uG} = (\bar{q}\sigma^{\mu\nu}\lambda^A u)\tilde{h}G^A_{\mu\nu} \quad (2.17\text{k})$$
$$O^t_{uW} = (\bar{q}\sigma^{\mu\nu}\tau^I u)\tilde{h}W^I_{\mu\nu} \quad (2.17\text{l})$$
$$O^t_{uB} = (\bar{q}\sigma^{\mu\nu} u)\tilde{h}B_{\mu\nu} \quad (2.17\text{m})$$
$$O^t_{dG} = (\bar{q}\sigma^{\mu\nu}\lambda^A d)hG^A_{\mu\nu} \quad (2.17\text{n})$$
$$O^t_{dW} = (\bar{q}\sigma^{\mu\nu}\tau^I d)hW^I_{\mu\nu} \quad (2.17\tilde{\text{n}})$$
$$O^t_{dB} = (\bar{q}\sigma^{\mu\nu} d)hB_{\mu\nu} \quad (2.17\text{o})$$

All the operators in these two last sections need to be completed with their Hermitian conjugate.

We conclude reminding that each operator carry flavor indices and is coupled to a "flavored" coefficient. Our convention for these coefficients are:

- The flavor matrix α of the Hermitian conjugate of the operators will carry a dagger;
- For the operators $O^{(1)}_{\ell\ell}$ and O_{ee}, because of the symmetry between the two bilinears, we impose $[\alpha]_{ijkl} = [\alpha]_{klij}$;
- in order to ensure the hermiticity of the four fermion operators of classes $LLLL$, $RRRR$ and $LRRL$ we impose $[\alpha]_{ijkl} = [\alpha]^*_{jilk}$.

It is important to note that none of these conditions entails any loss of generality.

Chapter 3

Lepton Flavor violation in leptonic meson decays

In the last few years there has been a great experimental progress in quark and lepton flavor physics. On the quark side, several stringent tests of neutral-current flavor-changing processes have been performed finding no significant deviations from the Standard Model predictions. This fact naturally points towards new physics models with highly constrained flavor structures. In models with flavored degrees of freedom around the TeV scale, a natural option is the so-called hypothesis of Minimal Flavor Violation (MFV). Within a general Effective Field Theory approach, this hypothesis can be formulated in general terms as the assumption that the Yukawa couplings are the only relevant sources of flavor symmetry breaking both within and beyond the SM, at least in the quark sector [42]. As discussed in the recent literature, this hypothesis can naturally be implemented in supersymmetric extensions of the SM [43] or, in slightly modified forms, also in models with new strongly interacting dynamics at the TeV scale [44, 45].

The situation of the lepton sector is more uncertain but also more exciting. As we noted in the previous chapter, the discovery of neutrino oscillations provide an unambiguous indication that the SM is not a complete theory and a clear evidence about the existence of new flavor structures in addition to the three SM Yukawa couplings. In various frameworks these new flavor structures can have non-trivial implications in other sectors of the model. In particular, deviations from SM predictions are expected in FCNC decays of charged leptons and, possibly, in a few meson decays with lepton pairs in the final state (see e.g. Ref. [46] for a recent review).

As far as meson decays are concerned, an interesting role is played by the helicity suppressed $P \to \ell\nu$ decays and particularly by the lepton-universality ratios in these processes. Present experimental data on $R_K^{\mu e} = \mathcal{B}(K \to e\nu)/$

$\mathcal{B}(K \to \mu\nu)$ [47, 48], with their impressive $\mathcal{O}(0.4\%)$ precision level, already strongly constrain the parameter space of supersymmetric extensions of the SM and new experimental improvements are in sight [49]. A very significant test of lepton-flavor universality (LFU) will soon be performed also in $\pi \to \ell\nu$ decays, measuring the $R_\pi^{\mu e}$ ratio at the $\mathcal{O}(0.1\%)$ level [50]. Finally, also the purely leptonic decays of the heavy pseudoscalar mesons ($B^\pm$, $D^\pm$ and $D_s^\pm$) have been observed in the last years at the B factories [51, 52, 53, 54, 55] opening the possibility of interesting LFU tests also in these modes [56].

A general theoretical tool for analyzing the results of all these future experiments is provided by low-energy EFT approaches based on specific flavor-symmetry assumptions. This approach allows us to test the implications of flavor symmetries which are independent from specific dynamical details of the new-physics model. As far as lepton-flavor mixing is concerned, two general constructions of this type are particularly interesting: the EFT based on the Minimal Lepton Flavor Violation (MLFV) hypothesis and the implementation of the MFV hypothesis in a Grand Unified Theory framework (MFV-GUT) [6]. The purpose of this chapter is to analyze the role of the $P \to \ell\nu$ decays in both these frameworks.

The chapter is organized as follows: in Section 3.1 we analyze the dimension-six effective operators contributing to $P \to \ell\nu$ decays and discuss their flavor structure according to the MLFV hypothesis. In Section 3.2 we present the results for the $P \to \ell\nu$ decay rates and discuss their natural size in the MLFV framework. The phenomenology is discussed in Section 3.4, starting from the model-independent bounds derived from FCNC processes within the EFT approach. The final results concerning the maximal deviations from SM predictions on $R_K^{\ell\ell'}$ ratios are presented in Section 3.4 and summarized in the Conclusions of the chapter.

3.1. Operator basis and flavor structures

The effective theory relevant to the analysis we will develop in the following sections is essentially the same that we discussed in Chapter 2. However, as we are interested in theories with new *flavored* degrees of freedom, we will substitute the generic NP energy scale $\Lambda_{\rm NP}$ with $\Lambda_{\rm LFV}$ (where LFV is short for lepton flavor violation), the scale at which new degrees of freedom carrying lepton-flavor quantum numbers appear. Following a theoretical argument based on a natural solution of the hierarchy problem we require that this scale doesn't exceed few TeV, stabilizing in this way the Higgs mass. On the other hand we introduce $\Lambda_{\rm LN}$ (or M_ν), a very high energy scale (well above $\Lambda_{\rm LFV}$) associated to the breaking of total lepton number. The only di-

mension five operator allowed by gauge symmetry is suppressed by the $\Lambda_{\rm LN}$ scale and then can be safely neglected.

In order to determine the relevant effective operators contributing to $P \to \ell\nu$ decays we need to specify the structure of the low-energy EFT. This is, as we discussed before, characterized by the low-energy field content and the symmetries of the theory. A part from imposing the SM gauge symmetry, we will focus on the role of the flavor symmetries, specifying the flavor symmetry breaking terms. We assume that the low-energy field content of the EFT is the SM one, with the exception of the Higgs sector, where we we consider two Higgs doublets coupled separately to up-type quarks (h_u), and down-type quarks and charged leptons (h_d). This way we avoid large contributions to FCNC, but we explore possible $\tan\beta = \langle h_u\rangle/\langle h_d\rangle$ enhancements of flavor-violating effects.

With these hypothesis the most general Lagrangian, up to dimension-six terms, is basically the one we described in Section 2.1. However two important modifications are needed:

- In order to take into account the larger Higgs sector, that we are considering in this chapter, new operators have to be introduced. There are small modifications of the existing operators involving Higgs fields. In what follows we will introduce explicitly the new operators when they are relevant for the processes we are analyzing.

- We will specify the operator flavor structure considering first the two MLFV frameworks introduced in Ref. [4], and briefly summarized below. Since in these two cases the deviations from the SM turn out to be very small, in Section 3.3 we analyse the GUT framework of Ref. [6] with the aim of identifying if, and under which conditions, larger deviations from the SM are possible.

3.1.1. Minimal Lepton Flavor Violation

The Minimal Flavor Violation principle [57, 58] was first introduced in the context of EFT in [42], whereas the extension to the lepton sector (called Minimal Lepton Flavor Violation) was discussed in [4]. In this framework the sources of LFV are linked in a minimal way to the known structure of the neutrino and charged-lepton mass matrices.

In order to reach a working definition for an EFT satisfying the MFV principle, we start with the basic observation that the largest group of unitary field transformations that commutes with the SM gauge group is $\mathrm{U}(3)^5$ [59].

This can be decomposed as:

$$G_F \equiv \mathrm{SU}(3)_q^3 \otimes \mathrm{SU}(3)_\ell^2 \otimes \mathrm{U}(1)_B \otimes \mathrm{U}(1)_L \otimes \mathrm{U}(1)_Y \otimes \mathrm{U}(1)_{\mathrm{PQ}} \otimes \mathrm{U}(1)_{e_R} \ , \quad (3.1)$$

where:

$$\begin{aligned} \mathrm{SU}(3)_q^3 &= \mathrm{SU}(3)_{q_L} \otimes \mathrm{SU}(3)_{u_R} \otimes \mathrm{SU}(3)_{d_R} \ , \\ \mathrm{SU}(3)_\ell^2 &= \mathrm{SU}(3)_{\ell_L} \otimes \mathrm{SU}(3)_{e_R} \ . \end{aligned} \quad (3.2)$$

Out of the five U(1) charges, three can be identified with baryon (B) and lepton (L) numbers and hypercharge (Y), which are respected by Yukawa interactions. The two remaining U(1) groups can be identified with the Peccei-Quinn symmetry of two-Higgs-doublet models [60] and with a global rotation of a single $\mathrm{SU}(2)_L$ singlet. Rearranging these two groups, we denote by $\mathrm{U}(1)_{\mathrm{PQ}}$ a rotation which affects only and in the same way d_R and e_R, and by $\mathrm{U}(1)_{e_R}$ a rotation of e_R only.

In the SM the Yukawa interactions break the symmetry group $\mathrm{SU}(3)_q^3 \otimes \mathrm{SU}(3)_\ell^2 \otimes \mathrm{U}(1)_{\mathrm{PQ}} \otimes \mathrm{U}(1)_{e_R}$. We can formally recover flavor invariance by introducing dimensionless auxiliary fields (called spurion fields or simply spurions from now on) with the right transformations under the flavor group.

Then an effective theory is defined to satisfy the criterion of MFV if all higher-dimensional operators, constructed from SM and spurion fields, are invariant under CP and (formally) under the flavor group G_F. In this way the dynamics of flavor violation is completely determined by the structure of the ordinary Yukawa couplings and all CP violation originates from the CKM phase.

We will now analyze two possible scenarios in which the MFV principle is implemented in the lepton sector. An overview on the phenomenology associated to these frameworks can be found in [61].

MLFV minimal field content

In this first scenario the lepton flavor symmetry group is:

$$G_{\mathrm{LF}} = SU(3)_{\ell_L} \times SU(3)_{e_R} \ , \quad (3.3)$$

and the lepton sector is invariant under two $U(1)$ symmetries which can be identified with the total lepton number, $U(1)_{\mathrm{LN}}$, and the weak hypercharge. In order to describe charged-lepton and neutrino masses we introduce the symmetry-breaking Lagrangian:

$$\mathcal{L}^{\min}_{\mathrm{Sym.Br.}} = -\lambda_e^{ij}\, \bar{e}_R^i (h_d^\dagger \ell_L^j) - \frac{1}{2\Lambda_{\mathrm{LN}}}\, g_\nu^{ij} (\bar{\ell}_L^{ci} \tau_2 h_u)(h_u^T \tau_2 \ell_L^j) + \mathrm{h.c.} \quad (3.4)$$

where λ_e and g_ν are the two irreducible sources of $G_{\rm LF}$ breaking.[1] As anticipated, $\Lambda_{\rm LN}$ denotes the scale of the flavor-independent breaking of the $U(1)_{\rm LN}$ symmetry. The smallness of neutrino masses, $m_\nu \equiv g_\nu v_u^2/\Lambda_{\rm LN}$, is attributed to the smallness of $v_u/\Lambda_{\rm LN}$.

It is convenient to treat the matrices λ_e and g_ν as spurions of $G_{\rm LF}$, such that the Lagrangian (3.4) and the complete low-energy EFT is formally invariant under $G_{\rm LF}$. The transformation properties of λ_e and g_ν are

$$\lambda_e \to V_R\,\lambda_e V_L^\dagger\ , \qquad\qquad g_\nu \to V_L^*\,g_\nu V_L^\dagger\ , \tag{3.5}$$

where $V_L \in SU(3)_{\ell_L}$ and $V_R \in SU(3)_{e_R}$. The simplest spurion combination controlling LFV transitions in the charged-lepton sector is $g_\nu^\dagger g_\nu$. Working in the basis where λ_e is diagonal we can write:

$$g_\nu^\dagger g_\nu = \frac{\Lambda_{\rm LN}^2}{v_u^4}\ U_{\rm PMNS}\ \bar m_\nu^2\ U_{\rm PMNS}^\dagger\ , \tag{3.6}$$

where $\bar m_\nu = {\rm diag}(m_{\nu_1}, m_{\nu_2}, m_{\nu_3})$ and $U_{\rm PMNS}$ is the usual PMNS mixing matrix (see Ref. [4] for notations). Up to the overall normalization, the LFV spurion in (3.6) is completely determined in terms of physical observables of the neutrino sector. Its explicit form in the case of normal hierarchy ($m_{\nu_1} < m_{\nu_2} \ll m_{\nu_3}$) or inverted hierarchy ($m_{\nu_3} \ll m_{\nu_1} < m_{\nu_2}$) is

$$\begin{aligned}
\left[g_\nu^\dagger g_\nu\right]_{ij}^{(\rm norm.)} &= \frac{\Lambda_{\rm LN}^2}{v^4}\ \left[m_{\nu_1}^2\,\delta_{ij}\ +\ U_{i2}U_{j2}^*\,\Delta m^2_{\rm sol} + U_{i3}U_{j3}^*\,\Delta m^2_{\rm atm}\right]\ , \\
\left[g_\nu^\dagger g_\nu\right]_{ij}^{(\rm inv.)} &= \frac{\Lambda_{\rm LN}^2}{v^4}\ \left[m_{\nu_3}^2\,\delta_{ij}\ +\ U_{i1}U_{j1}^*\,(\Delta m^2_{\rm atm} - \Delta m^2_{\rm sol}) + U_{i2}U_{j2}^*\,\Delta m^2_{\rm atm}\right]\ .
\end{aligned} \tag{3.7}$$

Here we used $U \equiv U_{\rm PMNS}$. For simplicity, in the numerical analysis of the following sections we assume that the mass of the lightest neutrino vanishes ($m_{\nu_1} = 0$ in the normal hierarchy and $m_{\nu_3} = 0$ in the inverted one). Furthermore, we adopt the convention where $s_{13} \geq 0$ and $0 \leq \delta < 2\pi$ [38].

MLFV extended field content

In this second case we assume the existence of three right-handed neutrino singlets under the SM gauge group, beside the SM degrees of freedom. The

[1] In Eq. (3.4) the indices i, j are lepton-flavor indices (that in the following will often be omitted, or equivalently indicated up or down), and $\psi^c \equiv -i\gamma^2\psi^*$. ℓ_L and e_R denote the lepton doublet and the right-handed lepton singlet, respectively ($\ell_L^T \equiv (\nu_L, e_L)$, $\bar\ell_L^c \equiv (\bar\nu_L^c, \bar e_L^c)$). We also denote by v_u and v_d the vacuum expectation values (vevs) of the Higgs doublets: $v_u \equiv v\sin\beta = \langle h_u\rangle$ and $v_d \equiv v\cos\beta = \langle h_d\rangle$, where $v \approx 174$ GeV, as defined in Eq. (1.7).

Majorana mass matrix of these neutrinos is flavor-blind [$(M_R)_{ij} = M_\nu\,\delta_{ij}$], it is the only source of $U(1)_{\rm LN}$ breaking and it is assumed to be much heavier that the electroweak scale ($|M_\nu| \gg v$). The lepton flavor symmetry group is

$$SU(3)_{\ell_L} \times SU(3)_{e_R} \times O(3)_{\nu_R} = G_{\rm LF} \times O(3)_{\nu_R}\ . \tag{3.8}$$

The irreducible sources of flavor symmetry breaking are λ_e and λ_ν, defined by

$$\mathcal{L}^{\rm ext}_{\rm Sym.Br.} = -\lambda_e^{ij}\,\bar e^i_R(h_d^\dagger \ell^j_L) + i\lambda_\nu^{ij}\,\bar\nu^i_R(h_u^T\tau_2\ell^j_L) + \text{h.c.}\ , \tag{3.9}$$

which have the following spurion transformation properties

$$\lambda_e \to V_R\lambda_e V_L^\dagger\ , \qquad \lambda_\nu \to O_\nu\lambda_\nu V_L^\dagger\ , \tag{3.10}$$

with $V_L \in SU(3)_{\ell_L}$, $V_R \in SU(3)_{e_R}$ and $O_\nu \in O(3)_{\nu_R}$. Integrating out the heavy right-handed neutrinos the effective left-handed Majorana mass matrix is $m_\nu = (v_u^2/M_\nu)\lambda_\nu^T\lambda_\nu$.

In this framework the basic spurion combination controlling LFV transitions in the charged-lepton sector is $\lambda_\nu^\dagger\lambda_\nu$. This can be unambiguously connected to the low-energy neutrino mass matrix only if we impose a further hypothesis, namely if we neglect CP violation in the neutrino mass matrix [4]:

$$\lambda_\nu^\dagger\lambda_\nu \overset{\text{CP limit}}{\longrightarrow} \frac{M_\nu}{v_u^2}\,U_{\rm PMNS}\,\bar m_\nu\,U^\dagger_{\rm PMNS}\ . \tag{3.11}$$

In the CP limit and neglecting the mass of the lightest neutrino, we can write

$$\left[\lambda_\nu^\dagger\lambda_\nu\right]^{(\text{norm.})}_{ij} = \frac{M_\nu}{v_u^2}\left[U_{i2}U_{j2}\sqrt{\Delta m^2_{\rm sol}} + U_{i3}U_{j3}\sqrt{\Delta m^2_{\rm atm}}\right]\ , \tag{3.12}$$

$$\left[\lambda_\nu^\dagger\lambda_\nu\right]^{(\text{inv.})}_{ij} = \frac{M_\nu}{v_u^2}\left[U_{i1}U_{j1}\sqrt{\Delta m^2_{\rm atm} - \Delta m^2_{\rm sol}} + U_{i2}U_{j2}\sqrt{\Delta m^2_{\rm atm}}\right] \tag{3.13}$$

3.1.2. Relevant effective operators and mixing matrices

We will now analyze the effective operator basis relevant for $P \to \ell\nu$ decays. We are interested in operators of dimension up to six (we will then refer to the effective basis of Section 2.1, paying special attention to the operator flavor structure) that can contribute to LFV processes with a single charged-lepton-neutrino pair and a single meson. The presence of a single meson implies we can neglect all operators with a tensor Lorentz structure, because of their vanishing hadronic matrix element.

The basic building blocks for the relevant dimension-six operators are the bilinears

$$\bar\ell_L\Delta_{LL}\ell_L \qquad \text{and} \qquad \bar e_R\Delta_{RL}\ell_L\ , \tag{3.14}$$

where Δ_{LL} and Δ_{RL} are spurions transforming under G_{LF} as $(\mathbf{8},\mathbf{1})$ and $(\bar{\mathbf{3}},\mathbf{3})$ respectively. The specific structure of the two spurions depends on the considered scenario. The lepton bilinears in (3.14) must be combined with corresponding quark bilinears, that we construct following the MFV rules [42]. Restricting the attention to terms with at most one power of the quark Yukawa couplings, the basis of relevant dimension-six operators is:

$$\begin{aligned}
O_{RL}^{(1)} &= \left(\bar{\ell}_R\,\Delta_{RL}\ell_L\right)\ \left(\bar{q}_L\lambda_d d_R\right) & O_{LL}^{(1)} &= \left(\bar{\ell}_L\gamma^\mu\tau_a\Delta_{LL}\ell_L\right)\ \left(iD_\mu h_u\right)^\dagger\tau_a h_u \\
O_{RL}^{(2)} &= \left(D_\mu h_d\right)^\dagger\ \left(\bar{\ell}_R\,\Delta_{RL}D_\mu\ell_L\right) & O_{LL}^{(2)} &= \frac{1}{2}\ \left(\bar{\ell}_L\gamma^\mu\tau_a\Delta_{LL}\ell_L\right)\ \left(\bar{q}_L\gamma_\mu\tau_a q_L\right) \\
O_{RL}^{(3)} &= \epsilon_{\alpha\beta}\left(\bar{\ell}_R\,\Delta_{RL}\ell_L^\alpha\right)\ \left(\bar{u}_R\lambda_u^\dagger q_L^\beta\right)
\end{aligned} \tag{3.15a}$$

In principle an additional independent operator is obtained replacing h_u with h_d in $O_{LL}^{(1)}$. However, this operator has the same flavor and Lorentz structure as $O_{LL}^{(1)}$ and it is suppressed in the large $\tan\beta$ limit, therefore we ignore it.

In Eq. (3.15a) we changed the notation for the operators in order to distinguish these specific flavor structures from the general form of the operators in Section 2.1. Some comments are in order:

- Operators $O_{RL}^{(1)}$ and $O_{LL}^{(1)}$ are the Hermitian conjugates of O_{qde} of Eq. (2.9i) and $O_{h\ell}^{(3)}$ of Eq. (2.17b), respectively;
- Operator $O_{RL}^{(2)}$ can be expressed in terms of other operators included in the effective basis of Section 2.1;
- Operator $O_{LL}^{(2)}$ is exactly equal to $O_{\ell q}^{(3)}$ of Eq. (2.7e), whereas operator $O_{RL}^{(3)}$ is equal to the Hermitian conjugate of $O_{\ell q}$ of Eq. (2.10c).

Taking into account the effective basis previously developed, the effective Lagrangian encoding new physics contributions reads:

$$\mathcal{L}_{\rm LFV}^{\rm eff} = \frac{1}{\Lambda_{\rm LFV}^2}\sum_{n=1}^{2}\alpha_{LL}^{(n)}O_{LL}^{(n)} + \frac{1}{\Lambda_{\rm LFV}^2}\sum_{n=1}^{3}\alpha_{RL}^{(n)}O_{RL}^{(n)} + \text{h.c.}\ , \tag{3.16}$$

where $\alpha_{\rm x}$ are the effective coefficients that describe the short distance physics in the EFT framework. They are matrices in flavor space. It is worth stressing that the coefficients considered in this work can be decomposed in two parts:

$$\left[\alpha_{\rm x}\right]_{ijkl} = \left[\alpha_{\rm x}^{\ell}\right]_{ij}\times\left[\alpha_{\rm x}^{q}\right]_{kl}\ , \tag{3.17}$$

where $\alpha_{\rm x}^{\ell(q)}$ is the flavor matrix for the lepton (quark) bilinear. Taking the operator $O_{RL}^{(1)}$ as an example, we get:

$$\left[\alpha_{RL}^{(1)}\right]^{\ell} = \Delta_{RL} \quad \text{and} \quad \left[\alpha_{RL}^{(1)}\right]^{q} = \lambda_d \ . \tag{3.18}$$

Expanding the lepton spurions in powers of λ_e, g_ν and λ_ν and retaining only the leading terms in the expansion (we assume all these couplings have perturbative elements), the explicit form of Δ_{LL} and Δ_{RL} in the charged-lepton mass basis is:

- *minimal case*

$$\Delta_{LL} = \frac{\Lambda_{\rm LN}^2}{v_u^4} U_{\rm PMNS}\, \bar{m}_\nu^2\, U_{\rm PMNS}^\dagger \ , \qquad \Delta_{RL} = \bar{\lambda}_e \left[\frac{\Lambda_{\rm LN}^2}{v_u^4} U_{\rm PMNS}\, \bar{m}_\nu^2\, U_{\rm PMNS}^\dagger\right] \ , \tag{3.19}$$

- *extended case*

$$\Delta_{LL} = \frac{M_\nu}{v_u^2} U_{\rm PMNS}\, \bar{m}_\nu\, U_{\rm PMNS}^\dagger \ , \qquad \Delta_{RL} = \bar{\lambda}_e \left[\frac{M_\nu}{v_u^2} U_{\rm PMNS}\, \bar{m}_\nu\, U_{\rm PMNS}^\dagger\right] \ . \tag{3.20}$$

3.2. $P \to \ell\nu$ matrix elements and decay rates

Having defined the operator basis and the effective Lagrangian $\mathcal{L}^{\rm eff}$ in Eq. (3.16), we compute the decay rates using $\mathcal{L}_{\rm tot} = \mathcal{L}_{\rm SM} + \mathcal{L}_{\rm LFV}^{\rm eff}$. At the level of accuracy we are working, the SM amplitude for the $P^- \to \ell\bar{\nu}_\ell$ decay is:

$$A_{\rm SM} = \frac{4G_{\rm F}\,[V_{\rm CKM}]_{ab}}{\sqrt{2}} \,\langle \ell\bar{\nu}_\ell|\, \bar{e}_L^\ell \gamma^\mu \nu_L^\ell \,|\, 0\rangle \ \langle 0|\, \bar{u}_L^a \gamma_\mu d_L^b \,|\, P^-\rangle \ , \tag{3.21}$$

where a, b are the quark-flavor indices of the corresponding meson and $V_{\rm CKM}$ is the CKM matrix. Defining the meson decay constant, $\langle 0|\bar{u}^a\gamma_\mu\gamma_5 d^b|\, P^-(p)\rangle = i\sqrt{2}F_P p^{\mu\,2}$, the corresponding rate is:

$$\Gamma(P^- \to \ell\bar{\nu}_\ell)_{\rm SM} = \frac{G_{\rm F}^2}{4\pi} \left|[V_{\rm CKM}]_{ab}\right|^2 \ F_P^2 m_\ell^2 M_P \left(1 - \frac{m_\ell^2}{M_P^2}\right)^2 \ . \tag{3.22}$$

[2]Note that there is a precise relation between the flavor of the quarks u, d and the type of meson we indicate generically by P. For example, if $P = K^-$, the flavor indices must be $a = 1$ (up quark) and $b = 2$ (strange quark).

The LL operators of $\mathcal{L}^{\rm eff}_{\rm LFV}$ have SM-like matrix elements, while the RL operators have a different structure:

$$A_{RL} \sim \langle \ell\bar\nu_k|\, \bar e^\ell_R \nu^k_L \,|0\rangle \times \begin{cases} \langle 0|\, \bar u^a \gamma_5 d^b \,|P\rangle & O^{(1)}_{RL}\,, O^{(3)}_{RL}\,, \\ (p_\ell)_\mu \,\langle 0|\, \bar u^a_L \gamma^\mu d^b_L \,|P\rangle & O^{(2)}_{RL}\,. \end{cases} \tag{3.23}$$

For light mesons (π and K), the hadronic matrix element of the pseudoscalar current

$$\langle 0|\, \bar u^a \gamma_5 d^b \,|P^-(p)\rangle = -i\sqrt{2} F_P B_0\,, \qquad B_0 = M_P^2/(m_a+m_b) \tag{3.24}$$

leads to a substantial enhancement of the first two terms in Eq. (3.23). Looking at the complete structure of the RL terms, it is easy to realise that $O^{(1)}_{RL}$ is the potentially dominant one: $O^{(2)}_{RL}$ is suppressed by the extra charged-current interaction needed to mediate $P\to\ell\nu$ decays, while $O^{(3)}_{RL}$ is suppressed by the small value of the up-quark mass (appearing because of λ_u). On the other hand, there is no clear difference among the two LL operators. Since we are interested in evaluating the maximal deviations from the SM, we concentrate the following phenomenological analysis on the three potentially dominant terms: $O^{(1)}_{RL}$, $O^{(1)}_{LL}$ and $O^{(2)}_{LL}$.

In order to analyse the relative strength of SM and new-physics contributions, for each of these operators we define the ratio

$$R_{P\ell\nu}[O^{(n)}_{XX}] = \frac{\Gamma(P^-\to\ell\bar\nu_\ell)_{\rm SM} + \delta\Gamma(P^-\to\ell\bar\nu_\ell)_{\rm int} + \sum_{k\neq\ell}\Gamma(P^-\to\ell\bar\nu_k)_{\rm LFV}}{\Gamma(P^-\to\ell\bar\nu_\ell)_{\rm SM}}\,, \tag{3.25}$$

where $\delta\Gamma_{\rm int}$ takes into account the lepton-flavor-conserving contributions generated by $\mathcal{L}^{\rm eff}_{\rm LFV}$ (including the interference with SM amplitude). The explicit expressions of this ratio for the three dominant operators are:

$$\begin{aligned} R_{P\ell\nu}[O^{(1)}_{LL}] &= \left|1 + \frac{2v_u^2\alpha^{(1)}_{LL}}{\Lambda^2_{\rm LFV}}\,\Delta^{\ell\ell}_{LL}\right|^2 + \sum_{k\neq\ell}\frac{4v_u^4|\alpha^{(1)}_{LL}|^2}{\Lambda^4_{\rm LFV}}\,|\Delta^{\ell k}_{LL}|^2\,, \\ R_{P\ell\nu}[O^{(2)}_{LL}] &= \left|1 - \frac{\alpha^{(2)}_{LL}}{\sqrt{2}G_{\rm F}\Lambda^2_{\rm LFV}}\,\Delta^{\ell\ell}_{LL}\right|^2 + \sum_{k\neq\ell}\frac{|\alpha^{(2)}_{LL}|^2}{2G_{\rm F}^2\Lambda^4_{\rm LFV}}\,|\Delta^{\ell k}_{LL}|^2\,, \\ R_{P\ell\nu}[O^{(1)}_{RL}] &= \left|1 - \frac{\alpha^{(1)}_{RL}}{2\sqrt{2}G_{\rm F}\Lambda^2_{\rm LFV}}\,\Delta^{\ell\ell}_{RL}\,\frac{m_d B_0}{v_d m_\ell}\right|^2 + \sum_{k\neq\ell}\frac{|\alpha^{(1)}_{RL}|^2|\Delta^{\ell k}_{RL}|^2}{8G_{\rm F}^2\Lambda^4_{\rm LFV}}\left(\frac{m_d B_0}{v_d m_\ell}\right)^2\,, \end{aligned} \tag{3.26}$$

where m_d is the mass of the down-type quark inside the hadron (the apparent dependence on the QCD renormalization scale is canceled by the corresponding dependence of B_0).

A closer look to these expressions allows us to identify the potentially dominant terms and the maximal size of the NP effects. The basic hypothesis of our approach is that $\Lambda_{\rm LFV}$ is around the TeV scale and that all the Wilson coefficients are at most of $\mathcal{O}(1)$. This implies that the dimensionless coefficients of the Δ_{LL} terms in Eq. (3.26) are at most of $\mathcal{O}(10^{-1})$. The size of Δ_{LL} is controlled by the scale of lepton-number violation ($\Lambda_{\rm LN}$ or M_ν): as shown in [4], within this general EFT approach the scale of lepton-number violation cannot be too large because of the bounds from $\mu \to e\gamma$. We shall come back on the precise bounds from LFV processes in Section 3.4.1, here we simply note that an order of magnitude estimate give $\Delta_{LL} \sim \Lambda^2_{\rm LN}\Delta m^2_{\rm atm}/v_u^4 \lesssim \mathcal{O}(10^{-4})$. Thus for $R_{P\ell\nu}[O^{(1)}_{LL}]$ and $R_{P\ell\nu}[O^{(1)}_{LL}]$ the non-standard effect is necessarily small and the interference terms dominate.

The coefficients of the Δ_{RL} terms in $R_{P\ell\nu}[O^{(1)}_{RL}]$ are apparently enhanced by an inverse dependence from the lepton mass. However, as shown in Eqs. (3.19)–(3.20), in the MLFV framework the Δ_{RL} spurion contains a charged lepton Yukawa that cancels this dependence:

$$\Delta^{\ell k}_{RL}\frac{m_d B_0}{v_d m_\ell} \approx (\tan\beta)^2\frac{m_P^2}{v_u^2}\left(\frac{\Delta^{\ell k}_{RL}}{\bar\lambda_e}\right) \approx (\tan\beta)^2\frac{m_P^2}{v_u^2}\Delta^{\ell k}_{LL}\ . \tag{3.27}$$

The above result implies that the non-standard effect in $R_{P\ell\nu}[O^{(1)}_{RL}]$ are: i) negligible for π and K decays, even for large $\tan\beta$; ii) of similar size of those in $R_{P\ell\nu}[O^{(1,2)}_{LL}]$ in the B-meson case at large $\tan\beta$. We thus conclude that in the MLFV framework, both within the minimal and the extended field content, there is no way to generate large deviations from the SM in $P \to \ell\nu$ decays.

The key difference with respect to the case discussed in Ref. [62] is that the MLFV hypothesis imply the same helicity suppression for SM and non-standard amplitudes. A general EFT framework where such condition is not necessarily enforced is the MFV-GUT framework that we analyse below.

3.3. Beyond the minimal case: MFV-GUT framework

Following Ref. [6], we consider the implementation of the MFV principle in a GUT based on the $SU(5)$ gauge group: the three generations of SM fermions fall into a $\bar{\mathbf{5}}$ $[\psi_i \equiv (d^c_{iR}, \ell_{iL})]$ and a $\mathbf{10}$ $[\chi_i \equiv (q_{iL}, u^c_{iR}, e^c_{iR})]$ of $SU(5)$, and we add three singlets for the right-handed neutrinos $[N_i \equiv \nu_{iR}]$. The maximal flavor group is then reduced to $SU(3)_{\bar5} \times SU(3)_{10} \times SU(3)_1$.

Introducing three Higgs fields, h_5, $h_{\bar{5}}$ and Σ_{24}, with appropriate $U(1)$ charges to avoid tree-level FCNCs, the Yukawa Lagrangian defining the irreducible sources of flavor-symmetry breaking is

$$\begin{aligned}\mathcal{L}_{\rm Y-GUT} = \lambda_5^{ij}\ \psi_i^T \chi_j h_{\bar{5}} + \lambda_{10}^{ij}\ \chi_i^T \chi_j h_5 + \frac{1}{M}(\lambda_5')^{ij}\ \psi_i^T \Sigma_{24} \chi_j h_{\bar{5}} \\ + \lambda_1^{ij}\ N_i^T \psi_j h_5 + M_R^{ij} N_i^T N_j + \text{h.c.}\end{aligned} \tag{3.28}$$

Imposing the invariance of $\mathcal{L}_{\rm Y-GUT}$ under the $SU(3)_{\bar{5}} \times SU(3)_{10} \times SU(3)_1$ group implies

$$\lambda_5^{(\prime)} \to V_{\bar{5}}^*\ \lambda_5^{(\prime)}\ V_{10}^\dagger\ , \qquad \lambda_{10} \to V_{10}^*\ \lambda_{10}\ V_{10}^\dagger\ , \tag{3.29}$$

$$\lambda_1 \to V_1^*\ \ \lambda_1\ V_{\bar{5}}^\dagger\ , \qquad M_R \to\ V_1^*\ \ M_R\ V_1^\dagger\ . \tag{3.30}$$

with $V_{\bar{5}} \in SU(3)_{\bar{5}}$, $V_{10} \in SU(3)_{10}$ and $V_1 \in SU(3)_1$.

The non-renormalizable term in (3.28) has been introduced to break the exact GUT relations between down-type quark and charged-lepton masses, which are know to be violated in the case of the first two generations.[3] Expressing the low-energy Yukawa couplings in terms of the high-energy ones we have

$$\lambda_u = a_u \lambda_{10}\ , \quad \lambda_d = a_d\,(\lambda_5 + \lambda_5')\ , \quad \lambda_e^T = a_e \left(\lambda_5 - \frac{3}{2}\lambda_5'\right)\ , \quad \lambda_\nu = a_\nu \lambda_1\ , \tag{3.31}$$

where $a_i = \mathcal{O}(1)$ are appropriate renormalization-group factors and we have redefined the spurion λ_5' incorporating a suppression factor $\sim \langle\Sigma_{24}\rangle/M$. In the basis where the down-type quark Yukawa coupling is diagonal, the complete set of low-energies Yukawa couplings assume the form:

$$\begin{aligned}&\lambda_d = \bar{\lambda}_d\ , \qquad \lambda_u = {V_{\rm CKM}}^T\, \bar{\lambda}_u\, V_{\rm CKM}\ \ , \qquad \lambda_e = C^T\, \bar{\lambda}_e\, G^*\ , \\ &\left[\lambda_\nu^\dagger \lambda_\nu\right]_{\rm CP-limit}\ =\ \frac{M_\nu}{v_u^2} G^T U_{\rm PMNS}\, \bar{m}_\nu\, U_{\rm PMNS}^\dagger G^*\ ,\end{aligned} \tag{3.32}$$

where, in analogy with the MLFV case with extended field content, we have assumed that M_R is flavor blind $[(M_R)_{ij} = M_\nu\, \delta_{ij}]$.

The two new mixing matrices C and G appearing in (3.32) control the diagonalization of λ_e in the basis where λ_d is diagonal. In the spirit of minimising the unknown sources of flavor symmetry breaking, in the following we work in the limit $C = G = I$. This assumption, which is justified in the

[3] The high-scale vev of Σ_{24} breaks $SU(5)$ preserving $SU(2)_L \times U(1)_Y$, $\langle\Sigma_{24}\rangle = M_{\rm GUT}{\rm diag}(1,1,1,-3/2,-3/2)$. Moreover, we assume $M \gg M_{\rm GUT}$, such that this non-renormalizable term is negligible but for the first two generations.

limit where we can neglect the breaking of the flavor symmetry induced by λ'_5 ($C, G \to I$ in the limit $\lambda'_5 \to 0$ [6]), allows us to express all mixing effects in terms of the CKM and the PMNS matrices.

In the GUT framework the number of independent spurion combinations contributing to LFV processes is much larger than in the MLFV case; however, only few of them can give rise to a substantial parametrical difference. The potentially most interesting effect is obtained replacing the Δ_{RL} spurion of the MLFV case with $\Delta^{\rm GUT}_{RL} = \lambda_u \lambda_u^\dagger \lambda_d^T$. In the basis where the charged-lepton Yukawa is diagonal, this spurion takes the form

$$[\Delta^{\rm GUT}_{RL}]_{\ell k} = \left[C \Delta^{(q)} \bar{\lambda}_d G^\dagger\right]^*_{\ell k} \quad \stackrel{\rm C=G=I}{\longrightarrow} \quad \left[\Delta^{(q)} \bar{\lambda}_d\right]^*_{\ell k} \ , \tag{3.33}$$

where

$$\Delta^{(q)}_{ij} \equiv \left[V^\dagger_{\rm CKM}\, \bar{\lambda}_u^2\, V_{\rm CKM}\right]_{ij} \approx \frac{m_t^2}{v_u^2} \left[V_{\rm CKM}\right]^*_{3i} \left[V_{\rm CKM}\right]_{3j} \ . \tag{3.34}$$

The key feature of $\Delta^{\rm GUT}_{RL}$ in (3.33) is the presence of the suppressed down-type Yukawa coupling on the right, and not on the left, as in Eqs. (3.19)–(3.20). This could allow to overcome the SM helicity suppression in LFV processes with light charged leptons and neutrinos of the third generation.

3.4. Phenomenology

3.4.1. Bounds from FCNC processes

One of the advantage of the EFT approach is that we can derive model-independent bounds on the coefficients of the effective Lagrangian in (3.16) from experiments. In particular, we can extract some interesting bounds from FCNC transitions of charged leptons which receive tree-level contributions from the operators in (3.16).

At present the most stringent bound is obtained by the bounds on the $\mu - e$ conversion in nuclei and in particular by this result:

$$\mathcal{B}_{\mu\to e} = \sigma(\mu^- {\rm Au} \to e^- {\rm Au})/\sigma(\mu^- {\rm Au} \to {\rm capture}) < 7 \times 10^{-13} \ [38] \ . \tag{3.35}$$

Starting from the Lagrangian (3.16), assuming $\tan\beta \gg 1$ and using the notation of [63], we get:

$$\mathcal{B}_{\mu\to e} = \frac{m_\mu^5}{\Gamma_{\rm capt} \Lambda^4_{\rm LFV}} \left| \left[\left(1 - 4 s_w^2\right) V^{(p)} - V^{(n)}\right] \alpha^{(1)}_{LL} \Delta^{\mu e}_{LL} + \left(-V^{(p)} + V^{(n)}\right) \alpha^{(2)}_{LL} \Delta^{\mu e}_{LL} \right.$$
$$\left. + \left(\tilde{g}^{(p)}_{RS} S^{(p)} + \tilde{g}^{(n)}_{RS} S^{(n)}\right) \alpha^{(1)}_{RL} \left[\Delta^{\mu e}_{RL} + (\Delta^\dagger_{RL})^{\mu e}\right] \right|^2 \ , \tag{3.36}$$

Coefficients	MLFV min.	MLFV ext.		MFV GUT
		Norm. hier.	Inv. hier.	
$\lvert\alpha^{(1)}_{LL}\rvert\ (1\ \text{TeV}/\Lambda_{\text{LFV}})^2$	$< 1.9 \times 10^{-1}$	$< 2.7 \times 10^{-2}$	$< 3.5 \times 10^{-2}$	–
$\lvert\alpha^{(2)}_{LL}\rvert\ (1\ \text{TeV}/\Lambda_{\text{LFV}})^2$	$< 5.3 \times 10^{-1}$	$< 3.8 \times 10^{-2}$	$< 5.0 \times 10^{-2}$	–
$\lvert\alpha^{(1)}_{LR}\rvert \left(\frac{\tan\beta}{50}\right)^2 \left(\frac{1\ \text{TeV}}{\Lambda_{\text{LFV}}}\right)^2$	< 36	< 4.9	< 6.6	< 6.3

Table 3.1: Bounds on the Wilson coefficients of the LFV effective Lagrangian, from $\mu \to e$ conversion, in different flavor symmetry breaking frameworks. In the MLFV with minimal field content we used $\Lambda_{\text{LN}} = 10^{13}$ GeV. For the MLFV extended we set $M_\nu = 10^{12}$ GeV. In the MFV-GUT case we report the values in the $C, G \to I$ limit (see text), and only for the potentially dominant operator ($O^{(1)}_{RL}$).

where $\tilde{g}^{(p)}_{RS} = 4.3\lambda_d + 2.5\lambda_s$, $\tilde{g}^{(n)}_{RS} = 5.1\lambda_d + 2.5\lambda_s$ and $V^{(p,n)}$, $S^{(p,n)}$ are dimensionless nucleus-dependent overlap integrals, whose numerical value can be found in [63].

Barring accidental cancelations among the contributions of different operators, expressing the Δ's in terms of neutrino masses and mixing angles, according to Eqs. (3.19)–(3.20), we extract the bounds on the ratios of Wilson coefficients and effective scales reported in Table 3.1.[4] For simplicity, in the case of the two MLFV frameworks we show the bounds obtained for reference values of Λ_{LN} and M_ν: for different values of these energy scales, the bounds can easily be rescaled according to Eqs. (3.19)–(3.20). This overall normalization problem does not appear in the GUT case: here we report the bound in the $C, G \to I$ limit and we analyse only the case of the potentially dominant operator $O^{(1)}_{RL}$.

3.4.2. Predictions for the lepton universality ratios

Using the general expressions for the ratios in Eq. (3.26) and the bounds on the Wilson coefficients reported in Table 3.1, we are ready to derive predictions for the possible deviations from the SM in $P \to \ell\nu$ decays. The most interesting observables are the lepton universality ratios, $R^{\ell\ell'}_P = \mathcal{B}(P \to \ell\nu)/\mathcal{B}(P \to \ell'\nu)$, whose values can be computed with high accuracy within the SM [64]. We parametrise possible deviations from the SM in the $R^{\ell\ell'}_P$ as follows:

$$\frac{R^{\ell\ell'}_P|_{\text{exp}}}{R^{\ell\ell'}_P|_{\text{SM}}} \equiv 1 + \Delta r^{\ell\ell'}_P \ . \tag{3.37}$$

[4] The numerical values of neutrino masses and mixing angles used in the analysis are those reported in Ref. [4].

Operators	MLFV minimal	MLFV extended Norm. hier.	MLFV extended Inv. hier.	MFV-GUT
		Bounds on $\lvert\Delta r_\pi^{e\mu}\rvert$:		
$O_{LL}^{(1)}$	$< 2.7 \times 10^{-6}$	$< 2.3 \times 10^{-6}$	$< 3.3 \times 10^{-6}$	–
$O_{LL}^{(2)}$	$< 7.7 \times 10^{-6}$	$< 3.3 \times 10^{-6}$	$< 4.7 \times 10^{-6}$	–
$O_{RL}^{(1)}$	$< 2.1 \times 10^{-7}$	$< 1.7 \times 10^{-7}$	$< 2.5 \times 10^{-7}$	$< 6.3 \times 10^{-5}$
		Bounds on $\lvert\Delta r_K^{e\mu}\rvert$:		
$O_{LL}^{(1)}$	$< 2.7 \times 10^{-6}$	$< 2.3 \times 10^{-6}$	$< 3.2 \times 10^{-6}$	–
$O_{LL}^{(2)}$	$< 7.7 \times 10^{-6}$	$< 3.3 \times 10^{-6}$	$< 4.7 \times 10^{-6}$	–
$O_{RL}^{(1)}$	$< 5.0 \times 10^{-6}$	$< 4.1 \times 10^{-6}$	$< 5.9 \times 10^{-6}$	$< 5.0 \times 10^{-2}$

Table 3.2: Bounds on $|\Delta r_\pi^{e\mu}|$ and $|\Delta r_K^{e\mu}|$ and in the various symmetry-breaking frameworks.

The maximal allowed values for $\Delta r_\pi^{e\mu}$ and $\Delta r_K^{e\mu}$ are shown in Table 3.2. As can be seen, in the two MLFV frameworks these values are far too small compared to the experimental precision expected in future experiments: few $\times 0.01\%$ in R_π and few $\times 0.1\%$ in R_K. Undetectable effects are found also in the $B \to \ell\nu$ system, within the two MLFV frameworks.

In the MFV-GUT case the situation is definitely more interesting. According to the last column of Table 3.2, in such case $\Delta r_K^{e\mu}$ might be within the reach of future experiments. However, this result must be taken with some care. The bounds in Table 3.2 are obtained saturating the constraints on the Wilson coefficients from $\mu \to e$ conversion: in the MFV-GUT framework these are not very stringent and are saturated only for unnatural large values of the Wilson coefficients or unnatural low values of the effective scale $\Lambda_{\rm LFV}$. Imposing natural constraints on the parameters of the EFT, such as $|\alpha_{LR}^{(1)}| < 1$, $\tan\beta < 50$, and $\Lambda_{\rm LFV} > 1$ TeV, the deviations from the SM in $R_K^{e\mu}$ are at most around 0.1%, beyond the reach of future experiments.

The reason why our bounds on $\Delta r_K^{e\mu}$ are stronger with respect to the maximal effects discussed in Ref. [62], even in the MFV-GUT framework, is the assumption of minimal breaking of the flavor symmetry. We have assumed that both M_R and the new mixing matrices C and G are flavor blind. In this limit the mixing structure of $[\Delta_{RL}^{\rm GUT}]_{\ell k}$ is controlled by the CKM matrix. This implies that the enhancement of $[\Delta_{RL}^{\rm GUT}]_{i3}$ due to the large Yukawa coupling of the third generation is partially compensated by the suppression of $|V_{i3}| \ll 1$ $(i = 1, 2)$. This suppression could be removed only with new flavor-mixing structures. We thus conclude that if some violation of LFU will be observed in π decays at the 0.1% level, or in K decays at

	$R_B^{\mu\tau}$	$R_B^{e\mu}$	$R_B^{e\tau}$
SM	$\approx 4.4 \times 10^{-3}$	$\approx 2.4 \times 10^{-5}$	$\approx 1.1 \times 10^{-7}$
MFV − GUT (mod. ind.)	$< 7.0 \times 10^{-3}$	$< 1.6 \times 10^{-2}$	$< 7.4 \times 10^{-5}$
MFV − GUT ($\lvert\alpha_{LR}^{(1)}\rvert < 1$)	$< 6.5 \times 10^{-3}$	$< 4.2 \times 10^{-4}$	$< 2.8 \times 10^{-6}$

Table 3.3: Bounds on the universality ratios $R_B^{\ell\ell'}$ in the MFV-GUT framework. The model-independent bounds are obtained saturating the constraint on $\alpha_{LR}^{(1)}$ reported in Table 3.1 and imposing $\mathcal{B}(B \to \tau\nu) = \mathcal{B}(B \to \tau\nu)_{\rm SM}$ (see text). The bounds in the last line are obtained evaluating all the decays with the *natural* conditions $|\alpha_{LR}^{(1)}| < 1$, $\tan\beta < 50$ and $\Lambda_{\rm LFV} > 1$ TeV.

the 1% level, this would unambiguously signal the presence of *non-minimal* sources of lepton-flavor symmetry breaking.

The only system were sizable violations of LFU universality can be produced in the minimal set-up we are considering is the case of $B \to \ell\nu$ decays (assuming the MFV-GUT framework). Here the large meson mass provides a substantial enhancement of the contribution of the Δ_{RL} terms (see Eq. (3.27)). As a result, in the helicity suppressed modes $B \to \mu\nu$ and, especially, $B \to e\nu$, the contribution of the Δ_{RL} terms is large enough to compete with the SM.

The enhancement of $\mathcal{B}(B \to e\nu)$ allowed by the model-independent bound on $\alpha_{LR}^{(1)}$ (Table 3.1) is huge ($\sim 10^3\times$ SM), and even imposing $|\alpha_{LR}^{(1)}| < 1$ large non-standard effects are possible. The maximal deviations from the SM for the three LFU ratios[5] are shown in Table 3.3. Given the suppression of the $B \to \ell\nu$ rates, the experimental sensitivity needed to go below these bounds is still far from the presently available one. However, it could possibly be reached in future with high-statistics dedicated experiments.

3.5. Conclusions

Within the SM $P \to \ell\nu$ decays are mediated only by the Yukawa interaction (the decay amplitudes can indeed be computed to an excellent accuracy in the gauge-less limit of the model). This implies a strong helicity suppression and a

[5] The model-independent bound on $\alpha_{LR}^{(1)}$ allow a lepton-flavor conserving contribution to $B \to \tau\nu$, from $O_{RL}^{(1)}$, of the same order of the SM amplitude. Since the experimental measurement of $\mathcal{B}(B \to \tau\nu)$ is consistent with the SM expectation and we have not systematically analysed all the lepton-flavor conserving dimension-six operators, in Table 3.3 we report the model-independent bounds on the $R_B^{\ell\ell'}$ assuming $\mathcal{B}(B \to \tau\nu) = \mathcal{B}(B \to \tau\nu)_{\rm SM}$.

corresponding enhanced sensitivity to possible physics beyond the SM. In particular, the lepton-flavor universality ratios $R_P^{\ell\ell'} = \mathcal{B}(P \to \ell\nu)/\mathcal{B}(P \to \ell'\nu)$, which can be predicted within high accuracy, are interesting probes of the underlying lepton-flavor symmetry-breaking structure.

In this work we have analyzed the deviations from the SM in the $R_P^{\ell\ell'}$ ratios using a general effective theory approach, employing different ansätze about the flavor-symmetry breaking structures of physics beyond the SM. The main results can be summarized as follows:

- In models with Minimal Lepton Flavor Violation, both in the minimal and in the extended version (as defined in [4]), we find that the effects are too small to be observed in the next generations of experiments in all relevant meson systems ($P = \pi, K, B$). This is because the MLFV hypothesis, by construction, implies the same helicity suppression of $P \to \ell\nu$ amplitudes as in the SM.

- In a Grand Unified framework with a minimal breaking of the flavor symmetry (as defined in Section 3.3) the effects remain small in π and K decays, while large violations of lepton-flavor universality are possible in the B system (see Table 3.3). These are possible mainly because of the enhancement of the flavor-violating $B \to e\nu_\tau$ rate.

Chapter 4

Violation of lepton universality in leptonic W decays

One of the features of the SM of particle physics is, as we noted before, the universality of the lepton couplings, i.e. the fact that the coupling of the $W^{\pm}$ to the leptons does not depend on their flavor. However the experimental results from LEP-II on this issue [7, 8, 9, 10, 11] showed a slight deviation from universality coming from the third family, giving [38]:

$$R^W_{\tau\ell} = \frac{2\,\mathrm{BR}\,(W \to \tau\,\overline{\nu}_\tau)}{\mathrm{BR}\,(W \to e\,\overline{\nu}_e) + \mathrm{BR}\,(W \to \mu\,\overline{\nu}_\mu)} = 1.055(23), \tag{4.1}$$

resulting in 2.4 standard deviations[1] (all correlations included) from the SM prediction $R^W_{\tau\ell}|_{\mathrm{SM}} = 0.999$ [66], which uncertainty is negligible compared with the experimental error. Recalling also the following ratio:

$$R^W_{\mu e} = \mathrm{BR}\,(W \to \mu\,\overline{\nu}_\mu)\,/\mathrm{BR}\,(W \to e\,\overline{\nu}_e) = 0.983(18), \tag{4.2}$$

and the correspondent SM prediction $R^W_{\mu e}|_{\mathrm{SM}} = 1.000$, it can be concluded that the two lightest families seem to attach to the universality principle. Although the discrepancy in Eq. (4.1) is not large, it is a result that has been around for already seven years and it is worth studying its possible implications on the present experimental scenario. The confirmation or refutation of this measurement is obviously very important, since such a violation by the third family would be a clear indication of NP [67, 68]. However, it will not be easy for the LHC to reach such a precision in this observable, given the theoretical uncertainties associated to a hadronic machine. For this reason it is interesting to check indirectly this anomaly through its interplay with other related measurements.

[1] The result given in Eq. (4.1) is obtained from the PDG fit to the branching ratios of the W [38], that uses LEP2 and $p\bar{p}$ colliders data. It is worth mentioning that considering only LEP2 data the discrepancy grows to 2.8 σ [11] (2.6 σ using only published data [65]), all correlations included.

Precision electroweak observables (EWPO), as well as other precise low energy measurements, provide constraints on new models looking for deviations that could foresee the NP structure. We study in this chapter if it is possible to accommodate the apparent discrepancy on the $W \to \tau\bar{\nu}_\tau$ channel within the present situation provided by EWPO, where essentially no disagreements have been found. In particular, lepton universality has been tested successfully at the per-mil level in $Z \to \ell^+\ell^-$ [38] and $\tau \to \nu_\tau \ell \nu_\ell$ decays (see e.g. Table 3 in Ref. [1]), what makes very challenging to find a NP explanation for the large anomaly shown in Eq. (4.1). Just for the sake of illustration, we show the values obtained in leptonic Z decays [38]:

$$\begin{aligned} \mathrm{BR}\big(Z \to \mu^+\mu^-\big)/\mathrm{BR}\big(Z \to e^+e^-\big) &= 1.001(3), \\ \mathrm{BR}\big(Z \to \tau^+\tau^-\big)/\mathrm{BR}\big(Z \to \mu^+\mu^-\big) &= 1.001(3), \end{aligned} \tag{4.3}$$

in good agreement with the SM predictions, 1.000 and 0.998 respectively.

Instead of adhering to a specific model we will follow an Effective Field Theory approach, where, as we explained in Chapter 2, NP is parameterized by a tower of higher-dimensional operators. Guided by the above-mentioned experimental data on lepton universality, we will consider different frameworks where the NP does not affect operators involving first and second generation fermions. As we will explain, this can be implemented through the adoption of specific flavor symmetries.

For the numerical analysis, we greatly benefit from Ref. [69], where constraints on these effective operators were obtained via a global fit to precision electroweak data. We modify the associated fitting code to introduce additional observables and operators[2]. These fit procedures are a powerful tool to analyze the impact of current constraints on different models.

We apply this method to study the possible NP effects in leptonic W decays allowed by electroweak precision data. We will emphasize the role that the leptonic tau decay and the exclusive channel $\tau^- \to \pi^-\nu_\tau$ play in constraining specific directions of the parameter space of our theory, and the need to include these observables in this kind of analyses. We will see that the observed departure from universality cannot be accommodated within the current experimental scenario under quite general assumptions. Thus in order to be able to explain the observed deviation from lepton universality as a genuine NP effect, it seems to be necessary to resort to a different description of NP that could involve the introduction of new light degrees of freedom or a strongly interacting sector.

A closely related issue driven by the $W\ell\nu_\ell$ vertex is the ratio of widths involving the leptonic decays of pseudoscalar heavy mesons, $P \to \ell\,\overline{\nu}_\ell$. Accordingly, if any violation of universality is at work it also should be exposed in ratios of these decays into different charged leptons. Similarly, any modification of the SM coupling of W with the tau lepton could show up, due to gauge symmetry, in the anomalous magnetic moment of the tau. We will comment how our results translate into these subjects.

[2]The code can be freely downloaded at the web page `http://ific.uv.es/lhcpheno/`.

In the next section the EFT framework is introduced, focusing on the different flavor symmetries and the relevant effective operators. In Section 4.2 we identify the operators that can generate a lepton universality violation in the third family, whereas in Section 4.3 we analyze through a global fit the bounds on these operators from EWPO and other low-energy measurements. Section 4.4 is devoted to study the sensitivity of the leptonic decays of heavy mesons to the lepton universality violation, and Section 4.5 contains a summary of the main results of this chapter.

4.1. The Effective Field Theory framework

In this chapter we consider the study of the apparent violation of universality in the couplings of W to leptons within the EFT framework described in Chapter 2, with the goal of finding out if the observed deviation can be explained in terms of NP effects once constraints from precise electroweak observables are taken into account. Motivated by the data and for the sake of simplicity, we will assume two different flavor symmetries that we introduce in the next subsections. For the list of operators and the notation used please refer to Chapter 2.

To set the stage for this discussion, we recall first the simpler case of $U(3)^5$ flavor symmetry. In the absence of Yukawa couplings, the SM Lagrangian shows a

$$U(3)^5 = U(3)_q \times U(3)_u \times U(3)_d \times U(3)_\ell \times U(3)_e \tag{4.4}$$

flavor symmetry, corresponding to the independent rotation of each SM fermion field: the quark and lepton doublets q and ℓ and the up-quark, down-quark and charged lepton singlets u, d and e. We can also decompose this symmetry group in the following way:

$$U(3)^5 = SU(3)^5 \times U(1)_L \times U(1)_B \times U(1)_Y \times U(1)_{PQ} \times U(1)_e \tag{4.5}$$

where the five global $U(1)$ symmetries can be identified with the Total Lepton (L) and Baryon (B) number, the hypercharge, the Peccei-Quinn symmetry and a remaining global symmetry that we choose to be the rotation of the charged lepton singlet. In the presence of Yukawa couplings this flavor symmetry breaks down to the subgroup $G = U(1)_L \times U(1)_B \times U(1)_Y$.

Requiring that the higher dimensional operators respect the $U(3)^5$ flavor symmetry reduces significantly their number, suppresses undesired Flavor Changing Neutral Current effects and leads to the Minimal Flavor Violation (MFV) framework after the introduction of the Yukawa spurions [42]. The complete list of the twenty-one dimension-six $U(3)^5$ invariant operators can be found in Refs. [70, 71], where this flavor symmetry was assumed in the context of an EFT analysis of electroweak precision data.

It is clear that in this special framework it is impossible to generate any departure from lepton universality, as the $U(3)^5$ symmetry allows only for flavor independent NP contributions. For this reason we will relax this symmetry group to smaller groups where the third family is singled out.

4.1.1. $[U(2) \times U(1)]^5$ flavor symmetry

Motivated by the experimental observations shown in Eqs. (4.1) and (4.2), it is an interesting possibility to assume the flavor symmetry $[U(2) \times U(1)]^5$, that singularizes the third family with respect to the light ones, allowing for different NP contribution to the processes involving the heavy fermions: top, bottom and, in particular, τ and ν_τ.

This framework was indeed studied in Ref. [69], and we will use the same notation, in which q_i, ℓ_i, u_i, d_i and e_i $(i = 1, 2)$ represent only the two first generations of fermions, whereas Q, L, t, b and τ represent the third family fields. The new notation makes clear which combinations of flavor indices are allowed by the flavor symmetry. The operators that do not involve fermions are the same as in the $U(3)^5$ case, whereas those involving one or two fermion bilinears split in several operators; for instance:

$$O_{he} = \left(h^\dagger i D_\mu h\right)(\bar{e}\gamma_\mu e) \quad \rightarrow \quad \begin{aligned} O_{he} &= \left(h^\dagger i D_\mu h\right)(\bar{e}\gamma_\mu e), \\ O_{h\tau} &= \left(h^\dagger i D_\mu h\right)(\bar{\tau}\gamma_\mu \tau). \end{aligned} \tag{4.6}$$

The list of invariant operators is much longer than in the $U(3)^5$ symmetric case, but not all the operators affect the EWPO. For this reason, and following Ref. [69], we do NOT include in our numerical analyses:

- Operators involving top quarks;
- Operators involving only third-generation fermions;
- Operators involving light quarks and third generation leptons[3].

Moreover, motivated by the experimental result shown in Eq. (4.2) and for the sake of simplicity we will assume that 2- and 4-fermion operators that only have light generation fermions can be neglected. In this way we are left with the following six operators with one fermion bilinear:

$$O_{hf_1} = \left(h^\dagger i D_\mu h\right)(\overline{f}_1 \gamma_\mu f_1) + \text{h.c.}\,, \tag{4.7}$$

$$O^{(1)}_{hf_2} = \left(h^\dagger i D_\mu h\right)(\overline{f}_2 \gamma_\mu f_2) + \text{h.c.}\,, \tag{4.8}$$

$$O^{(3)}_{hf_2} = \left(h^\dagger i \tau^I D_\mu h\right)\left(\overline{f}_2\, \gamma^\mu\, \tau^I\, f_2\right) + \text{h.c.}\,, \tag{4.9}$$

where $f_1 = \tau, b$ and $f_2 = L, Q$. We also have the following four-fermion operators

[3] We noticed that the operator $O^{(3)}_{Lq}$ in Eq. (4.10a) can be strongly constrained by the experimental value of the $\tau \to \pi\nu_\tau$ process and it is consequently included in our analysis. Ref. [69], not considering this observable, didn't include $O^{(3)}_{Lq}$.

[69]:

$$
\begin{aligned}
&O_{Lq}^{(3)} = (\overline{L}\gamma^\mu\tau^I L)(\overline{q}\gamma_\mu\tau^I q) \ , && O_{\ell Q}^{(3)} = (\overline{\ell}\gamma^\mu\tau^I \ell)(\overline{Q}\gamma_\mu\tau^I Q) \ , \\
&O_{\ell Q}^{(1)} = (\overline{\ell}\gamma^\mu \ell)(\overline{Q}\gamma_\mu Q) \ , && O_{Qe} = (\overline{Q}\gamma^\mu Q)(\overline{e}\gamma_\mu e) \ , \\
&O_{eb} = (\overline{e}\gamma^\mu e)(\overline{b}\gamma_\mu b) \ , && O_{\ell b} = (\overline{\ell}\gamma^\mu \ell)(\overline{b}\gamma_\mu b) \ , \\
&O_{\ell L}^{(1)} = (\overline{\ell}\gamma^\mu \ell)(\overline{L}\gamma_\mu L) \ , && O_{\ell L}^{(3)} = (\overline{\ell}\gamma^\mu\tau^I \ell)(\overline{L}\gamma_\mu\tau^I L) \ , \\
&O_{Le} = (\overline{L}\gamma^\mu L)(\overline{e}\gamma_\mu e) \ , && O_{\ell\tau} = (\overline{\ell}\gamma^\mu \ell)(\overline{\tau}\gamma_\mu \tau) \ , \\
&O_{e\tau} = (\overline{e}\gamma^\mu e)(\overline{\tau}\gamma_\mu \tau) \ . &&
\end{aligned}
\tag{4.10a}
$$

Irrespective of the flavor symmetry assumed, we also include the following non-fermionic operators:

$$
\begin{aligned}
O_{WB} &= \left(h^\dagger \tau^I h\right) W^I_{\mu\nu} B^{\mu\nu}, \\
O_{hD} &= \left(h^\dagger D_\mu h\right)^* \left(h^\dagger D_\mu h\right) \ , \\
O_W &= \epsilon_{IJK}\, W^{I\nu}_\mu W^{J\lambda}_\nu W^{K\mu}_\lambda \ .
\end{aligned}
\tag{4.11}
$$

4.1.2. $U(2)^5$ flavor symmetry

In the limit of vanishing Yukawa couplings the SM Lagrangian is invariant under the $[U(2)\times U(1)]^5$ group symmetry considered in the previous section. We can work with a more realistic scenario keeping the third family Yukawas:

$$
\mathcal{L} = -\lambda_t\, \bar{Q}\, \tilde{h}\, t - \lambda_b\, \bar{Q}\, h\, b - \lambda_\tau\, \bar{L}\, h\, \tau \tag{4.12}
$$

and neglecting only those of the two lightest generations. In this case the flavor symmetry breaks down to $U(2)^5 \times U(1)^3$, that we will just call $U(2)^5$, since the three $U(1)$ subgroups are simply the lepton and baryon number and hypercharge of the third generation[4].

Among the new operators that appear due to the reduction of the symmetry group, only the following four chirality-flipping operators will affect EWPO:

$$
\begin{aligned}
O^t_{\tau B} &= \left(\overline{L}\,\sigma^{\mu\nu}\,\tau\right) h\, B_{\mu\nu} + \text{h.c.} \ , \\
O^t_{bB} &= \left(\overline{Q}\,\sigma^{\mu\nu}\, b\right) h\, B_{\mu\nu} + \text{h.c.} \ , \\
O^t_{\tau W} &= \left(\overline{L}\,\sigma^{\mu\nu}\,\tau^I\,\tau\right) h\, W^I_{\mu\nu} + \text{h.c.} \ , \\
O^t_{bW} &= \left(\overline{Q}\,\sigma^{\mu\nu}\,\tau^I\, b\right) h\, W^I_{\mu\nu} + \text{h.c.} \ .
\end{aligned}
\tag{4.13}
$$

[4] A recent analysis of the implications of current flavor data for the quark-sector component of this symmetry, i.e. $U(2)^3$, suitably broken by spurions à la MFV, can be found in Ref. [72].

Their chirality-flipping structure translates, in the processes of our interest here, into contributions proportional to the fermion masses, i.e. suppressed by the factor m_f/v with respect to other NP contributions from dimension-six operators. Given that we focus here on the $W \to \tau\,\overline{\nu}_\tau$ decay we will not consider in the following the operators O^t_{bB} and O^t_{bW}.

4.2. $W \to \tau\,\overline{\nu}_\tau$ decay in the EFT framework

When the $U(2)^5$ flavor symmetry is assumed, the SM term and dimension-six operators contributing to the $W \to \tau\,\overline{\nu}_\tau$ decay are:

$$\begin{aligned}\mathcal{L}_{\rm EFT} &= i\,\bar{\ell}\not{D}\,\ell + \frac{1}{\Lambda^2}\left\{\alpha^{(3)}_{hL}\mathcal{O}^{(3)}_{hL} + \alpha^t_{\tau W}\mathcal{O}^t_{\tau W} + \text{h.c.}\right\} \\ &\supset \frac{g}{\sqrt{2}}\Big[\Big(1+2\hat{\alpha}^{(3)}_{hL}\Big)\bar{\tau}_L\gamma^\mu\nu_\tau W^-_\mu + \frac{2}{gv}\hat{\alpha}^t_{\tau W}\bar{\tau}_R\sigma^{\mu\nu}\nu_\tau W^-_{\mu\nu}\Big],\end{aligned} \tag{4.14}$$

where $W^-_\mu = (W^1_\mu + iW^2_\mu)/\sqrt{2}$, and we used the normalized couplings:

$$\hat{\alpha}_X \equiv \frac{v^2}{\Lambda^2}\,\alpha_X\ , \tag{4.15}$$

that we assume to be real hereafter. Working at linear order in the $\hat{\alpha}$ coefficients, the full decay width reads:

$$\Gamma\left(W \to \tau\,\overline{\nu}_\tau\right) = \frac{G_F\,M_W^3}{6\sqrt{2}\,\pi}\left(1-w_\tau^2\right)^2\left\{\left(1+4\hat{\alpha}^{(3)}_{hL}\right)\left(1+\frac{w_\tau^2}{2}\right) + 6\sqrt{2}\,w_\tau\,\hat{\alpha}^t_{\tau W}\right\},$$

where $w_\tau = m_\tau/M_W$ and G_F is the tree level Fermi coupling constant defined by $G_F/\sqrt{2} = g^2/(8M_W^2)$. The new contributions to the decay width have the following features:

- There are only two dimension-six operators contributing to this process: $\mathcal{O}^{(3)}_{hL}$ and $\mathcal{O}^t_{\tau W}$. This can be seen if the equations of motion are properly used to reduce the number of operators in the effective basis, as done in Ref. [40], instead of using directly all the operators appearing in the original list of Ref. [3, 73].

- The lepton universality feature of the SM implies that $g_\tau = g$. The operator $\mathcal{O}^{(3)}_{hL}$ simply shifts the SM result in such a way that its effect can be encoded in the following redefinition:

$$g_\tau \equiv g\,(1+\delta g_\tau) = g\left(1+2\ \hat{\alpha}^{(3)}_{hL}\right)\ . \tag{4.16}$$

  This operator is allowed in the two flavor symmetries that we consider.

- The magnetic operator $\mathcal{O}^t_{\tau W}$ provides a new structure not present in the SM [74, 75, 76]. Contrarily to $\mathcal{O}^{(3)}_{hL}$ this is a chirality flipping operator and it gives a contribution suppressed by m_ℓ/M_W due to the derivative dependence. Assuming the $[U(2)\times U(1)]^5$ flavor symmetry this term vanishes.

In what follows we will consider the universality ratios:

$$R^W_{\ell\ell'} = \Gamma(W\to\ell\nu_\ell)/\Gamma(W\to\ell'\nu'_\ell)\ , \tag{4.17}$$

instead of the simple decay rate, in such a way that we do not have to worry about the NP corrections associated to the experimental determination of the Fermi constant G_F, since they cancel in the ratio.

4.3. Fit procedure and results

Once we have identified in the previous section the effective operators that can contribute to $R^W_{\tau\ell}$, generating a deviation from lepton universality, we study now the constraints that can be derived on these operators from EWPO and low-energy measurements.

Looking for example at the experimental result (4.3) it can be understood that one single operator will not be able to explain simultaneously the EWPO and the anomaly in the $W\tau\nu$ vertex shown in Eq. (4.1), due to the gauge symmetry that connects W and Z bosons. However, when several operators are present one can have cancelations between them and a careful numerical analysis is needed.

With that purpose we updated and modified the Mathematica code developed in Ref. [69], that included electroweak observables at the Z line and at higher energies and other low energy measurements. In addition we included the leptonic tau decay and the exclusive channel $\tau\to\pi\nu_\tau$, that have an experimental error well below the 1% level and a theoretical error under control. We considered also the anomalous magnetic moment of the tau lepton that, despite its very large experimental uncertainty, is able to constrain the magnetic operators poorly bounded by other observables. The associated formulas will be presented in the following subsections and the complete list of the observables used in our analysis can be found in Table 4.1.

We included in the program also the contribution to the different observables coming from the magnetic operators $O^t_{\tau W}$ and $O^t_{\tau B}$, not included in Ref. [69] since the $U(2)^5\times U(1)^5$ symmetry was assumed in that work.

With the above-mentioned observables O^i, we build a standard χ^2 function as:

$$\chi^2(\hat{\boldsymbol{\alpha}}) = \sum_i \left[O^i_{\rm th}(\hat{\boldsymbol{\alpha}}) - O^i_{\rm exp}\right]\left[\sigma^2_{\rm O}\right]^{-1}_{ij}\left[O^j_{\rm th}(\hat{\boldsymbol{\alpha}}) - O^j_{\rm exp}\right]\ , \tag{4.18}$$

where the error matrix $\sigma^2_{\rm O}$ includes the experimental error and the uncertainty on the SM prediction combined in quadrature. The theoretical value $O^i_{\rm th}$ contains

Classification	Std. Notation	Measurement
Atomic parity violation	$Q_W(Cs)$	Weak charge in Cs
	$Q_W(Tl)$	Weak charge in Tl
DIS	g_L^2, g_R^2	ν_μ-nucleon scattering (NuTeV)
	R^ν	ν_μ-nucleon scatt. (CDHS, CHARM)
	κ	ν_μ-nucleon scatt. (CCFR)
	$g_V^{\nu e}, g_A^{\nu e}$	ν-e scatt. (CHARM II)
Z-pole	Γ_Z	Total Z width
	σ_0	e^+e^- hadronic cross section
	$R^0_{f=e,\mu,\tau,b,c}$	Ratios of decay rates
	$A_{FB}^{0,f=e,\mu,\tau,b,c}$	FB asymmetries
	$A_{f=e,\mu,\tau,s,b,c}$	Polarized asymmetries
	$\sin^2\theta^{lept}_{eff}$	Hadronic charge asymmetry
LEPII fermion production	$\sigma_{f=q,c,b\mu,\tau}$	Total cross sections for $e^+e^- \to f\overline{f}$
	$A_{FB}^{f=c,b,\mu,\tau}$	FB asymmetries for $e^+e^- \to f\overline{f}$
	$d\sigma_e/d\cos\theta$	$e^+e^- \to e^+e^-$ diff. cross section
W pair	$d\sigma_W/d\cos\theta$	$e^+e^- \to W^+W^-$ diff. cross section
	M_W	W mass
$V_{\rm CKM}$ unitarity	Δ_{CKM}	V_{ud} and V_{us} extractions [71]
τ decays	$\tau \to \nu_\tau \ell \bar{\nu}_\ell$	Leptonic τ decay ($\ell = e, \mu$) [38]
	$\tau \to \nu_\tau \pi$	Exclusive hadronic τ decay [38]
Anomalous magnetic moment	a_τ	$e^+e^- \to e^+e^-\tau^+\tau^-$ cross section [77]

Table 4.1: Measurements included in this analysis. See Ref. [70] and references therein for detailed descriptions. References are shown only for the new observables considered in this work.

the up-to-date SM prediction and the contribution of higher dimensional operators through interference with SM vertices, i.e. linear in the $\hat{\alpha}$ couplings.

As a result of this fit we determine the value of the different Wilson coefficients $\hat{\alpha}$, with their relative errors and the corresponding correlations, or in other words the bounds on the different NP effective operators. In particular we are interested in the bounds associated to the two operators that could generate a lepton universality violation in the W decay (see Eq. (4.14)), and finally in the determination of the universality ratio $R^W_{\tau\ell}$ extracted from our fit, to be compared with the experimental determination given in Eq. (4.1).

New observables considered for the fit

Leptonic Z decays

We calculated the $Z \to \tau^+\tau^-$ decay using the following effective Lagrangian, the most general Lagrangian contributing to this process once we choose the flavour $U(2)^5$ symmetry group:

$$\mathcal{L}_{\rm EFT} = i\,\bar{\ell}\not{D}\,\ell + \frac{1}{\Lambda^2}\left\{\alpha_{hL}^{(1)}\mathcal{O}_{hL}^{(1)} + \alpha_{hL}^{(3)}\mathcal{O}_{hL}^{(3)} + \alpha_{h\tau}\mathcal{O}_{h\tau} + \alpha_{\tau W}^{t}\mathcal{O}_{\tau W}^{t} + \alpha_{\tau B}^{t}\mathcal{O}_{\tau B}^{t} + \text{h.c.}\right\}, \tag{4.19}$$

The corresponding decay width is given by:

$$\begin{aligned}\Gamma\left(Z \to \tau^+\,\tau^-\right) = \frac{G_F M_Z^3}{24\sqrt{2}\,\pi}\sqrt{1-4\,z_\tau^2}\Big\{&\left(1-4\,v^-\right)\left(1-4\,z_\tau^2\right) - 24\sqrt{2}\,z_\tau\,t^Z\left(4s_W^2-1\right)\\ &+\left[\left(4s_W^2-1\right)-4v^+\right]\left(4s_W^2-1\right)\left(1+2\,z_\tau^2\right)\Big\},\end{aligned} \tag{4.20}$$

where:

$$\begin{aligned} v^- &= \hat{\alpha}_{h\tau} - \hat{\alpha}_{hL}^{(1)} - \hat{\alpha}_{hL}^{(3)},\\ v^+ &= \hat{\alpha}_{h\tau} + \hat{\alpha}_{hL}^{(1)} + \hat{\alpha}_{hL}^{(3)},\\ t^Z &= c_W\hat{\alpha}_{\tau W}^{t} + s_W\hat{\alpha}_{\tau B}^{t}, \end{aligned} \tag{4.21}$$

being s_W and c_W the sine and cosine of the weak angle θ_W respectively, and $z_\tau = m_\tau/M_Z$. As discussed in relation with Eq. (4.16) it can be noticed that the linear contribution of the tensor operators $\mathcal{O}_{\tau W}^{t}$ and $\mathcal{O}_{\tau B}^{t}$ is suppressed by the lepton mass over the Z mass. Moreover operators $\mathcal{O}_{h\tau}$, $\mathcal{O}_{hL}^{(1)}$ and $\mathcal{O}_{hL}^{(3)}$ simply modify the weight of the SM vertices.

Anomalous magnetic moment

The two magnetic operators provide also a local contribution to the anomalous magnetic moment of the tau lepton. The generic $\gamma\,\tau\,\overline{\tau}$ vertex is given by

$$-\,i\,e\,\varepsilon^{\mu}(q)\,\overline{u}(p')\,V_\mu\,u(p)\ , \tag{4.22}$$

where:

$$V_\mu = F_1(q^2)\,\gamma_\mu\ +\ i\,F_2(q^2)\,\sigma_{\mu\nu}\,\frac{q^\nu}{2\,m_\tau} + F_3(q^2)\,\gamma^5\,\sigma_{\mu\nu}\,\frac{q^\nu}{2\,m_\tau}\ , \tag{4.23}$$

and the anomalous magnetic moment of the τ lepton is given by $a_\tau = (g_\tau - 2)/2 = F_2(0)$. By using $\mathcal{L}_{\rm EFT}$ in Eq. (2.1) we find the following expression for the τ lepton anomalous magnetic moment:

$$a_\tau\ =\ a_\tau^{\rm SM}\ +\ \frac{2\sqrt{2}}{s_W}\,\frac{m_\tau}{M_W}\,\left(\,c_W\hat{\alpha}_{\tau B}^{t} - s_W\hat{\alpha}_{\tau W}^{t}\right)\ , \tag{4.24}$$

where the first term in the right-hand side is the SM contribution [78]:

$$a_\tau^{\rm SM} = 1.17721(5) \times 10^{-3} \ . \tag{4.25}$$

The current experimental result is given by $-0.052 < a_\tau < 0.013$ at 95% C.L. [77], though other analyses establish more stringent limits [76].

Other observables

In the original Mathematica program were already present observables based on the $e^+e^- \to \tau^+\tau^-$ cross section (total cross section, FB and polarized asymmetries). We introduced the contribution coming from magnetic operators, using the formulas taken from of Ref. [76].

The leptonic decays of heavy pseudoscalar mesons ($B^\pm$, $D^\pm$, $D_{\rm S}^\pm$) could in principle be considered in order to constrain NP effects in leptonic W decays, but they have not reached yet the necessary experimental precision: the relative error of the current data on the decays into tau are approximately $\mathcal{O}(6\%)$ for $D_{\rm S}$ decays and $\mathcal{O}(20\%)$ for B decays, and some of the decays into muon and electron have not been seen yet, preventing a complete analysis of the lepton universality ratios. For these reasons, these observables have not been included in the fit. We will comment on them in Section 4.4.

Concerning LHC measurements, the natural channels to analyze for the purpose of this work are $pp \to \tau\bar{\nu}X$ and $pp \to \tau^+\tau^-X$, where possible modifications of the $W\tau\nu$ vertex and its gauge counterpart $Z\tau^+\tau^-$ can be probed, but unfortunately there is no data available for these particular channels yet. On the theoretical side, the contribution to these processes coming from effective operators has been worked out in Refs. [18, 79] for first generation leptons. In any case, as we will see, the list of observables included in our fit is exhaustive enough to reach a solid answer to the possible lepton universality violations.

(Semi)leptonic τ decays as precise EW observables

In a general analysis involving a big number of operators (free parameters in the fit) it is possible to encounter flat directions, i.e. directions in the parameter space that are not bounded by the experimental data. This means that some operators appear always in the same combination throughout all the observables considered in the fit and then only that combination can be constrained, and not each operator separately. In Ref. [69] four flat directions were identified in the particular fit we are using in this work. However, we show now how the addition of the leptonic tau decay to the list of EWPO included in the fit removes one of these flat directions.

In the limit of $U(2)^5$ flavor symmetry the rate for the leptonic decay of the τ

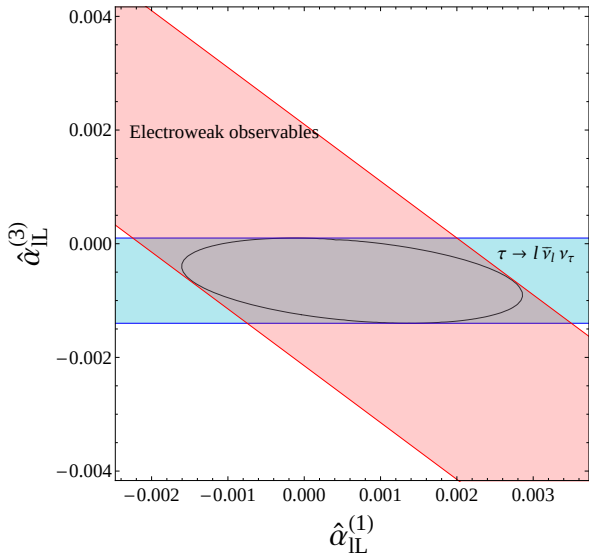

Figure 4.1: Phenomenological constraints on the operators $O^{(1)}_{\ell L}$ and $O^{(3)}_{\ell L}$ from electroweak observables (red diagonal band) and leptonic tau decay rate (blu horizontal band). See Table 4.1 for the complete list of observables considered. The black ellipse is the 1σ C.L. region when considering all observables together.

lepton reads:

$$\Gamma_{\tau\to\nu_\tau\ell\bar{\nu}_\ell} = \frac{G_F^2 m_\tau^5}{192\,\pi^3}\left\{\left[1+4\,\hat{\alpha}^{(3)}_{hL}+4\,\hat{\alpha}^{(3)}_{h\ell}-4\,\hat{\alpha}^{(3)}_{\ell L}\right]f\left(\frac{m_\ell^2}{m_\tau^2}\right) +2\sqrt{2}\,\hat{\alpha}^t_{\tau W}\,\frac{m_\tau}{M_W}\,g\left(\frac{m_\ell^2}{m_\tau^2}\right)\right\}(1+\delta_{RC})\ , \tag{4.26}$$

where $\ell = e,\mu$, δ_{RC} contains the radiative corrections to the SM contribution [80] and

$$\begin{aligned} f(x) &= 1-8x-12x^2\ln x+8x^3-x^4, \\ g(x) &= 1-6x+18x^2-10x^3+12x^3\ln x-3x^4. \end{aligned} \tag{4.27}$$

In Eq. (4.26) we used the coefficient $\hat{\alpha}^{(3)}_{h\ell}$, corresponding to the operator:

$$O^{(3)}_{hL} = (h^\dagger i\tau^I D_\mu h)(\bar{\ell}\gamma^\mu\tau^I\ell)\ . \tag{4.28}$$

The self-explanatory notation used for the name of this operator will be adopted hereafter for operators involving only light fermions. Although we neglect these operators in the subsequent numerical analysis we keep them in the analytic expressions for the sake of completeness.

In order to show the constraining power of the tau decays let us consider the simple situation in which only the operators $O^{(1)}_{\ell L}$ and $O^{(3)}_{\ell L}$ are not vanishing. As

shown in Figure 4.1 the electroweak observables, and in particular the $e^+e^- \to \tau^+\tau^-$ cross section and the forward-backward asymmetry, are able to constrain only the combination $O^{(1)}_{\ell L} + O^{(3)}_{\ell L}$. The inclusion of the leptonic tau decay into the fit allows to reduce the one sigma C.L. region to the black ellipse. The two operators are then constrained at the 0.4% and 0.2% level, corresponding to an effective NP scale $\Lambda > 2.7$ TeV and $\Lambda > 4.1$ TeV (90% C.L.) respectively: very strong bounds that show the importance of leptonic tau decays as electroweak precision observable.

A similar role is played by the pionic τ decay, where experimental results and SM calculations are also below the per-mil level of precision. The expression for the $\tau \to \pi\nu_\tau$ decay rate within our $U(2)^5$ flavor symmetric EFT framework is the following:

$$\Gamma_{\tau^-\to\pi^-\nu_\tau} = \frac{G_F^2 F_\pi^2}{8\pi}|V_{ud}|^2 m_\tau^3 \left(1 - \frac{M_\pi^2}{m_\tau^2}\right)^2 (1+\delta'_{RC}) \left(1 + 4\,\hat{\alpha}^{(3)}_{hL} + 4\,\hat{\alpha}^{(3)}_{hq} - 4\,\hat{\alpha}^{(3)}_{Lq}\right) , \tag{4.29}$$

where F_π denotes the pion decay constant and δ'_{RC} radiative corrections [81]. It is convenient to work once again with a normalized ratio, namely:

$$\begin{aligned} R_{\tau/\pi} &\equiv \frac{\Gamma_{\tau^-\to\pi^-\nu_\tau}}{\Gamma_{\pi^-\to\mu^-\overline{\nu}_\mu}} \\ &= \frac{m_\tau^3}{2\,m_\mu^2 M_\pi} \left(\frac{1 - \frac{M_\pi^2}{m_\tau^2}}{1 - \frac{m_\mu^2}{M_\pi^2}}\right)^2 \left(1+\delta_{\tau/\pi}\right) \left(1 + 4\left(\hat{\alpha}^{(3)}_{hL} - \hat{\alpha}^{(3)}_{h\ell}\right) - 4\left(\hat{\alpha}^{(3)}_{Lq} - \hat{\alpha}^{(3)}_{\ell q}\right)\right) . \end{aligned} \tag{4.30}$$

where $\delta_{\tau/\pi} = 0.0016(14)$ denotes the radiative corrections to the SM contributions [82]. As we can see, this observable represents another probe of the $\hat{\alpha}^{(3)}_{hL}$ coefficient, and moreover it represents the only observable in our analysis sensitive to the $\hat{\alpha}^{(3)}_{Lq}$ coefficient. Comparing the experimental value of $R_{\tau/\pi}$ [38, 83] and its SM prediction we get a bound of $\Lambda > 3.1$ TeV (90% C. L.) on the NP effective scale for the four Wilson coefficients appearing in Eq. (4.30).

4.3.1. $[U(2) \times U(1)]^5$ symmetric case: results

In order to study if the $R^W_{\tau\ell}$ anomaly of Eq. (4.1) can be accommodated in our EFT framework as a genuine New Physics effect and not just a statistical fluctuation, we start with a single operator analysis where only the $\hat{\alpha}^{(3)}_{hL}$ is present and all the observables of Table 4.1 are included. In this case we obtain the expected strong bound:

$$R^W_{\tau\ell} = 0.9997 \pm 0.0015 , \tag{4.31}$$

in good agreement with the SM prediction. As shown in Figure 4.2, the very precise measurements of leptonic Z and τ decays dominate our fit, and makes impossible to accommodate the $R^W_{\tau\ell}$ anomaly.

Once we include additional operators, things become less intuitive because cancelations between operators are possible, opening the possibility to explain the $R^W_{\tau\ell}$ anomaly and the leptonic Z and τ decays at the same time.

As a first global analysis, we assume the $[U(2) \times U(1)]^5$ flavor symmetry and we include the 17 operators given in Eqs. (4.7-4.11). It is worth repeating that in order to simplify the discussion and given that the experimental data show no sign of NP related to the light families of fermions, we have assumed that the operators involving only light fermions can be neglected.

Somehow surprisingly we find that even with so many operators, the constraint on $\hat{\alpha}^{(3)}_{hL}$ is very strong, namely:

$$-3.6 \times 10^{-3} \leq \hat{\alpha}^{(3)}_{hL} \leq -0.5 \times 10^{-3} \qquad (90\%\ \text{C.L.}) \tag{4.32}$$

Interestingly enough, this value is two sigmas away from zero, giving the following bound on the universality ratio:

$$R^W_{\tau\ell} = 0.991 \pm 0.004\ , \tag{4.33}$$

where we quoted the error at 1σ level in order to be comparable with the experimental result in Eq. (4.1).Thus we find the curious result that our fit is indeed able to accommodate a violation of lepton universality in the W decays, but *in the opposite direction* than the direct experimental measurement. The explanation for this fact is simple: when we take into account the effect of many higher-dimension operators, the fit introduces some non-zero Wilson coefficients in order to alleviate the small tensions between the experimental values and the SM predictions (see e.g. σ^0_{had} in Figure 4.2). These non-zero contributions then cancel in those observables where the agreement with the SM is perfect. And it turns out that one of these non-zero NP coefficients is $\hat{\alpha}^{(3)}_{hL}$. This is exactly why global analyses are interesting: they can find regions on the parameter space where these cancelations between operators take place, offering new possibilities not accessible in single-operator analyses, and difficult to foresee in a naive analysis. Obviously the inclusion of $R^W_{\tau\ell}$ as an additional observable in our fit will reduce this "tension" moving the value of $\hat{\alpha}^{(3)}_{hL}$ closer to zero, giving a 90% C.L. bound:

$$-3.2 \times 10^{-3} \leq \hat{\alpha}^{(3)}_{hL} \leq -0.08 \times 10^{-3} \tag{4.34}$$

The conclusion is once more that we cannot accommodate the $R^W_{\tau\ell}$ along with our long list of precision observables, and thus we are forced to consider it a mere statistical fluctuation. Unlike the single operator case where it could be naively expected, this represents a non-trivial result in a fit with seventeen free parameters.

For the sake of completeness, let us mention that in a truly global $[U(2)\times U(1)]^5$ fit, where operators only involving light fermions (like e.g. $\mathcal{O}^{(3)}_{h\ell}$) are also included, the NP bounds become extremely weak and the current experimental value of $R^W_{\tau\ell}$ cannot be excluded anymore.

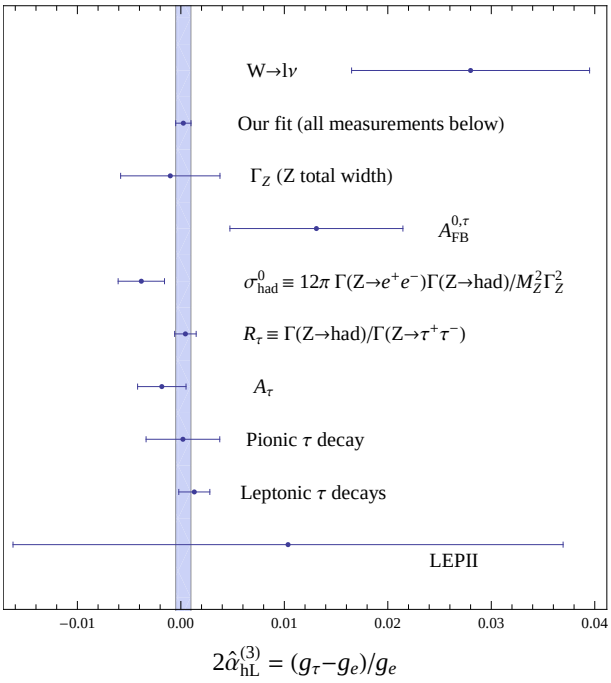

Figure 4.2: Bounds obtained for the NP coefficient $\hat{\alpha}^{(3)}_{hL}$ from the different set of measurements included in our fit. Equivalently, these are the bounds on the deviation from lepton universality in the electroweak coupling to third generation leptons g_τ (see Eq. (4.16)). For comparison we also show the value obtained, using the experimental data in Eq. (4.1), from leptonic W decays (not included in our fit). $A^{0,\tau}_{FB}$ is the forward-backward asymmetry measured at LEP1 for tau pairs, A_τ includes the SLD measurement and the LEP1 total τ polarization and the LEP2 bound comes from τ pair cross sections and asymmetries. See PDG [38], chapter 10, for more details.

4.3.2. $U(2)^5$ symmetric case: results

Reducing the symmetry group to $U(2)^5$ introduces the chirality-flipping operators $O^t_{\tau W}$ and $O^t_{\tau B}$, offering additional NP contributions to the observables and higher cancellations between operators.

From the associated global fit[5] with 19 free parameters, we get the following 90% bounds on the two operators involved in the W decays:

$$-3.7\times10^{-3} \leq \hat{\alpha}^{(3)}_{hL} \leq -0.6\times10^{-3} \tag{4.35}$$

and

$$0.04\times10^{-3} \leq \hat{\alpha}^{t}_{\tau W}\frac{m_\tau}{M_W} \leq 5.0\times10^{-3}\ , \tag{4.36}$$

[5]We do not include in this $U(2)^5$-symmetry fit the leptonic polarization asymmetries A_ℓ, since they have been extracted assuming only vector and axial-vector couplings.

where we have explicitly shown the m_τ/M_W suppression that multiplies the $\hat{\alpha}^t_{\tau W}$ coefficient in the observables. From these values we calculate the prediction for the universality ratio at 1σ level:

$$R^W_{\tau\ell} = 1.01 \pm 0.01 \ . \tag{4.37}$$

While the constraints on $\hat{\alpha}^{(3)}_{hL}$ are very similar to the previous case, the presence of a second contribution from the magnetic operator increases the error (and the central value) of $R^W_{\tau\ell}$. This increase is however not enough to nicely accommodate the experimental value of $R^W_{\tau\ell}$ shown in Eq. (4.1).

4.4. Leptonic decays of heavy mesons

The leading SM contribution to the $P^- \to \ell^- \overline{\nu}_\ell$ decays is given by the W exchange and hence it is interesting to point out how these decays get modified by possible deviations from family universality in the $W\ell\nu$ coupling. In particular we are interested in the D, D_S and B decays because they are heavy enough to decay into the tau lepton. Although two dimension-six operators modify the vertex of the W gauge boson with leptons, namely $\mathcal{O}^{(3)}_{h\ell}$ and $\mathcal{O}^t_{eW}$, only the first contributes to the leptonic decay of heavy mesons, due to the fact that the tensor coupling has no spin-0 component.

In order to get rid of the hadronic uncertainties and the NP corrections to the Fermi constant or the CKM elements appearing in the individual decay widths, we will focus again on the ratio between the tau channel and a light lepton channel:

$$R^P_{\tau\ell} = \frac{\mathrm{BR}\left(P \to \tau\, \overline{\nu}_\tau\right)}{\mathrm{BR}\left(P \to \ell\, \overline{\nu}_\ell\right)} \ , \tag{4.38}$$

where $\ell = e, \mu$. The effective Lagrangian that mediates these decays, including linear corrections in the $\hat{\alpha}$ coefficients, can be found in Eq. (34) of [71]. Assuming the $U(2)^5$ flavor symmetry we find the following expressions for the ratios[6]:

$$\begin{aligned} R^{D_{(s)}}_{\tau\ell} &= \frac{h_{D_{(s)}}(m_\tau)}{h_{D_{(s)}}(m_\ell)} \left\{1 + 4\left(\hat{\alpha}^{(3)}_{hL} - \hat{\alpha}^{(3)}_{h\ell}\right) - 4\left(\hat{\alpha}^{(3)}_{Lq} - \hat{\alpha}^{(3)}_{\ell q}\right)\right\} \ , \\ R^{B}_{\tau\ell} &= \frac{h_{B}(m_\tau)}{h_{B}(m_\ell)} \left\{1 + 4\left(\hat{\alpha}^{(3)}_{hL} - \hat{\alpha}^{(3)}_{h\ell}\right) - 4\left(\hat{\alpha}^{(3)}_{LQ} - \hat{\alpha}^{(3)}_{\ell Q}\right)\right\} \ , \end{aligned} \tag{4.39}$$

where $h_P(m) = m^2\left(1 - m^2/M_P^2\right)^2$.

As expected, we find that the $\hat{\alpha}^{(3)}_{hL}$ coefficient modifies these ratios. However, the bound on this coefficient from our analysis of EWPO and low-energy measurements

[6] In the B decays we neglect the contribution from a new $U(2)^5$-invariant operator $O_{Qb\tau} = (\bar{L}\tau)(\bar{b}Q) + \mathrm{h.c.}$, since this operator does not affect the EWPO included in our fit.

is below the per-cent level (see Section 4.3), a precision very far from current experimental results in these decays. The only ratio where we actually have a value, and not just an upper or lower limit, is $R_{\tau\mu}^{D_s} = 9.2(7)$ [38]. We can compare this $\sim 8\%$ experimental error with the $\sim 0.7\%$ determination of the $R_{\tau/\pi}$ ratio, where exactly the same linear combination of NP couplings is probed, as shown in Eq. (4.30). This level of precision can actually be considered a benchmark sensitivity for future D and D_s meson experiments to become competitive in the NP search within our EFT framework.

On the other hand the leptonic B decays are interesting since they probe a different linear combination of NP coefficients, and therefore are complementary to other observables.

4.5. Conclusions

In the SM the coupling of leptons to the gauge bosons is flavor blind, a property that has been tested successfully in several different observables and experiments, sometimes even at the per-mil level of precision. The latest results from the LEP2 experiment in 2005 showed however a quite sizable deviation ($\sim 5\%$) from universality in the $W\ell\nu_\ell$ coupling of more than two sigmas when comparing the third leptonic family with the two light ones, as shown in Eq. (4.1).

We have considered in this chapter the possibility that this deviation represents a real NP effect. We have performed an Effective Field Theory analysis where the NP effects are parameterized by a series of Wilson coefficients $\hat{\alpha}$, that appear in the effective Lagrangian multiplying dimension-six operators. In order to reduce the number of unknown coefficients and motivated by the possible deviation from lepton universality in the $W\tau\nu_\tau$ vertex, we have assumed different flavor symmetries where the third family plays a special role.

Within this framework we have analyzed if it is possible to accommodate the $R_{\tau\ell}^W$ anomaly of Eq. (4.1) as a real NP effect without spoiling the nice agreement between SM predictions and EWPO observables. As expected, it is not possible to do such a thing with just one effective operator at play, due mainly to the very precise Z and τ leptonic decays, as nicely shown in Figure 4.2. More surprisingly we have found that EWPO are such strong constraints that not even in a global analysis where all the operators affecting the third family are present one can accommodate the $R_{\tau\ell}^W$ anomaly.

Should this departure from universality be confirmed by new data, then our analysis disfavor the possibility of explaining it through a weakly coupled theory standing at the TeV scale, unless a quite non-trivial flavor structure occurs. Instead, it would be necessary to resort to a different description of NP that could involve the introduction of new light degrees of freedom or a strongly interacting sector with flavor dependent couplings to leptons. For example previous studies of this deviation from universality in W decays have focused on the possibility that pair production of light charged Higgs bosons, almost degenerate with the W and

decaying largely into heavy fermions, could mimic $W \to \tau\,\overline{\nu}_\tau$ decays [13, 84]. Modifications on the electroweak gauge group in order to singularize the third family have also been considered [85].

Last but not least we have shown the importance of the current measurements in leptonic and semileptonic τ decays as New Physics constraining observables that probe new directions in the parameter space of our EFT framework, and we have analyzed the sensitivity of the leptonic decays of pseudoscalar mesons to the violations of lepton universality.

Chapter 5

Constraining novel Scalar and Tensor interactions

Nuclear and neutron beta decays have historically played a central role in determining the $V - A$ structure of weak interactions and in shaping what we now call the Standard Model [86, 87]. Nowadays, precision measurements of low-energy processes such as neutron decay can be used to probe the existence of non-SM interactions, such as novel scalar and tensor structures. Considerable experimental efforts using both cold and ultracold neutrons are underway worldwide, with the aim to improve the precision of various neutron decay observables [16, 17]: lifetime [88, 89, 90, 91, 92], beta asymmetry (A) [93, 94, 95, 96] neutrino asymmetry (B) [97, 95], electron-neutrino correlation (a) [98, 99, 100], and Fierz interference term (b) [98, 101]. In some of the asymmetry measurements there are prospects to reach experimental sensitivities between 10^{-3} and 10^{-4}; this makes these observables very interesting probes of New Physics effects originating at the TeV scale that have expected size $(v/\Lambda_{\rm NP})^2$, the ratio between the weak scale v and the New Physics scale.

The overall goal of the work presented in this chapter is to assess the discovery potential and discriminating power of planned precision beta-decay measurements with cold and ultracold neutrons. In particular we wish to study the sensitivity of neutron decay to new physics in the context of and in competition with: (i) other low-energy precision measurements in nuclear beta decays and pion decays; and (ii) high-energy collider searches (Tevatron, LHC). We work within the effective field theory setup presented in Chapter 2 and we will develop the matching between the effective Lagrangian at the electroweak scale and the Lagrangian describing the neutron decay, written in terms of nucleon fields. In the absence of a clear new-physics signal from collider searches, we find this way of proceeding the most attractive and general: all specific model analyses of beta decays can be cast in the EFT language and the constraints on effective operators that we will derive can be readily converted into constraints on the parameters of any SM extension.

Among various Beyond Standard Model (BSM) contributions we identify new scalar and tensor operators involving left-handed neutrinos as the most promising to probe with neutron decay, because they interfere with the SM amplitude and thus contribute at *linear* order to decay parameters. Motivated by this, we present a comprehensive analysis of constraints on such scalar and tensor BSM interactions from a broad range of low-energy probes (neutron decay, nuclear decays, pion decays) as well as collider searches.[1] To our knowledge such an analysis is missing in the literature, despite being essential to judging the relative merits of various low-energy experiments.

Extracting bounds on short-distance scalar and tensor couplings from neutron and nuclear beta decays requires knowledge of the nucleon scalar and tensor form factors at zero momentum transfer, denoted here by $g_{S,T}$. In previous beta-decay studies, g_S and g_T have been assumed to be $O(1)$ based on quark-model estimates (see, for example, Ref. [102]). The importance of the hadronic form factors can be appreciated by considering the extreme case in which $g_{S,T} \ll 1$, which would dilute the sensitivity of beta decays to new physics. We will use new estimates of these form factors to asses the real constraining power of present and future low energy experiments.

The chapter is organized as follows. In Section 5.1 we present the effective theory description of low-energy charged-current processes and briefly discuss how the coefficients may be constrained. In Section 5.2 we explain our notation for the matrix elements required to describe the neutron beta decay and discuss how this decay constrains the parameters in the effective field theory. In Section 7.1, we discuss the low-energy phenomenological constraints on chirality-violating scalar and tensor operators in the effective Lagrangian. In Section 5.4 we provide the first estimate of g_S from lattice QCD and a new average of existing calculations of g_T. In Section 5.5 we summarize the impact of lattice estimates of $g_{S,T}$ on the phenomenology of scalar and tensor BSM interactions. In Section 7.3 we present the constraints on the short-distance couplings obtained from an analysis of high-energy scattering experiments and discuss the improvement expected in the next few years. We present the concluding remarks on the chapter in Section 5.7.

5.1. Effective description of low-energy charged-current processes

The model independent effective theory setup we described in Chapter 2 can be easily applied to the study of neutron decay observables and other related low-energy and collider measurements. Following Ref. [71], we describe new physics contributions to low-energy charged-current (CC) processes using an effective Lagrangian derived from the general basis in Section 2.1. We truncate the expansion

[1] The EFT analysis of collider searches is valid as long as the particles that mediate the new interactions are above threshold for production at colliders.

of the effective Lagrangian to the lowest non-trivial order, given by dimension-six operators.

Effective Lagrangian

In Ref. [71] a minimal basis of $SU(2) \times U(1)$ invariant dimension-six operators contributing to low-energy charged-current processes was identified. In this framework one can derive the low-scale $O(1\text{ GeV})$ effective Lagrangian for semi-leptonic transitions. It receives contributions from both W-exchange diagrams (with modified W-fermion couplings) and the four-fermion operators $O_{lq}^{(3)}$, O_{qde}, O_{lq}, O_{lq}^{t} defined in Section 2.1. This matching procedure leads to [71]:

$$\begin{aligned}\mathcal{L}_{\rm CC} = \frac{-g^2}{2M_W^2}\, V_{ij} \Bigg[&\Big(1 + [v_L]_{\ell\ell ij}\Big)\ \bar{\ell}_L \gamma_\mu \nu_{\ell L}\ \bar{u}^i_L \gamma^\mu d^j_L \ +\ [v_R]_{\ell\ell ij}\ \bar{\ell}_L \gamma_\mu \nu_{\ell L}\ \bar{u}^i_R \gamma^\mu d^j_R \\ &+ [s_L]_{\ell\ell ij}\ \bar{\ell}_R \nu_{\ell L}\ \bar{u}^i_R d^j_L \ +\ [s_R]_{\ell\ell ij}\ \bar{\ell}_R \nu_{\ell L}\ \bar{u}^i_L d^j_R \\ &+ [t_L]_{\ell\ell ij}\ \bar{\ell}_R \sigma_{\mu\nu} \nu_{\ell L}\ \bar{u}^i_R \sigma^{\mu\nu} d^j_L \Bigg] \ +\ \text{h.c.}\ , \end{aligned} \tag{5.1}$$

where we explicitly use chiral fields to distinguish them from the non-chiral fields we will use in other formulas of this chapter and we defined:

$$V_{ij} \cdot [v_L]_{\ell\ell ij} = 2\, V_{ij}\ \left[\hat{\alpha}^{(3)}_{\varphi l}\right]_{\ell\ell} + 2\, V_{im} \left[\hat{\alpha}^{(3)}_{\varphi q}\right]^*_{jm} - 2\, V_{im} \left[\hat{\alpha}^{(3)}_{lq}\right]_{\ell\ell mj}\ , \tag{5.2a}$$

$$V_{ij} \cdot [v_R]_{\ell\ell ij} = -\,[\hat{\alpha}_{\varphi\varphi}]_{ij}\ , \tag{5.2b}$$

$$V_{ij} \cdot [s_L]_{\ell\ell ij} = -\,[\hat{\alpha}_{lq}]^*_{\ell\ell ji}\ , \tag{5.2c}$$

$$V_{ij} \cdot [s_R]_{\ell\ell ij} = -V_{im}\,[\hat{\alpha}_{qde}]^*_{\ell\ell jm}\ , \tag{5.2d}$$

$$V_{ij} \cdot [t_L]_{\ell\ell ij} = -\left[\hat{\alpha}^{t}_{lq}\right]^*_{\ell\ell ji}\ . \tag{5.2e}$$

Here $V \equiv V_{\rm CKM}$ and we use the notation $\hat{\alpha}_X \equiv \alpha_X v^2/\Lambda^2_{NP}$. The SM effective Lagrangian corresponds to $v_L = v_R = s_L = s_R = t_L = 0$. We want to stress two important features of these coupling constants:

- v_L involves a linear combination of three weak-scale effective couplings: a quark-gauge boson vertex correction, a lepton-gauge boson vertex correction, and a four-fermion operator coupling left-handed quarks and leptons (same chirality structure as the SM). An important consequence is that by $SU(2)\times U(1)$ gauge invariance, v_L is related to Z^0 fermion-antifermion vertex corrections and neutral-current four-fermion vertices.

- v_R and s_L, s_R, t_L are in one-to-one correspondence with weak-scale effective couplings. v_R describes a right-handed charged-current quark coupling, while s_L, s_R, t_L correspond to scalar and tensor four-quark operators.

Again, $SU(2)$ gauge invariance implies that these couplings mediate not only charged-currrent processes but also processes such as $\bar{e}e \leftrightarrow \bar{u}u, \bar{d}d$, with scalar or tensor Dirac structure.

In what follows, we will work in the limit in which the effective non-standard couplings $v_{L,R}$, $s_{L,R}$, and t_L are real and we will focus only on CP-even observables (for a discussion of CP-odd observables refer to Ref. [102]). To simplify the notation, we will omit flavor indices, e.g. $[v_L]_{eeud} \to v_L$. In addition, we will use the tree-level definition of the Fermi constant $g^2/(8M_W^2) \equiv G_F^{(0)}/\sqrt{2}$. Working to linear order in the non-standard couplings, and focusing on the $ij = ud$ component, the semi-leptonic effective Lagrangian can be written in the following useful form:

$$\begin{aligned}\mathcal{L}_{d\to u\ell^-\bar{\nu}_\ell} = -\frac{G_F^{(0)}V_{ud}}{\sqrt{2}}\Big(1+\epsilon_L+\epsilon_R\Big)\times \\ \times\Bigg[\bar{\ell}\gamma_\mu(1-\gamma_5)\nu_\ell\cdot\bar{u}\Big[\gamma^\mu\ -\ \big(1-2\epsilon_R\big)\gamma^\mu\gamma_5\Big]d \\ +\bar{\ell}(1-\gamma_5)\nu_\ell\cdot\bar{u}\Big[\epsilon_S-\epsilon_P\gamma_5\Big]d \\ +\epsilon_T\,\bar{\ell}\sigma_{\mu\nu}(1-\gamma_5)\nu_\ell\cdot\bar{u}\sigma^{\mu\nu}(1-\gamma_5)d\Bigg] + \text{h.c.},\end{aligned} \tag{5.3}$$

where we use non-chiral fields and we have defined the effective scalar, pseudoscalar, and tensor couplings as follows:

$$\epsilon_{L,R} \equiv v_{L,R}\ , \qquad \epsilon_S \equiv s_L + s_R\ , \qquad \epsilon_P \equiv s_L - s_R\ , \qquad \epsilon_T \equiv t_L\ . \tag{5.4}$$

While the physical amplitudes are renormalization scale and scheme independent, the individual effective couplings ϵ_i and hadronic matrix elements can display a strong scale dependence. Throughout the paper, we will quote estimates and bounds for the ϵ_i at the renormalization scale $\mu = 2$ GeV in the $\overline{\text{MS}}$ scheme, unless otherwise specified.

The Lagrangian (5.3) mediates all low-energy charged-current weak processes involving up and down quarks. For a recent analysis of flavor-dependent constraints, see Ref. [103]. In some of the charged-current processes involving first-generation quarks the theoretical and experimental precision has reached or will reach in the near future a level that allows stringent bounds on the new-physics effective couplings. In this work we are interested in assessing the sensitivity of neutron decay to new physics in the context of (i) other low-energy constraints from nuclear beta decays and pion decays; and (ii) constraints from high-energy colliders (LEP, Tevatron, LHC). To set the stage for the discussion, we summarize the observables that give us access to the couplings appearing in Eq. (5.3) (we will come back in detail to these in following sections):

- The combination $(\epsilon_L + \epsilon_R)$ affects the overall normalization of the effective Fermi constant. This is phenomenologically accessible through quark-lepton

universality tests (precise determination of V_{ud} from $0^+ \to 0^+$ nuclear decays under the assumption that $G_F = G_\mu$, where G_μ is the Fermi constant extracted from muon decay). An extensive analysis of the constraints on $(\epsilon_L + \epsilon_R)$ from universality tests and precision electroweak observables from the Z-pole was performed in Ref. [71], within BSM scenarios with minimal flavor violation. In this context it was shown that constraints from low-energy are at the same level or stronger (depending on the operator) than from Z-pole observables and $e^+e^- \to q\bar{q}$ cross-section measurements at LEP.

- The right-handed coupling ϵ_R affects the relative normalization of the axial and vector currents. In neutron decay ϵ_R can be reabsorbed in a redefinition of the axial coupling and experiments are only sensitive to the combination $(1 - 2\epsilon_R)g_A/g_V$ (g_V and g_A are the vector and axial form factors at zero momentum transfer, to be precisely defined below). Disentangling ϵ_R requires precision measurements of $(1 - 2\epsilon_R)g_A/g_V$ and precision calculations of g_A/g_V in LQCD.

- The effective pseudoscalar combination $\epsilon_P \equiv s_L - s_R$ contributes to leptonic decays of the pion. It is strongly constrained by the helicity-suppressed ratio $R_\pi \equiv \Gamma(\pi \to e\nu[\gamma])/\Gamma(\pi \to \mu\nu[\gamma])$. Moreover, as discussed in Refs. [104, 105, 106], the low-energy coupling ϵ_P receives contributions proportional to $\epsilon_{S,T}$ through electroweak radiative corrections. We will discuss the resulting constraints on $\epsilon_{S,P,T}$ in Section 5.3.1.

- Both the scalar combination $\epsilon_S \equiv s_L + s_R$ and the tensor coupling $\epsilon_T \equiv t_L$ contribute at linear order to the Fierz interference terms in beta decays of neutrons and nuclei, and the neutrino-asymmetry correlation coefficient B in polarized neutron and nuclear decay (see Appendix A for notation). Because of the peculiar way in which the Fierz interference term appears in many asymmetry measurements, bounds on ϵ_S and ϵ_T can also be obtained by observation of the beta-asymmetry correlation coefficient A, electron-neutrino correlation a, and positron polarization measurements in various nuclear beta decays. Finally, the tensor coupling ϵ_T can also be constrained through Dalitz-plot studies of the radiative pion decay $\pi \to e\nu\gamma$.

- All of the above operators can provide signatures at colliders. Currently there are no competitive collider bounds on the chirality-flipping scalar and tensor couplings $\epsilon_{S,P,T}$, because their interference with the SM amplitude carries factors of m_f/E_f (where m_f is a light fermion mass, $f \in \{e, u, d\}$), which at collider energies strongly suppresses the whole effect. So we immediately see that low-energy physics provides a unique opportunity to probe these couplings, to which collider searches are sensitive only quadratically (i.e. via non-interference terms). We will derive in Section 7.3 the current bounds on $\epsilon_{S,T}$ from searches at the LHC, and we will show that with higher center-of-mass energy and integrated luminosity they will become competitive with

low-energy searches.

Next, we review the analysis of neutron decay in the SM and beyond within the EFT framework described above.

5.2. Neutron β decay

The amplitude for neutron decay $n(p_n) \to p(p_p)e^-(p_e)\bar{\nu}_e(p_\nu)$ mediated by the effective Lagrangian (5.3) involves in principle the matrix elements between the neutron and proton of all possible quark bilinears. These can be parameterized in terms of Lorentz-invariant form factors as follows [107]:

$$\langle p(p_p)|\,\bar{u}\gamma_\mu d\,|\,n(p_n)\rangle \;= \bar{u}_p(p_p)\left[g_V(q^2)\,\gamma_\mu + \frac{\tilde{g}_{T(V)}(q^2)}{2M_N}\,\sigma_{\mu\nu}q^\nu + \frac{\tilde{g}_S(q^2)}{2M_N}\,q_\mu\right]u_n(p_n)\;, \tag{5.5a}$$

$$\langle p(p_p)|\,\bar{u}\gamma_\mu\gamma_5 d\,|\,n(p_n)\rangle \;= \bar{u}_p(p_p)\left[g_A(q^2)\gamma_\mu + \frac{\tilde{g}_{T(A)}(q^2)}{2M_N}\sigma_{\mu\nu}q^\nu + \frac{\tilde{g}_P(q^2)}{2M_N}q_\mu\right]\gamma_5 u_n(p_n)\;, \tag{5.5b}$$

$$\langle p(p_p)|\,\bar{u}\,d\,|\,n(p_n)\rangle \;= g_S(q^2)\;\bar{u}_p(p_p)\,u_n(p_n)\;, \tag{5.5c}$$

$$\langle p(p_p)|\,\bar{u}\,\gamma_5\,d\,|\,n(p_n)\rangle \;= g_P(q^2)\;\bar{u}_p(p_p)\,\gamma_5\,u_n(p_n)\;, \tag{5.5d}$$

$$\begin{aligned}\langle p(p_p)|\,\bar{u}\,\sigma_{\mu\nu}\,d\,|\,n(p_n)\rangle \;&= \bar{u}_p(p_p)\Big[g_T(q^2)\,\sigma_{\mu\nu} + g_T^{(1)}(q^2)\,(q_\mu\gamma_\nu - q_\nu\gamma_\mu)\\ &\quad + g_T^{(2)}(q^2)\,(q_\mu P_\nu - q_\nu P_\mu) + g_T^{(3)}(q^2)\,\big(\gamma_\mu \not{q}\gamma_\nu - \gamma_\nu \not{q}\gamma_\mu\big)\Big]\,u_n(p_n)\;,\end{aligned} \tag{5.5e}$$

where $u_{p,n}$ are the proton and neutron spinor amplitudes, $P = p_n + p_p$, $q = p_n - p_p$ is the momentum transfer, and $M_N = M_n = M_p$ denotes a common nucleon mass.[2] Note that all the above spinor contractions are $O(1)$, except for $\bar{u}_p\gamma_5 u_n$ which is $O(q/M_N)$. Moreover, as discussed below, second-class current contributions $\tilde{g}_S$ and $\tilde{g}_{T(A)}$ affect the amplitude at levels below the expected experimental sensitivities.

Our goal here is to identify TeV-induced new physics contaminations to the amplitude of typical size $\epsilon_{P,S,T} \sim (v/\Lambda_{\rm BSM})^2 \sim 10^{-3}$. The effect we are after is of the same size as recoil corrections $q/M_N \sim 10^{-3}$ as well as radiative corrections α/π. So in our analysis we perform a simultaneous expansion in new physics contributions, recoil, and radiative corrections keeping terms up to first order and neglecting higher-order terms, as they are smaller than the current and planned experimental sensitivity. In light of this simultaneous expansion in $\epsilon_{P,S,T}$, q/M_N, and α/π, we now discuss contributions from all quark-bilinear operators:

[2] In the case of vector and axial bilinears, the induced tensor term proportional to $\sigma_{\mu\nu}q^\nu$ can be traded for an independent "scalar" form factor proportional to P_μ. Here we choose to follow the parameterization of Ref. [107].

- **Vector current**: The form factor $g_V(0)$ contributes at $O(1)$ to the amplitude and $\tilde{g}_{T(V)}(0)$ contributes at first order in q/M_N. Also, up to isospin-breaking corrections of order $(M_n - M_p)/M_N \sim q/M_N$, the weak magnetism form factor $\tilde{g}_{T(V)}(0)$ can be related to the difference of proton and neutron magnetic moments, that are well known. On the other hand, the induced-scalar form factor $\tilde{g}_S(q^2)$ vanishes in the isospin limit [107], so it is of order $(M_n - M_p)/M_N \sim q/M_N$. Since it multiplies one power of q_μ/M_N, its contribution to the amplitude is effectively second order in the recoil expansion, so we drop it.

- **Axial current**: From the axial current only $g_A(0)$ contributes up to first order. The induced-tensor form factor $\tilde{g}_{T(A)}(q^2)$ vanishes in the isospin limit [107], and since it multiplies one power of q_μ/M_N its contribution to the amplitude is of second order in q/M_N, so we drop it. Similarly, the contribution associated with the induced-pseudoscalar form factor $\tilde{g}_P$ is quadratic in our counting, because the pseudoscalar bilinear is itself of order q/M_N, and it comes with an explicit q/M_N suppression, so we neglect it.[3]

- **Pseudoscalar bilinear**: The pseudoscalar bilinear $\bar{u}_p\gamma_5 u_n$ is itself of order q/M_N. Since it necessarily multiplies a new-physics effective coupling ϵ_P (there is no pseudoscalar coupling in the SM), this term is also of second order in our expansion, and we drop it.

- **Scalar and tensor bilinears**: These bilinears enter into the analysis multiplied by new-physics effective couplings $\epsilon_{S,T}$. So we need the matrix elements to zeroth order in the recoil expansion, which leaves us with $g_S(0)$ and $g_T(0)$. $g_T^{(1,2,3)}(q^2)$ are all multiplied by one power of q and $g_T^{(3)}$ vanishes in the isospin limit [107].

In summary, to the order we are working, the amplitudes depend only on $g_i \equiv g_i(0)$ $(i \in \{V, A, S, T\})$ and $\tilde{g}_{T(V)}(0)$. Up to second-order corrections in isospin breaking, one has $g_V = 1$ [109, 110]. For notational convenience, it is also useful to define the ratio of the axial to vector form factors as $\lambda \equiv g_A/g_V$. As noted earlier, in presence of non-standard right-handed interactions the axial form factor is always multiplied by the correction factor $(1 - 2\epsilon_R)$, so that the neutron-decay amplitude is actually a function of $\tilde{\lambda} \equiv \lambda(1 - 2\epsilon_R)$.

Finally, in order to make contact with the existing standard references on neutron and nuclear beta-decay phenomenology [111, 112, 87], let us note here that Eq. (5.5) can be viewed as the matching conditions from our quark-level effective theory Eq. (5.3) to a nucleon-level effective theory, such as the one originally

[3]This effect is, however, enhanced. Using partially conserved axial current one can show that the form factor $\tilde{g}_P$ is of order $M_N/m_q \sim 100$, making the contribution to the amplitude of order 10^{-4}. The effect of $\tilde{g}_P$ on the neutron beta-decay rate has been worked out in Ref. [108], and it should be included when the experiments reach that level of precision.

written down by Lee and Yang [111]. The Lee-Yang effective couplings C_i, C_i' ($i \in \{V, A, S, T\}$) can be expressed in terms of our parameters as

$$C_i = \frac{G_F}{\sqrt{2}} V_{ud} \bar{C}_i \ , \tag{5.6a}$$

$$\bar{C}_V = g_V \left(1 + \epsilon_L + \epsilon_R\right) \ , \tag{5.6b}$$

$$\bar{C}_A = -g_A \left(1 + \epsilon_L - \epsilon_R\right) \ , \tag{5.6c}$$

$$\bar{C}_S = g_S \, \epsilon_S \ , \tag{5.6d}$$

$$\bar{C}_T = 4 \, g_T \, \epsilon_T \ , \tag{5.6e}$$

with $C_i' = C_i$, since we only have left-handed neutrinos in our low-energy effective theory. Operators involving right-handed neutrinos do not interfere with the SM amplitude and therefore contribute at second order to all observables. Finally, notice that Ref. [102] defines the couplings $C_A, C'_{V,S,T}$ with an overall minus sign compared to ours.

5.2.1. Differential decay distribution

Including the effect of recoil corrections, radiative corrections, and BSM couplings, the differential decay rate for polarized neutrons reads [113, 114, 115, 116]:

$$\begin{aligned} \frac{d\Gamma}{dE_e d\Omega_e d\Omega_\nu} = \frac{(G_F^{(0)})^2 \, |V_{ud}|^2}{(2\pi)^5} \left(1 + 2\epsilon_L + 2\epsilon_R\right) \left(1 + 3\,\tilde{\lambda}^2\right) \times \\ \times w(E_e) \, D(E_e, \mathbf{p}_e, \mathbf{p}_\nu, \boldsymbol{\sigma}_n) \, , \end{aligned} \tag{5.7}$$

where $\mathbf{p}_e$ and $\mathbf{p}_\nu$ denote the electron and neutrino three-momenta, while $\boldsymbol{\sigma}_n$ denotes the neutron polarization. The bulk of the electron spectrum is described by:

$$w(E_e) = p_e E_e (E_0 - E_e)^2 \ F(Z = 1, E_e) \ \left(1 + \frac{\alpha}{2\pi} e_V^R + \frac{\alpha}{2\pi} \delta_\alpha^{(1)}(E_e)\right) \ , \tag{5.8}$$

where $E_0 = \Delta - (\Delta^2 - m_e^2)/(2M_n)$ (with $\Delta = M_n - M_p$) is the electron endpoint energy, m_e is the electron mass, and $F(Z, E_e)$ is the Fermi function that captures the Coulomb radiative corrections (Z denotes the charge of the daughter nucleus, which coincides with the proton in this case). The function $\delta_\alpha^{(1)}(E_e)$ [115, 116] captures model-independent ("outer") radiative corrections, while the coupling e_V^R is sensitive to the short-distance ("inner") radiative correction [117, 115]. The differential decay distribution function $D(E_e, \mathbf{p}_e, \mathbf{p}_\nu, \boldsymbol{\sigma}_n)$ is given by [115, 116]:

$$\begin{aligned} D(E_e, \mathbf{p}_e, \mathbf{p}_\nu, \boldsymbol{\sigma}_n) = 1 + c_0 + c_1 \frac{E_e}{M_N} + \frac{m_e}{E_e} \bar{b} + \bar{a}(E_e) \frac{\mathbf{p}_e \cdot \mathbf{p}_\nu}{E_e E_\nu} + \bar{A}(E_e) \frac{\boldsymbol{\sigma}_n \cdot \mathbf{p}_e}{E_e} \\ + \bar{B}(E_e) \frac{\boldsymbol{\sigma}_n \cdot \mathbf{p}_\nu}{E_\nu} + \bar{C}_{(aa)}(E_e) \left(\frac{\mathbf{p}_e \cdot \mathbf{p}_\nu}{E_e E_\nu}\right)^2 \\ + \bar{C}_{(aA)}(E_e) \frac{\mathbf{p}_e \cdot \mathbf{p}_\nu}{E_e E_\nu} \frac{\boldsymbol{\sigma}_n \cdot \mathbf{p}_e}{E_e} + \bar{C}_{(aB)}(E_e) \frac{\mathbf{p}_e \cdot \mathbf{p}_\nu}{E_e E_\nu} \frac{\boldsymbol{\sigma}_n \cdot \mathbf{p}_\nu}{E_\nu} \ , \end{aligned} \tag{5.9}$$

where $\bar{b}$ is an effective Fierz interference term and $\bar{a}(E_e)$, $\bar{A}(E_e)$, $\bar{B}(E_e)$ and $\bar{C}_{aa,aA,aB}(E_e)$ are effective energy-dependent correlation coefficients, whose full expressions [115, 116, 118] we report in Appendix A, where one can also find the coefficients $c_{0,1}$ generated by recoil corrections. In absence of radiative corrections, recoil corrections and BSM contributions, the effective correlation coefficients $\bar{a}(E_e)$, $\bar{A}(E_e)$ and $\bar{B}(E_e)$ reduce to the following well-known leading-order expressions:

$$\bar{a}(E_e) \to \frac{1-\lambda^2}{1+3\lambda^2} \ , \quad \bar{A}(E_e) \to \frac{2\lambda(1-\lambda)}{1+3\lambda^2} \ , \quad \bar{B}(E_e) \to \frac{2\lambda(1+\lambda)}{1+3\lambda^2} \ , \tag{5.10}$$

with the rest of coefficients $(c_{0,1}, \bar{b}, \bar{C}_{(aa,aA,aB)}(E_e))$ vanishing in this limit.

The impact of new-physics contributions can be summarized as follows:

- The effect of $\epsilon_{L/R}$ was already evident from the effective Lagrangian of Eq. 5.3: they induce (i) an overall correction proportional to $(1+2\epsilon_L+2\epsilon_R)$, and (ii) the shift $\lambda \to \tilde{\lambda} = \lambda(1-2\epsilon_R)$. As a consequence of this second effect, working to linear order in new-physics contributions, the measurements of different correlation coefficients by themselves cannot disentangle λ and ϵ_R; they simply provide independent measures of $\tilde{\lambda}$. In order to probe ϵ_R from correlation measurements, one needs to independently know g_A/g_V from LQCD calculations.

- The scalar and tensor interactions $\epsilon_{S,T}$ appear to linear order only through the Fierz interference term $\bar{b}$ and the analogue term b_ν in the neutrino-asymmetry parameter (b_ν is the part of $\bar{B}(E_e)$ proportional to m_e/E_e, see Appendix A for a precise definition):

$$b^{\rm BSM} = \frac{2}{1+3\lambda^2}\left[g_S\,\epsilon_S - 12\lambda\, g_T\,\epsilon_T\right] \approx 0.34\, g_S\,\epsilon_S - 5.22\, g_T\,\epsilon_T \ , \tag{5.11a}$$

$$b_\nu^{\rm BSM} = \frac{2}{1+3\lambda^2}\left[g_S\,\epsilon_S\,\lambda - 4 g_T\,\epsilon_T\,(1+2\lambda)\right] \approx 0.44\, g_S\,\epsilon_S - 4.85\, g_T\,\epsilon_T \ . \tag{5.11b}$$

  To the order we are working, in the above expressions we can use either λ or $\tilde{\lambda}$.

Experimentally, one can probe the new-physics contributions in $\tilde{\lambda}$, $b^{\rm BSM}$, and $b_\nu^{\rm BSM}$ through (i) measurements of the electron spectrum, aimed to isolate the term $\bar{b}$ in Eq. (5.9); or (ii) correlation measurements, aimed to isolate $\bar{a}(E_e)$, $\bar{A}(E_e)$, and $\bar{B}(E_e)$ in the same equation. Correlation measurements involve the construction of asymmetry ratios [114]. For example, in order to isolate $\bar{A}(E_e)$ one constructs the ratio $A_{\rm exp}(E_e) = (N_+(E_e) - N_-(E_e))/(N_+(E_e) + N_-(E_e))$ where $N_\pm(E_e)$ are the spectra corresponding to events with $\boldsymbol{\sigma}_n \cdot \mathbf{p}_e > 0$ and $\boldsymbol{\sigma}_n \cdot \mathbf{p}_e < 0$. Similarly,

in order to isolate $\bar{B}(E_e)$ one can use the simple ratio $B_{\rm exp}(E_e) = (Q_{++}(E_e) - Q_{--}(E_e))/(Q_{++}(E_e)+Q_{--}(E_e))$, where $Q_{++}(E_e)$ and $Q_{--}(E_e)$ are the spectra of events with $\boldsymbol{\sigma}_n\cdot\mathbf{p}_e > 0$, $\boldsymbol{\sigma}_n\cdot\mathbf{p}_p > 0$ and $\boldsymbol{\sigma}_n\cdot\mathbf{p}_e < 0$, $\boldsymbol{\sigma}_n\cdot\mathbf{p}_p < 0$, respectively. One can immediately see that through the total spectra in the denominator, both $A_{\rm exp}(E_e)$ and $B_{\rm exp}(E_e)$ are sensitive to the Fierz interference term $\bar{b}$, so that asymmetry measurements involving simple ratios as described above really measure:

$$\tilde{Y}(E_e) = \frac{\bar{Y}(E_e)}{1+\bar{b}\,m_e/E_e}\ , \tag{5.12}$$

where $Y \in \{A, B, a, ...\}$. Moreover, each individual experiment applies optimization cuts in E_e, thus mesuring a specific weighted average of Eq. (5.12).

The above observation has important consequences for the phenomenology of neutron decay:

- The m_e/E_e component of $B_{\rm exp}(E_e)$ is sensitive not to $b_\nu^{\rm BSM}$ but rather to the combination:

$$(1+3\lambda^2)/(2\lambda(1+\lambda))\, b_\nu^{\rm BSM} - b^{\rm BSM} \approx b_\nu^{\rm BSM} - b^{\rm BSM}\ . \tag{5.13}$$

  Besides $B_{\rm exp}(E_e)$, it might be possible to construct a set of observables that disentangle the contribution of $b^{\rm BSM}$ and $b_\nu^{\rm BSM}$. In this case the BSM sensitivity of $b_\nu^{\rm BSM}$ alone is of interest. In our phenomenological analysis we will study both cases (constraints from $b_\nu^{\rm BSM} - b^{\rm BSM}$ and $b_\nu^{\rm BSM}$).

- More generally, correlation coefficients measurements traditionally used to determine $\lambda = g_A/g_V$ within the SM ($\epsilon_{L/R} = 0, b = b_\nu = 0$), provide information on three independent parameters in our EFT setup: $\tilde{\lambda} = \lambda(1-2\epsilon_R)$, $b^{\rm BSM}$, and $b_\nu^{\rm BSM}$. In other words, if $\epsilon_{S,T}$ are larger than the experimental errors, one has to observe an unexpected energy dependence of the form m/E in the measurements of the correlation coefficients (in addition to the various expected energy dependences due to sub-leading standard effects that are detailed in Appendix A). Thus, for a certain energy, a determination of λ from $a(A)$ would be actually extracting the quantity:

$$\tilde{\lambda}\left(1 + n_{a(A)} b^{\rm BSM} m/E\right)\ , \tag{5.14}$$

  whereas in a B-based determination of λ, we would have:

$$\tilde{\lambda}\left(1 + n_B (b_\nu^{\rm BSM} - b^{\rm BSM}) m/E\right)\ , \tag{5.15}$$

  where:

$$\begin{aligned} n_a &= \frac{(1-\lambda^2)(1+3\lambda^2)}{8\lambda^2} \approx -0.28\ , \\ n_A &= -\frac{(1-\lambda)(1+3\lambda^2)}{(1+\lambda)(1-3\lambda)} \approx -0.25\ , \\ n_B &= \frac{(1+\lambda)(1+3\lambda^2)}{(1-\lambda)(1+3\lambda)} \approx -10.2\ . \end{aligned} \tag{5.16}$$

A fit to the current data [119, 120, 121, 122] (with precision $\delta A/A \sim 0.005$, $\delta a/a \sim 0.05$, $\delta B/B \sim 0.005$) yields $-0.3 < b^{\rm BSM}, b_\nu^{\rm BSM} < 0.5$ at the 95% C.L. [17], which, as we will see, is not competitive with other bounds. It will be interesting, however, to explore the implications of future experimental improvements in the combined extraction of $\tilde{\lambda}$, $b^{\rm BSM}$ and $b_\nu^{\rm BSM}$ from a, A, and B measurements, along the lines described in Refs. [17, 123].

The main conclusion from the above discussion is that measurements of the differential neutron-decay distribution are mostly sensitive to new physics through $b^{\rm BSM}$ and $b_\nu^{\rm BSM}$, which depend on the scalar and tensor couplings, ϵ_S and ϵ_T, to linear order. Therefore, apart from the next section, which we include for completeness, in the rest of this chapter we restrict our discussion on these exotic scalar and tensor interactions, comparing the physics reach of neutron decay to other low-energy and collider probes.

5.2.2. Total decay rate and determination of $|V_{ud}|$

For completeness, we discuss here the BSM corrections to the neutron decay rate and the extraction of $|V_{ud}|$ from neutron decay. Expressing $G_F^{(0)}$ in terms of the Fermi constant determined in muon decay G_μ (this involves non-standard contributions to the purely leptonic charged-current interaction encoded in the coefficient $\tilde{v}_L$ [71]) and performing the phase-space integrations, the total decay rate reads:

$$\Gamma = \frac{G_\mu^2 |V_{ud}|^2 m_e^5}{2\pi^3} \left(1 + 3\tilde{\lambda}^2\right) \cdot f \cdot (1 + \Delta_{\rm RC}) \left[1 + 2\epsilon_L - 2\tilde{v}_L + 2\epsilon_R + b^{\rm BSM} \frac{I_1(x_0)}{I_0(x_0)}\right] . \tag{5.17}$$

In the above expression, the corrections from BSM physics are encoded in $\tilde{\lambda}$ and the terms in square brackets. $\Delta_{\rm RC} = 3.90(8) \times 10^{-2}$ is the SM electroweak radiative correction [117], and the phase-space integrals are defined by:

$$I_k(x_0) = \int_1^{x_0} x^{1-k} \, (x_0 - x)^2 \, \sqrt{x^2 - 1} \, dx \; , \qquad\qquad f = I_0(x_0)(1 + \Delta_f) \; , \tag{5.18}$$

where $x_0 = E_0/m_e$ and Δ_f encodes Coulomb and recoil corrections that are numerically quite important, $I_0(x_0) = 1.629$, $f = 1.6887$, $I_1(x_0)/I_0(x_0) = 0.652$ (see Ref. [117] for details). In order to extract $|V_{ud}|$ from neutron decays one needs (see Eq. 5.17) experimental input on the neutron lifetime $1/\Gamma$ [124, 125] and $\tilde{\lambda}$, which is usually extracted from beta-asymmetry $A_{\rm exp}(E_e)$ measurements [119, 120] (after accounting for recoil and radiative corrections). Taking into account Eq. (5.12), the usual method for extracting $\tilde{\lambda}$ actually determines $\tilde{\lambda}\left(1 + c\, b^{\rm BSM}\right)$, where c is a certain $O(1)$ number that depends on the specific experimental analysis. In summary

what we really extract from neutron beta decay is not $|V_{ud}|$ but the combination:

$$|V_{ud}|^2\Big|_{n\to pe\bar{\nu}} = |V_{ud}|^2\left[1+2\epsilon_L-2\tilde{v}_L+2\epsilon_R+b^{\rm BSM}\left(\frac{I_1(x_0)}{I_0(x_0)}-\frac{6\lambda^2}{1+3\lambda^2}c\right)\right]$$
$$\approx |V_{ud}|^2\left[1+2\epsilon_L-2\tilde{v}_L+2\epsilon_R+b^{\rm BSM}\left(0.65-1.66\,c\right)\right]. \qquad (5.19)$$

5.3. Low-energy phenomenology of scalar and tensor interactions

5.3.1. Other probes of scalar and tensor interactions

In order to assess the discovery potential of experiments planning to measure $\bar{b}$ and $\tilde{B}$ at the level of 10^{-3} and 10^{-4}, it is crucial to identify existing constraints on new scalar and tensor operators. As we discuss below in some detail, the most stringent constraint on the scalar coupling ϵ_S arises from $0^+\to 0^+$ nuclear beta decays. On the other hand, the most stringent bound on the tensor effective coupling ϵ_T arises from the Dalitz-plot study of the radiative pion decay $\pi\to e\nu\gamma$. For completeness, we will also briefly review (i) constraints on $\epsilon_{S,T}$ from other nuclear beta-decay observables, showing that they are not competitive at the moment; and (ii) constraints on $\epsilon_{S,P,T}$ arising from the helicity-suppressed $\pi\to e\nu$ decay. As we will show, the latter provides potentially the strongest constraints on $\epsilon_{S,T}$, once the flavor structure of the underlying theory is known. This provides very stringent constraints on model building.

$0^+\to 0^+$ transitions and scalar interactions

At leading order within the SM and new physics, the differential decay rate for an unpolarized nucleus is [112]:

$$\frac{d\Gamma_{0^+\to 0^+}}{dE_e d\Omega_e d\Omega_\nu} = 2\frac{(G_F^{(0)})^2\,|V_{ud}|^2}{(2\pi)^5}\,(1+2\epsilon_L+2\epsilon_R)\;p_eE_e(\tilde{E}_0-E_e)^2F(-Z,E_e)$$
$$\times\left\{1+a_{0^+}\frac{\mathbf{p_e}\cdot\mathbf{p}_\nu}{E_eE_\nu}+b_{0^+}\frac{m_e}{E_e}\right\}, \qquad (5.20)$$

where $\tilde{E}_0=M_P-M_D$ is the electron endpoint energy expressed in terms of the masses of parent and daughter nuclei, $F(-Z,E_e)$ is the Fermi function, Z is the atomic number of the daughter nucleus (the minus sign applies to β^+ emitters for which the most precise measurements exist). For $0^+\to 0^+$ transitions the coefficients: a,b are

$$a_{0^+}=1\,, \qquad (5.21a)$$
$$b_{0^+}=-2\gamma\,g_S\,\epsilon_S \qquad \text{with} \quad \gamma=\sqrt{1-\alpha^2Z^2}\,, \qquad (5.21b)$$

and the total rate is given by:

$$\Gamma_{0^+\to 0^+} = \frac{G_\mu^2 |V_{ud}|^2 m_e^5}{\pi^3} f_{0^+\to 0^+} \left(1 + \Delta_{\rm RC}^{(0^+\to 0^+)}\right) \left[1 + 2\epsilon_L - 2\tilde{v}_L + 2\epsilon_R + b_{0^+} \frac{I_1(\tilde{x}_0)}{I_0(\tilde{x}_0)}\right] , \tag{5.22}$$

where $\tilde{x}_0 = \tilde{E}_0/m_e$. In this last expression, the SM sub-effects have been included through $\Delta_{\rm RC}^{(0^+\to 0^+)}$ and also inside $f_{0^+\to 0^+}$, that up to Coulomb, nuclear distortion and recoil effects, is $f_{0^+\to 0^+} = I_0(\tilde{x}_0)$, similarly to what happens in the neutron-decay case. The various radiative corrections (including $\Delta_{\rm RC}^{(0^+\to 0^+)}$) are discussed in detail in Refs. [126, 127]. Comparing the values of V_{ud} as extracted from neutron and nuclear decays, we find (see Eq. (5.19) and the preceding discussion):

$$\frac{|V_{ud}^{0^+\to 0^+}|^2}{|V_{ud}^{n\to pe\bar{\nu}}|^2} = 1 + b_{0^+}^{\rm BSM} \frac{I_1(\tilde{x}_0)}{I_0(\tilde{x}_0)} - b_n^{\rm BSM} \left(\frac{I_1(x_0)}{I_0(x_0)} - \frac{6\lambda^2}{1+3\lambda^2} c\right) , \tag{5.23}$$

which in principle provides another handle on scalar and tensor interactions.

Let us now come to the point of greatest interest for this paper's discussion. From a comparison of precisely known half-lives corrected by phase-space factors $f_{0^+\to 0^+}$, Hardy and Towner [127] found $b_{0^+} = -0.0022(26)$, which translates into the following bound on the product of nucleon scalar form factor and short-distance scalar coupling:

$$-1.0 \times 10^{-3} < g_S\, \epsilon_S < 3.2 \times 10^{-3} \qquad (90\%\ \text{C.L.}) . \tag{5.24}$$

This is the most stringent bound on scalar interactions from low-energy probes.

Radiative pion decay and the tensor interaction

An analysis of the Dalitz plot of the radiative pion decay $\pi^+ \to e^+\nu_e\gamma$ is sensitive to the same tensor operator that can be probed in beta decays. The experimental results from the PIBETA collaboration [128] put constraints on the product $\epsilon_T \times f_T$ of the short-distance coupling ϵ_T and the hadronic form factor f_T defined by [129]

$$\langle \gamma(\epsilon, p) | \bar{u}\sigma_{\mu\nu}\gamma_5 d | \pi^+ \rangle = -\frac{e}{2} f_T \, (p_\mu \epsilon_\nu - p_\nu \epsilon_\mu) , \tag{5.25}$$

where p_μ and ϵ_μ are the photon four-momentum and polarization vector, respectively. The analysis of Ref. [129], based on a large-N_c-inspired resonance-saturation model provides $f_T = 0.24(4)$ at the renormalization scale $\mu = 1$ GeV, with parametric uncertainty induced by the uncertainty in the quark condensate. The 90%-C.L. experimental constraint[4] $-2.0 \times 10^{-4} < \epsilon_T \times f_T < 2.6 \times 10^{-4}$, when combined with the above estimate for f_T run to 2 GeV implies:

$$-1.1 \times 10^{-3} < \epsilon_T < 1.36 \times 10^{-3} \qquad (90\%\ \text{C.L.}) . \tag{5.26}$$

[4]Note that there is a factor of 2 difference in the normalization of the tensor coupling ϵ_T compared to what was used in Refs. [105, 128].

Again, this is the most stringent constraint on the tensor coupling from low-energy experiments. The next best constraints, which we report in the next section, arise from measurements of nuclear beta decays.

Bounds on scalar and tensor structures from other nuclear beta decays

Bounds on scalar and tensor interactions can be obtained from a number of observables in nuclear beta decays, other than $0^+ \to 0^+$ transitions. Although these bounds are currently not competitive, we summarize them here for completeness.

The leading sensitivity to scalar and tensor operators appears through the Fierz interference term b, which in the limit of pure Gamow-Teller transitions is proportional to the tensor coupling ($b_{\rm GT} = -(8\gamma g_T \epsilon_T)/\lambda$), while in pure Fermi transitions is proportional to the scalar coupling ($b_{\rm F} = 2\gamma g_S \epsilon_S$). Significant constraints on b arise from electron-polarization observables [112] as well as in measurements of $\tilde{A}$ and $\tilde{a}$ in both Fermi and Gamow-Teller transitions. Here is a summary of current bounds on $\epsilon_{S,T}$:

- The most stringent constraint from the beta asymmetry in pure Gamow-Teller transitions ($\tilde{A}_{\rm GT}$) arises from ^{60}Co measurements and implies [130]

$$-2.9\times10^{-3} \;<\; g_T\,\epsilon_T \;<\; 1.5\times10^{-2} \qquad (90\%\ \text{C.L.})\ . \tag{5.27}$$

  Similar bounds can be obtained from measurements of $\tilde{A}_{\rm GT}$ in ^{114}In decay [131]: $-2.2\times10^{-2} \;<\; g_T\,\epsilon_T \;<\; 1.3\times10^{-2}$ (90 % C.L.).

- Measurements of the ratio $P_{\rm F}/P_{\rm GT}$ of longitudinal polarization in the positron emitted in pure Fermi and Gamow-Teller transitions [132, 133] imply:

$$-0.76\times10^{-2} \;<\; g_S\,\epsilon_S + \frac{4}{\lambda} g_T\,\epsilon_T \;<\; 1.0\times10^{-2} \qquad (90\%\ \text{C.L.})\ . \tag{5.28}$$

- Preliminary results have been reported on the measurement of the longitudinal polarization of positrons emitted by polarized ^{107}In nuclei [134]. The corresponding 90 % C.L. sensitivity to tensor interactions, $|g_T\,\epsilon_T| < 3.1\times10^{-3}$, is quite promising although not yet competitive with the radiative pion decay.

- Finally, the beta-neutrino correlation a has been measured in a number of nuclear transitions [135, 136, 137, 138]. The resulting constraints on scalar and tensor interactions are nicely summarized in Figure 7 of Ref. [135]. In terms of the coupling constants used here, the 90 % C.L. combined bound on the tensor interaction reads $|g_T\,\epsilon_T| < 5\times10^{-3}$, again not competitive with the radiative pion decay.

We observe that in order to improve on the existing bound on ϵ_T from $\pi \to e\nu\gamma$, future measurements sensitive to $b_{\rm GT}$ should aim at sensitivities of $\delta b_{\rm GT} \lesssim 6.3 \times g_T \times 10^{-3}$. For example, a 10^{-3} measurement of $b_{\rm GT}$ would probe $g_T\epsilon_T$ at the 2×10^{-4}-level, providing a very competitive bound.

Constraints on $\epsilon_{S,P,T}$ from $\pi \to e\nu$

The ratio $R_\pi \equiv \Gamma(\pi \to e\nu[\gamma])/\Gamma(\pi \to \mu\nu[\gamma])$ probes more than just the effective low-energy pseudoscalar coupling ϵ_P defined earlier as the coefficient of the operator $\bar{e}(1-\gamma_5)\nu_e \cdot \bar{u}\gamma_5 d$. In fact, since (i) R_π is defined as the ratio of electron-to-muon decay and (ii) the neutrino flavor in both the decays is not observed, this observable is sensitive to the whole set of parameters $\epsilon_P^{\alpha\beta}$ defined by:

$$\mathcal{L}_{\text{eff}} \quad \supset \quad \frac{G_F}{\sqrt{2}} V_{ud}\, \epsilon_P^{\alpha\beta} \;\; \bar{e}_\alpha(1-\gamma_5)\nu_\beta \cdot \bar{u}\gamma_5 d \;, \tag{5.29}$$

where $\alpha \in \{e, \mu\}$ refers to the flavor of the charged lepton and $\beta \in \{e, \mu, \tau\}$ refers to the neutrino flavor. One generically expects SM extensions to generate non-diagonal components in $\epsilon_{P,S,T}^{\alpha\beta}$, In the new notation the previously defined pseudoscalar, scalar, and tensor couplings reads $\epsilon_{P,S,T} \equiv \epsilon_{P,S,T}^{ee}$. It is important to note here that only ϵ_P^{ee} and $\epsilon_P^{\mu\mu}$ can interfere with the SM amplitudes, while the remaining $\epsilon_P^{\alpha\beta}$ contribute incoherently to both the numerator and denominator in R_π.[5] In summary, allowing for non-standard interactions and factoring out the SM prediction for R_π, one can write:

$$\frac{R_\pi}{R_\pi^{\text{SM}}} = \frac{\left[\left(1 - \frac{B_0}{m_e}\epsilon_P^{ee}\right)^2 + \left(\frac{B_0}{m_e}\epsilon_P^{e\mu}\right)^2 + \left(\frac{B_0}{m_e}\epsilon_P^{e\tau}\right)^2\right]}{\left[\left(1 - \frac{B_0}{m_\mu}\epsilon_P^{\mu\mu}\right)^2 + \left(\frac{B_0}{m_\mu}\epsilon_P^{\mu e}\right)^2 + \left(\frac{B_0}{m_\mu}\epsilon_P^{\mu\tau}\right)^2\right]} \;. \tag{5.30}$$

Here we are neglecting the overall effect of $v_{L/R}$, not enhanced by helicity arguments. In the above equation the factors of $B_0/m_{e,\mu}\epsilon_P$ represent the ratio of new-physics amplitude over SM amplitude. The latter is proportional to the charged-lepton mass due to angular-momentum conservation arguments, while the former is proportional to $\langle 0|\bar{u}\gamma_5 d|\pi\rangle$, characterized by the scale- and scheme-dependent parameter:

$$B_0(\mu) \equiv \frac{M_\pi^2}{m_u(\mu) + m_d(\mu)} \;. \tag{5.31}$$

Note that the scale and scheme dependence of $B_0(\mu)$ is compensated in physical quantities by the scale and scheme dependence of the Wilson coefficients $\epsilon_P^{\alpha\beta}$. Since $B_0^{\overline{\text{MS}}}(\mu = 1\ \text{GeV}) = 1.85\,\text{GeV}$ and consequently $B_0/m_e = 3.6 \times 10^3$, R_π has enhanced sensitivity to $\epsilon_P^{\alpha\beta}$, and one needs to keep quadratic terms in these new physics coefficients. This feature is specific to purely leptonic decays of pseudoscalar mesons. In beta decays one never encounters relative enhancement factors such as B/m_e, because ϵ_P is always multiplied by nucleon velocity factors and the SM

[5] While in our setup the incoherent contribution arises from "wrong-flavor" neutrinos, in general it could have a different nature. For example, the incoherent contribution to R_π discussed in Refs. [105, 102] is due to a right-handed light neutrino.

amplitude does not suffer anomalous suppression (as the helicity argument implies in the case of $\pi \to e\nu$).

Inspection of Eq. (5.30) reveals that if the new-physics couplings respect $\epsilon_P^{e\alpha}/m_e = \epsilon_P^{\mu\alpha}/m_\mu$, then $R_\pi/R_\pi^{\rm SM} = 1$, and there are no constraints on these couplings. On the other hand, if the effective couplings $\epsilon_P^{\alpha\beta}$ are all of similar size, one can neglect the entire denominator in Eq. (5.30), as it is suppressed with respect to the numerator by powers of m_e/m_μ. We will assume to be in this second scenario. In this case the constraint in Eq. (5.30) forces the couplings $\epsilon_P^{ee}, \epsilon_P^{e\mu}, \epsilon_P^{e\tau}$ to live in a spherical shell of radius $m_e/B_0\sqrt{R_\pi^{\rm exp}/R_\pi^{\rm SM}} \approx 2.75 \times 10^{-4}$ centered at $\epsilon_P^{ee} = m_e/B_0 \approx 2.75 \times 10^{-4}$, $\epsilon_P^{e\mu} = \epsilon_P^{e\tau} = 0$. The thickness of the shell is numerically 1.38×10^{-6} and is determined by the current combined uncertainty in $R_\pi^{\rm exp}$ [139, 140] and $R_\pi^{\rm SM}$ [141, 142]: $R_\pi^{\rm exp}/R_\pi^{\rm SM} = 0.996(5)$ (90% C.L.). This is illustrated in Figure 5.1, where we plot the allowed region in the two-dimensional plane given by ϵ_P^{ee} and a generic "wrong-flavor" coupling denoted by ϵ_P^{ex}. Note that the allowed region is given by the thickness of the curve in the figure, thus enforcing a strong correlation between ϵ_P^{ee} and ϵ_P^{ex}. Since $\epsilon_P^{\alpha\neq\beta}$ are essentially unconstrained by other measurements and can be of order 10^{-3}, we can marginalize over either one of the couplings to obtain a bound on the other. The resulting 90%-C.L. bounds are:

$$-1.4 \times 10^{-7} < \epsilon_P^{ee} < 5.5 \times 10^{-4} \,, \tag{5.32}$$

or, if $\alpha \neq e$

$$-2.75 \times 10^{-4} < \epsilon_P^{e\alpha} < 2.75 \times 10^{-4} \quad (\alpha \neq e) \,, \tag{5.33}$$

in qualitative agreement with the findings of Refs. [105, 102].

As originally discussed in Refs. [104, 105, 106], the pseudoscalar coupling ϵ_P^{ee} can be radiatively generated starting from nonzero $\epsilon_{S,T}$. Hence, the stringent constraint in Eq. (5.32) puts constraints on the same $\epsilon_{S,T}$ that can be probed in beta decays. The physics of this effect is very simple: once the scalar, pseudoscalar, and tensor operators are generated by some non-standard physics at the matching scale Λ, electroweak radiative corrections induce mixing among these three operators. So even if one engineers a small pseudoscalar contribution $\epsilon_P(\Lambda)$ at the matching scale, known SM physics generates a nonzero $\epsilon_P(\mu)$ at some lower energy scale μ via loop diagrams. The general form of the constraint can be worked out by using

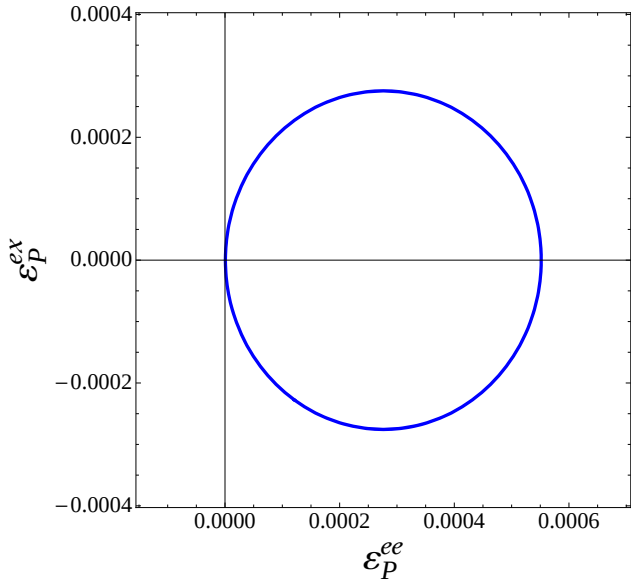

Figure 5.1: The allowed region in the two-dimensional plane ϵ_P^{ee}-ϵ_P^{ex} determined by R_π is given by an annulus of thickness 1.38×10^{-6}. In the absence of information on ϵ_P^{ex}, the 90 % C.L. bound on ϵ_P^{ee} is $-1.4 \times 10^{-7} < \epsilon_P^{ee} < 5.5 \times 10^{-4}$.

the three-operator mixing results from Ref. [106][6]. The leading-order result is:

$$\epsilon_P^{\alpha\beta}(\mu) = \epsilon_P^{\alpha\beta}(\Lambda)\left(1 + \gamma_{PP}\,\log\frac{\Lambda}{\mu}\right) + \epsilon_S^{\alpha\beta}(\Lambda)\,\gamma_{SP}\,\log\frac{\Lambda}{\mu} + \epsilon_T^{\alpha\beta}(\Lambda)\,\gamma_{TP}\,\log\frac{\Lambda}{\mu}\,, \tag{5.34a}$$

$$\gamma_{PP} = \frac{3}{4}\frac{\alpha_2}{\pi} + \frac{113}{72}\frac{\alpha_1}{\pi} \approx 1.3 \times 10^{-2}\,, \tag{5.34b}$$

$$\gamma_{SP} = \frac{15}{72}\frac{\alpha_1}{\pi} \approx 6.7 \times 10^{-4}\,, \tag{5.34c}$$

$$\gamma_{TP} = -\frac{9}{2}\frac{\alpha_2}{\pi} - \frac{15}{2}\frac{\alpha_1}{\pi} \approx -7.3 \times 10^{-2}\,, \tag{5.34d}$$

where $\alpha_1 = \alpha/\cos^2\theta_W$ and $\alpha_2 = \alpha/\sin^2\theta_W$ are the $U(1)$ and $SU(2)$ weak couplings, expressed in terms of the fine-structure constant and the weak mixing angle. Setting $\epsilon_P^{ee}(\Lambda) = 0$ and neglecting the small $O(\alpha/\pi)$ fractional difference between $\epsilon_{S,T}(\Lambda)$ and the observable $\epsilon_{S,T}(\mu)$ at the low scale, the 90% C.L. constraint on the ϵ_S-ϵ_T plane reads

$$\frac{-1.4 \times 10^{-7}}{\log(\Lambda/\mu)} \;<\; \gamma_{SP}\,\epsilon_S \;+\; \gamma_{TP}\,\epsilon_T \;<\; \frac{5.5 \times 10^{-4}}{\log(\Lambda/\mu)}\,. \tag{5.35}$$

[6]The authors of Ref. [106] focused only on the phenomenology of scalar-to-pseudoscalar mixing.

Even assuming $\log(\Lambda/\mu) \sim 10$ (e.g. $\Lambda \sim 10\,\text{TeV}$ and $\mu \sim 1\,\text{GeV}$), using the numerical values of $\gamma_{SP,TP}$, one can verify that the individual constraints are at the level of $|\epsilon_S| \lesssim 8 \times 10^{-2}$ and $|\epsilon_T| \lesssim 10^{-3}$, implying that this constraint on ϵ_T is roughly equivalent to the one arising from $\pi \to e\nu\gamma$. Of course, these bounds become logarithmically more stringent as the new-physics scale Λ grows.

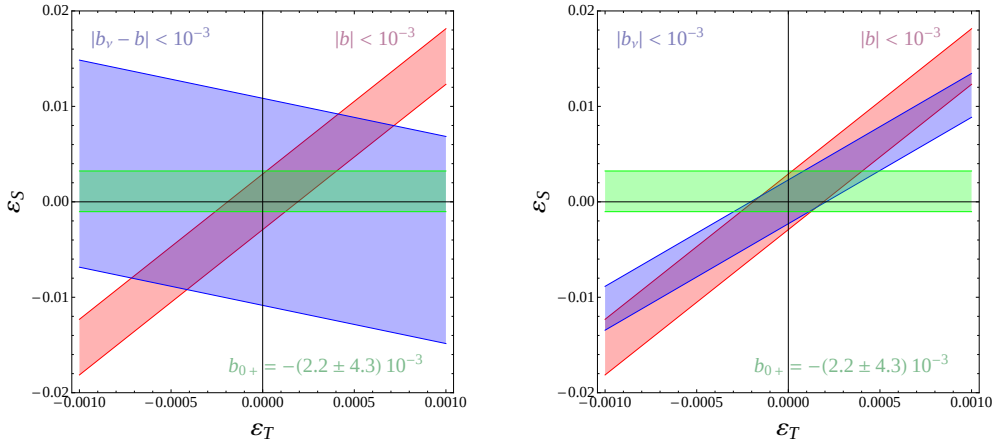

Figure 5.2: 90% C.L. allowed regions in the ϵ_S-ϵ_T plane implied by (i) the existing bound on b_{0+} (green horizontal band); (ii) projected 10^{-3}-level limits on b (red band), $b_\nu - b$ (blue band, left panel), and b_ν (blue band, right panel). The hadronic form factors are taken to be $g_S = g_T = 1$ in the ideal scenario of no uncertainty. The impact of hadronic uncertainties is discussed in Section 5.5.

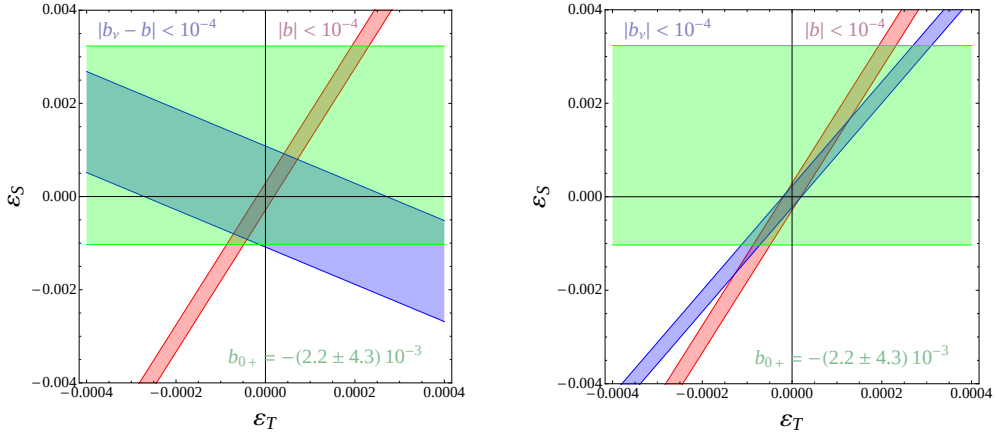

Figure 5.3: 90% C.L. allowed regions in the ϵ_S-ϵ_T plane implied by (i) the existing bound on b_{0+} (green horizontal band); (ii) projected 10^{-4}-level limits on b (red band), $b_\nu - b$ (blue band, left panel), and b_ν (blue band, right panel). The hadronic form factors are taken to be $g_S = g_T = 1$ in the ideal scenario of no uncertainty. The impact of hadronic uncertainties is discussed in Section 5.5.

5.3.2. The impact of future b and B neutron measurements

The discussion in the preceding subsection has shown that currently the most stringent low-energy constraints on novel scalar and tensor interactions arise, respectively, from the Fierz interference term in $0^+ \to 0^+$ nuclear beta decays (Eq. (5.24)) and from the radiative pion decay $\pi \to e\nu\gamma$ (Eq. (5.26)). It is important to realize that the allowed ϵ_S interval derived from Eq. (5.24) depends on the nucleon form factor g_S (as do all the constraints arising from neutron and nuclear beta decays). For a given experimental accuracy, the constraint on the short-distance couplings $\epsilon_{S,T}$ becomes stronger as $\delta g_{S,T}/g_{S,T} \to 0$. In this section, we will first explore the maximal constraining power of nuclear and neutron measurements in the ideal scenario of *no uncertainty* on $g_{S,T}$, and for illustrative purposes we assume the central values $g_S = g_T = 1$. We will quantify the implications of finite uncertainties on $g_{S,T}$ on the $\epsilon_{S,T}$ constraints in Section 5.5.

With the above assumptions on $g_{S,T}$, the currently allowed region (at 90% C.L.) on the ϵ_S-ϵ_T plane is given by the green horizontal band in Figures 5.2 and 5.3. The vertical (ϵ_S) boundaries of this region are determined by the constraint from b_{0^+}, while essentially the entire horizontal (ϵ_T) range on the scale of these plots is allowed by the $\pi \to e\nu\gamma$ limit (see Eq. (5.26)).

In this ideal scenario of no uncertainty on $g_{S,T}$, we can quantify the impact of future neutron measurements by plotting the 90% C.L. allowed region in the ϵ_S-ϵ_T plane implied by projected limits on b, $b_\nu - b$, and b_ν. The neutron constraints are derived using Eqs. (5.11) and in generating the plots we use the central value $\lambda = 1.269$. In Figure 5.2 we focus on the case in which the experimental sensitivity on b, $b_\nu - b$, and b_ν is at the 10^{-3} level. In the left panel we show the constraints from the existing b_{0^+} limit (green horizontal band) and 10^{-3}-level limits on b and $b_\nu - b$, (red and blue bands, respectively). In the right panel we replace the 10^{-3}-level limit on $b_\nu - b$ with the 10^{-3} limit on b_ν, which in principle can be isolated experimentally [143]. In Figure 5.3 we plot the constraints resulting from projected limits on b, $b_\nu - b$, and b_ν at the 10^{-4} level. The intersection of the various bands in Figures 5.2 and 5.3 denotes the combined allowed region in the ϵ_S-ϵ_T plane that would result after future neutron measurements. Two important remarks are in order here:

- For a given experimental sensitivity, the combination $b_\nu - b$ gives weaker constraints on $\epsilon_{S,T}$ than b or b_ν. This is easily understood: by taking the difference of Eqs. (5.11) one sees that $b_\nu - b \propto \lambda - 1$, which for $\lambda \approx 1.27$ provides a suppression factor.

- There is an almost exact “degeneracy" in the constraints from b and b_ν, again controlled by the form of Eqs. (5.11) and the numerical value of λ. For the purposes of constraining $\epsilon_{S,T}$, an upper limit on b is essentially equivalent to an upper limit on b_ν. This provides strong motivation to pursue exper-

imental determinations of both $b_\nu - b$ and b_ν via neutrino asymmetry (B) measurements. From the theoretical point of view, we can use either b or b_ν, and in subsequent sections we will use b for illustrative purposes.

Figure 5.2 clearly illustrates that with experimental sensitivity in neutron decay at the 10^{-3} level, the most stringent constraint arises from a combination of b_{0^+} and b or b_{0^+} and b_ν. The complementarity of these measurements would lead to a significant (four-fold) improvement in the bound on ϵ_T, compared to Eq. (5.26). The impact of 10^{-4} measurements of b, b_ν, and $b_\nu - b$ in neutron decay is even more dramatic (Figure 5.3), as in that case the constraint from b_{0^+} would become irrelevant and the combination of b and $b_\nu - b$ or b and b_ν would imply an improvement of one order of magnitude in the bound on ϵ_T and a factor of two in ϵ_S.

In Section 5.5 we will revisit the impact of proposed neutron measurements on $\epsilon_{S,T}$ in light of nonzero uncertainties in the hadronic matrix elements $g_{S,T}$.

5.4. Lattice calculation of matrix elements

To connect the measurements of b and b_ν in neutron decays to new physics at the TeV scale requires precision measurements of the matrix elements of isovector bilinear quark operators (the scalar operator $\bar{u}d$ and the tensor operator $\bar{u}\sigma_{\mu\nu}d$) between an initial neutron and final proton state, in particular of the scalar and tensor operators. Lattice QCD is a path-integral formulation of QCD on a discrete, four-dimensional Euclidean spacetime, and numerical simulations of it provide the best nonperturbative method for evaluating these matrix elements. It has been successfully employed to calculate hadron masses and their decay properties, such as matrix elements, with control over statistical and all systematic errors, in many cases at higher precision than can be measured experimentally [144, 145].

To obtain continuum results, estimates from LQCD obtained at a number of values of lattice spacing a and spacetime volume $L^3 \times T$ are extrapolated to $a \to 0$ and $L \to \infty$ to eliminate the artifacts introduced by formulating QCD in a finite discretized box. Another source of systematic uncertainty is introduced when estimates obtained at multiple values of u and d quark masses heavier than in nature are extrapolated to the physical point. One typically uses chiral perturbation theory to carry out this extrapolation, with low-energy constants determined by over-constraining the fits using experimental and lattice data [146]. Current state-of-the-art simulations are beginning to provide results at physical light-quark masses obviating the need for a chiral extrapolation.

A lattice calculation proceeds in two steps: First, a Monte-Carlo sampling of the QCD vacuum, called an "ensemble of gauge-field configurations", is generated using an appropriate discretization of the gauge and fermion actions. The particular choices of the actions have important implications for the computational cost of the calculation, for the size of the discretization errors and for which symmetries are violated at finite lattice spacing. The second step is to calculate expectation

values on these ensembles of gauge configurations and from these extract estimates of the desired observables.

It is interesting to stress that the matrix elements we are looking at have some simplifying features that allow us to make certain approximations:

- Current lattice simulations are done with degenerate u, d quarks, at zero momentum transfer, and do not include electromagnetic effects. The momentum transfer in neutron decay, $q^2 = 1.7$ MeV^2 is sufficiently small that the matrix elements can be calculated at $q_\mu = 0$. Also, the isospin-breaking and electromagnetic contributions are expected to be smaller than the statistical errors;

- Protons and neutrons are both stable asymptotic states of strong interactions, so there are no other hadronic final states that complicate the calculations.

Based on the analysis presented in [18], preliminary LQCD estimates are:

$$g_T(\overline{\rm MS}, \mu{=}2\,{\rm GeV}) = 1.05(35)\,, \qquad g_S(\overline{\rm MS}, \mu{=}2\,{\rm GeV}) = 0.8(4). \tag{5.36}$$

These values are used in the next section to explore bounds on new physics at the TeV scale. We emphasize that our focus at this point, given the preliminary nature of the estimates, is on the variation in the bounds under different scenarios of reduction of errors in lattice calculations.

5.5. Impact of lattice results on phenomenology

In Section 5.3.2, while studying the low-energy phenomenology of $\epsilon_{S,T}$, we ignored the uncertainty in the charges $g_{S,T}$. Clearly, the impact on $\epsilon_{S,T}$ of future 10^{-3}-level neutron measurements of b, b_ν, and $b_\nu - b$ depends on how well we know the nucleon matrix elements $g_{S,T}$. Since $g_{S,T}$ always multiply factors of the short-distance couplings in physical amplitudes, they determine the slope of the bands on the ϵ_S-ϵ_T plane represented in Figures 5.2 and 5.3. Moreover, if one accounts for the uncertainty in $g_{S,T}$ the bands Figures 5.2 and 5.3 acquire additional theory-induced thickness and their boundaries are mapped into characteristic "bow-tie" shapes. We illustrate this in Figure 5.4, assuming experimental sensitivities in b and $b_\nu - b$ at the 10^{-3} level. For the scalar and tensor charges we use in the left panel the ranges quoted in Ref. [102] (based on earlier quark-model estimates): $0.25 < g_S < 1.0$, $0.6 < g_T < 2.3$; while in the right panel we use the lattice estimates in Eq. (5.36) $g_S = 0.8(4)$ and $g_T = 1.05(35)$, corresponding to $\delta g_S/g_S \sim 50\%$ and $\delta g_T/g_T \sim 35\%$. Comparing these plots to the ones in Figure 5.2 the loss of constraining power is quite evident. Especially in the left panel one sees that the impact of neutron measurements is greatly diluted.

In Figure 5.5 we summarize the low-energy constraints on $\epsilon_{S,T}$, taking into account the effects of hadronic uncertainties. We plot the combined 90% C.L. regions in the ϵ_S-ϵ_T plane allowed by the current limit on b_{0^+} and future 10^{-3}-level measurements of b and $b_\nu - b$ in neutron decay. The different curves reflect four different scenarios for the hadronic matrix elements: the outer-most curve corresponds the range of Ref. [102], while the three inner curves correspond to lattice results with current central values from Eq. (5.36) and three different uncertainties: $\delta g_S/g_S \in \{50\%, 20\%, 10\%\}$ with $\delta g_T/g_T = 2/3\ \delta g_S/g_S$ (this choice assumes that the ratio of fractional uncertainties in g_S and g_T will remain approximately constant as these uncertainties decrease).

The confidence intervals on $\epsilon_{S,T}$ are obtained using the so-called R-Fit method, as described in Ref. [147]. In this approach the QCD parameters $g_{S,T}$ are bound to remain within allowed ranges determined by the lattice calculations and estimates of systematic uncertainties (in the case at hand the ranges are $0.4 \leq g_S \leq 1.2$ and $0.7 \leq g_T \leq 1.4$). The chi-squared function

$$\chi^2(\epsilon_S, \epsilon_T, g_S, g_T) = \sum_{i=1}^{N_{\rm obs}} \left(\frac{O_i^{\rm exp} - O_i^{\rm th}(\epsilon_S, \epsilon_T, g_S, g_T)}{\sigma_i^{\rm exp}} \right)^2 , \tag{5.37}$$

is then minimized with respect to $g_{S,T}$ (varying $g_{S,T}$ in their allowed ranges), leading to

$$\bar{\chi}^2(\epsilon_S, \epsilon_T) = \min_{g_{S,T}}\ \chi^2(\epsilon_S, \epsilon_T, g_S, g_T)\ . \tag{5.38}$$

Finally, the confidence intervals on $\epsilon_{S,T}$ are deduced applying the standard procedure [38] to $\bar{\chi}^2(\epsilon_S, \epsilon_T)$, with an effective number of degrees of freedom given by

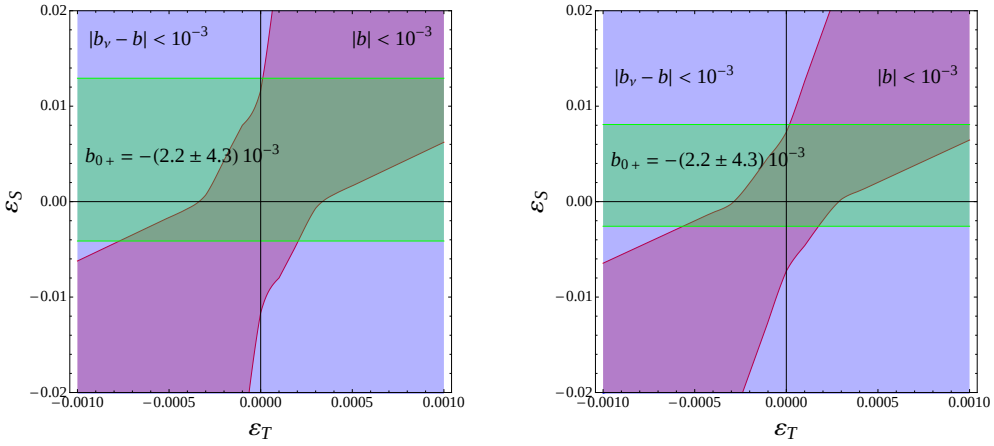

Figure 5.4: Left panel: 90% C.L. allowed regions in the ϵ_S-ϵ_T plane implied by (i) the existing bound on b_{0^+} (green horizontal band); (ii) projected measurements of b and $b_\nu - b$ in neutron decay (red and blue bow-tie shapes) at the 10^{-3} level; (iii) hadronic matrix elements taken in the ranges $0.25 < g_S < 1.0$, $0.6 < g_T < 2.3$ [102]. Right panel: same as left panel but with scalar and tensor charges taken from lattice QCD: $g_S = 0.8(4)$ and $g_T = 1.05(35)$. The effective couplings $\epsilon_{S,T}$ are defined in the $\overline{\rm MS}$ scheme at 2 GeV.

$\min(N_{\rm obs} - N_g, N_\epsilon)$, where $N_{\rm obs}$ is the number of experimental constraints, $N_g = 2$ is the number of QCD parameters ($g_{S,T}$), and $N_\epsilon = 2$ is the number of parameters we wish to constrain ($\epsilon_{S,T}$).

From Figure 5.5 several clear messages emerge:

- Hadronic uncertainties in $g_{S,T}$ strongly dilute the significance of new 10^{-3}-level experiments. Experimental progress without theoretical progress will not lead to competitive constraints on the short-distance scalar and tensor interactions.
- Our preliminary lattice results (curve labeled by $\delta g_S/g_S = 50\%$) already provide a significant improvement over previous knowledge of $g_{S,T}$ summarized in Ref. [102].
- In order to fully exploit the constraining power of planned 10^{-3} measurements of b and b_ν, the uncertainty on g_S should be reduced to 20%. Improvement beyond this level would not significantly increase the constraining power (see difference between the curves labeled as $\delta g_S/g_S = 20\%$ and $\delta g_S/g_S = 10\%$).

5.6. Collider limits

The contact interactions probed at low energy can also be directly probed at high-energy colliders. The rate, however, depends on whether the particles that generate the 4-fermi interaction are kinematically accessible at the collider energies. We begin in Section 5.6.1 under the assumption that the scalar and tensor interactions remain point-like at TeV scale energies. Then in Section 5.6.2 we derive a relation between ϵ_S and the production cross-section, Eq. 5.52 , when the scalar interaction is generated by the exchange of a resonance that is kinematically accessible at the LHC.

5.6.1. Model-independent limits

Assuming that the scalar and tensor interactions remain point-like at TeV-scale energies, we can employ the operator formalism to put bounds on $\epsilon_{S,T,P}$ from collider physics. $SU(2)$ gauge invariance implies that $\epsilon_{S,T,P}$ control not only charged-currrent processes but also the corresponding neutral-current versions, as the weak-scale effective Lagrangian includes terms proportional to $(\epsilon_S - \epsilon_P)\bar{e}_R e_L \bar{d}_L d_R$, $(\epsilon_S + \epsilon_P)\bar{e}_R e_L \bar{u}_R u_L$, and $\epsilon_T \bar{e}_R \sigma^{\mu\nu} e_L \bar{u}_R \sigma_{\mu\nu} u_L$. Exploiting this property, from an early CDF analysis [148] of contact interactions in $p\bar{p} \to e^+e^- + X$, after matching the different conventions for the effective couplings, we obtain the 90% C.L. limit $|\epsilon_S| < 0.135$. There are a number of LHC searches for contact interactions, specifically in dijet [149, 150, 151] and dimuon [152] final states. All of these studies,

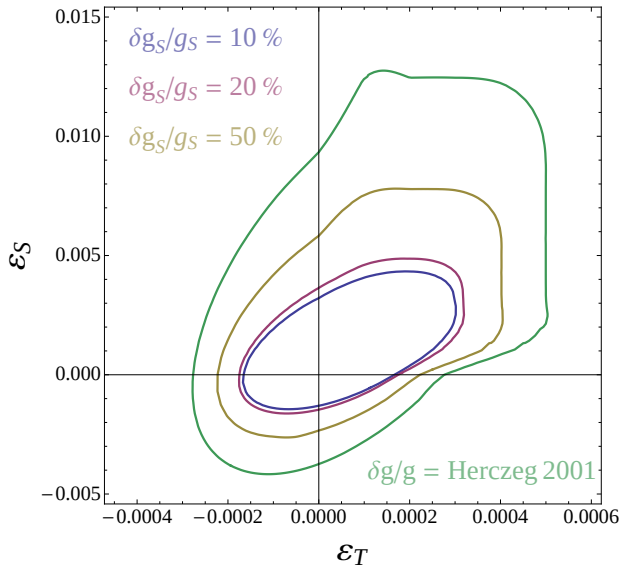

Figure 5.5: Combined 90% C.L. allowed regions in the ϵ_S-ϵ_T plane based on: (i) existing limit on b_{0^+} from $0^+ \to 0^+$ nuclear decays; (ii) future neutron decay measurements with projected sensitivity of 10^{-3} in b and $b_\nu - b$. The four curves correspond to four different scenarios for the hadronic matrix elements: $0.25 < g_S < 1.0$, $0.6 < g_T < 2.3$ as quoted in Ref. [102]; lattice results with current central values from Eq. (5.36) and $\delta g_S/g_S = 50\%, 20\%, 10\%$ with $\delta g_T/g_T = 2/3\ \delta g_S/g_S$ (this choice assumes that the ratio of fractional uncertainties in g_S and g_T will remain approximately constant as these uncertainties decrease). The effective couplings $\epsilon_{S,T}$ are defined in the $\overline{\text{MS}}$ scheme at 2 GeV.

however, focus only on specific vector-like interactions and do not consider scalar (i.e, helicity flipping) contact interactions.

Here we focus for definiteness on the charged-current part of the scalar and tensor effective operators. These contact interactions fall into the signature class of collider searches for an exotic W' gauge boson, since they both can contribute to the signature $pp \to e\nu + X$. We will use the analyses and results of searches for this process to obtain bounds on ϵ_S and ϵ_T. In the limit $m_l = 0$ the analysis is simplified, since these operators do not interfere with SM processes. We do include the interference between the scalar and tensor interactions, which does not vanish in the chiral limit. The relevant part of the effective Lagrangian is given by

$$\mathcal{L} = -\frac{\eta_S}{\Lambda_S^2} V_{ud}(\overline{u}d)(\overline{e}P_L\nu_e) - \frac{\eta_T}{\Lambda_T^2} V_{ud}(\overline{u}\sigma^{\mu\nu}P_L d)(\overline{e}\sigma_{\mu\nu}P_L\nu_e)\ , \tag{5.39}$$

where $\sigma^{\mu\nu} = i[\gamma^\mu, \gamma^\nu]/2$, and $\eta_S, \eta_T = \pm$ denotes the sign of the coefficients of the scalar and tensor operators. The relations between $\Lambda_{S,T}$ and the effective couplings $\epsilon_{S,T}$ at $\mu = 1$ TeV are given by $\epsilon_S \equiv 2\eta_S v^2/\Lambda_S^2$ and $\epsilon_T \equiv \eta_T v^2/\Lambda_T^2$. Note that since collider searches set limits on the effective couplings $\epsilon_{S,T}$ at the high renormalization scale $\mu = 1$ TeV, a direct comparison with the low-energy

constraints requires an appropriate rescaling down to the hadronic scale. Using the one-loop anomalous dimensions for scalar and tensor operators (see [153] and references therein), the one-loop beta function for the strong coupling constant, and including the appropriate heavy quark thresholds, we find in the $\overline{\rm MS}$ scheme $\epsilon_S(1\ {\rm TeV})/\epsilon_S(2\ {\rm GeV}) = 0.56$ and $\epsilon_T(1\ {\rm TeV})/\epsilon_T(2\ {\rm GeV}) = 1.21$. We will use these factors to rescale the collider limits and compare them to low-energy limits in Figures 5.6 and 5.7.

To determine the transverse mass distribution of the electron–neutrino pair we start with [154]

$$\frac{d^3\sigma}{dy\ dy'\ dm_T^2} = \frac{1}{64\pi s^2}\sum_{ij}\frac{f_i(x_1)}{x_1}\frac{f_j(x_2)}{x_2}\langle|\mathcal{M}|^2\rangle\ , \tag{5.40}$$

where i and j are summed over the initial partons (with parton distribution functions (PDF) $f_{i,j}$ and momentum fractions $x_{1,2}$), and y, y' are the rapidities of the electron and neutrino. One finds $x_1 = m_T(e^y+e^{y'})/2\sqrt{s}$, $x_2 = m_T(e^{-y}+e^{-y'})/2\sqrt{s}$. We also used the observation that the transverse mass of the electron and neutrino, $m_T \equiv \sqrt{2E_T^e E_T^\nu(1-\cos\Delta\phi_{e\nu})}$ (where $E_T^{e,\nu}$ is the transverse energy of the electron or neutrino, and $\Delta\phi_{e\nu}$ is the azimuthal angle between the two leptons), is simply $m_T = 2p_T$ at leading order, where p_T is the transverse momentum of the electron.

To leading order (LO), the contributions of the color- and spin-averaged scalar and tensor matrix elements to $pp \to e\nu + X$, including the interference term, is

$$\begin{aligned}\frac{\langle|\mathcal{M}|^2\rangle}{|V_{ud}|^2} &= \frac{2}{3}\frac{1}{\Lambda_S^4}(p\cdot p')(k\cdot k') - \frac{8}{3}\frac{\eta_S\eta_T}{\Lambda_S^2\Lambda_T^2}\left[(p\cdot k)(p'\cdot k') - (p\cdot k')(p'\cdot k)\right] \\ &\quad + \frac{16}{3}\frac{1}{\Lambda_T^4}\left[2(p\cdot k)(p'\cdot k') + 2(p\cdot k')(p'\cdot k) - (p\cdot p')(k\cdot k')\right]\ , \end{aligned}\tag{5.41}$$

where p, p' are the momenta of the incoming partons, and k, k' are the momenta of the electron and neutrino. The interference term is antisymmetric under $k \longleftrightarrow k'$, so it does not contribute to the transverse mass distribution obtained by integrating over y and y'. After some substitutions this expression becomes

$$\frac{\langle|\mathcal{M}|^2\rangle}{|V_{ud}|^2} = \frac{1}{6}\frac{\hat{s}^2}{\Lambda_S^4} - \frac{\eta_S\eta_T}{3}\frac{m_T^2\hat{s}}{\Lambda_S^2\Lambda_T^2}\sinh(y-y') + \frac{4}{3}\frac{\hat{s}^2}{\Lambda_T^4}\left(1-\frac{m_T^2}{\hat{s}}\right)\ , \tag{5.42}$$

with $\hat{s} = x_1x_2s$ and m_T is the transverse mass of the lepton-neutrino pair.

Next we need the cross-section with m_T greater than a threshold $m_{T,\rm cut}$. Using (5.40) and (5.42), one finds

$$\begin{aligned}&\sigma(m_T > m_{T,\rm cut}) = \\ &\frac{s}{48\pi}\int_{m_{T,\rm cut}^2/s}^1 d\tau\sqrt{\tau}\left[\frac{|V_{ud}|^2}{\Lambda_S^4}\sqrt{\tau - m_{T,\rm cut}^2/s} + \frac{8}{3}\frac{|V_{ud}|^2}{\tau\Lambda_T^4}\left(\tau - \frac{m_{T,\rm cut}^2}{s}\right)^{3/2}\right] \\ &\times\int_{\frac{1}{2}\ln\tau}^{-\frac{1}{2}\ln\tau} dy_P\left[f_{\overline{u}}(\sqrt{\tau}e^{y_P})f_d(\sqrt{\tau}e^{-y_P}) + (\overline{u},d)\to(u,\overline{d})\right]\ , \end{aligned}\tag{5.43}$$

where the sum over $i,j = \overline{u},d$ and $i,j = u,\overline{d}$ has been done, $\tau = x_1x_2$, and $y_P = 0.5\ln(x_1/x_2)$.

The ATLAS and CMS experiments have searched for new physics in $pp \to e\nu + X$ by looking for an excess of events at large transverse mass [155, 156]. The CMS study analyzes 1.03 fb^{-1} of data for the electron final state, and we begin by following their analysis in setting limits on the scalar and tensor interactions. The CMS search window is defined by specifying a cut on m_T and counting the number of events detected with transverse mass larger than the cut. Specifically, they looked for the production of a heavy W' with decay $W' \to e\nu$ by searching for events having transverse mass above a variable threshold $m_{T,\rm cut}$, finding 1 event for $m_{T,\rm cut} = 1$ TeV and 1 event for $m_{T,\rm cut} = 1.1$ TeV. In general the limit on the number of expected signal events depends on the expected background, $n_{\rm b}$, which for this search is quoted to be $n_{\rm b} = 2.2 \pm 1.1$ events for $m_{T,\rm cut} = 1$ TeV and $n_{\rm b} = 1.4 \pm 0.80$ events for $m_{T,\rm cut} = 1.1$ TeV [7].

To set a limit we follow Ref. [156] and use Bayesian statistics with a flat prior in the signal $n_{\rm s}$. The likelihood function $L(n|n_{\rm s})$ is given by the Poisson distribution for n detected events with $n_{\rm s}$ signal and $n_{\rm b}$ background events expected. The expected number of signal events is given by $n_{\rm s} = \epsilon\sigma\mathcal{L}$, where σ is given by (5.43), $\mathcal{L}$ is the integrated luminosity, and ϵ is the detection efficiency times the geometric acceptance. Ref. [156] quotes the signal efficiency for a W' to be 80%. Their earlier analysis (Ref. [157]), based on 36 pb^{-1} of data, quotes the product of the geometric acceptance and detection efficiency as being greater than 64% in the W' mass range of interest. In the absence of a detector simulation for our signal, in what follows we will assume our signal has a 80% detection times geometric acceptance efficiency.

The credibility level $1-\alpha$ for a flat prior in the signal is then derived from [38]

$$1 - \alpha = \frac{\int_0^{s_{\rm up}} dn_{\rm s}\; L(n|n_{\rm s})}{\int_0^{\infty} dn_{\rm s}\; L(n|n_{\rm s})}\ , \tag{5.44}$$

which is equivalent to [38]

$$\alpha = e^{-s_{\rm up}} \frac{\sum_{m=0}^{n} \frac{1}{m!}(s_{\rm up}+n_{\rm b})^m}{\sum_{m=0}^{n} \frac{1}{m!} n_{\rm b}^m}\ . \tag{5.45}$$

To set a limit on $s_{\rm up}$, we choose the lower value of $m_{T,\rm cut} = 1$ TeV in order to maximize the signal rate. Then for $n_{\rm b} = 2.2$ expected background events and $n = 1$ event detected, one finds that $s_{\rm up} = 3.0$ at the 90% credibility level. Dividing by ϵ, we obtain a 90% upper credibility limit of 3.7 produced signal events.

In Figure 5.6 we show the corresponding limits on ϵ_S and ϵ_T (red, solid curve), using Eq. (5.43) with 1.03 fb^{-1} of integrated luminosity at $\sqrt{s} = 7$ TeV. LO MSTW

[7] These $n_{\rm b}$ values are taken from Table 1 of Ref. [156]. Different central values for $n_{\rm b}$ appear in Figure 2 of Ref. [156]: for example $n_{\rm b} = 1.15$ for $m_{T,\rm cut} = 1$ TeV. The two sets of $n_{\rm b}$ are consistent within the quoted error bars and lead to minor (5%) differences in the bounds on $\epsilon_{S,T}$.

2008 [158] PDFs are used and evaluated at $Q^2 = 1$ TeV^2. We also checked that limits obtained using the CTEQ6 PDF set [159] are quantitatively in good agreement. When only one of these operators is present, the bounds on $\epsilon_{S,T}$ correspond to $\Lambda_S > 2.5$ TeV and $\Lambda_T > 2.7$ TeV. As illustrated by Figure 5.6, our LHC bound on ϵ_S is a factor of 7 stronger than the old CDF limit, but about 4 times weaker than the bound from nuclear beta decay. Similarly, our new collider bound on ϵ_T is a factor of 3 weaker than the bound from radiative pion decay.

We have performed a parallel analysis using the ATLAS results [155] on W' search. Use of the ATLAS results requires an extra step, since their quoted efficiency for a given $m_{T,\rm cut}$ includes the fraction of total $W' \to e\nu$ events with $m_T > m_{T,\rm cut}$. After determining this fraction with a leading-order calculation, we infer the ATLAS detection times geometric acceptance efficiency for $m_{T,\rm cut} = 1$ TeV to be 80%, the same as quoted by CMS for their experiment. Using then the fact that for $m_T > 1$ TeV ATLAS observes $n = 1$ event with an expected number of background events $n_{\rm b} = 0.89(20)$, we find that the ATLAS limits on $\epsilon_{S,T}$ differ from the CMS ones only at the 5% level, well within the uncertainties of our leading order calculation. We also estimate that the bounds on $\epsilon_{S,T}$ can be reduced by at least a factor of 2 once the full data set collected at $\sqrt{s} = 7$ TeV is analyzed (see dotted, gold line in Figure 5.6). We expect that stronger limits can be obtained by a combined analysis of the ATLAS and CMS data, which goes beyond the scope of this work.

To obtain projected limits at higher luminosities and $\sqrt{s} = 7$ TeV or $\sqrt{s} = 14$ TeV, we repeat the same LO analysis, assuming the same 80% detection times acceptance efficiency for the signal as before. We choose an aggressive cut to make the expected background small. The location of the cut on the transverse mass $m_{T,\rm cut} \sim$ TeV is estimated by computing at tree-level the transverse mass distribution of the dominant SM physics background, due to the production of a high-p_T lepton from an off-shell W, and finding the value above which the expected background is less than 1 event. At $\sqrt{s} = 7$ TeV and with an integrated luminosity of 10 fb^{-1}, we find that the number of background events drops below one for $m_{T,\rm cut} = 1.5$ TeV. At $\sqrt{s} = 14$ TeV, with $m_{T,\rm cut} = 2.5$ TeV and an integrated luminosity of 10 fb^{-1} we find 0.5 background events expected above the cut. We also consider an ultimate luminosity of 300 fb^{-1}, finding that for $m_T > 4$ TeV there are 0.3 expected background events. We therefore impose $m_{T,\rm cut} = 2.5$ TeV (4 TeV), and assume an integrated luminosity of 10 fb^{-1} (300 fb^{-1}). To set a limit we will assume that no events are found, which is consistent with less than 1 background event expected. From Eqs. (5.44) and (5.45) we then obtain a 90% Credibility Limit of 3 produced events. The anticipated joint 90% credibility level limits on ϵ_S and ϵ_T from LHC at $\sqrt{s} = 14$ TeV are shown in Figure 5.7.

From an inspection of Figure 5.7 we find that at high luminosity and center-of-mass energy the expected improvement in the limits are nearly an order of magnitude compared to the existing collider limits. Even with only 10 fb^{-1} taken at 14 TeV we expect the limits to improve substantially from the current collider limit.

At these energies and luminosities the bound on ϵ_S from the LHC will become stronger than anticipated future bounds from low-energy experiments. This conclusion is illustrated in Figure 5.7, where we also overlay the projected low-energy bounds presented in Figure 5.5.

We expect these projected limits can be tightened, since we have chosen hard cuts to reduce the expected leading background to below one event, at the cost of significantly cutting into the signal. Optimizing the choice of the cut to maximize the sensitivity to the contact interactions will require including additional backgrounds, such as QCD and top quarks, and more generally, a better understanding of the systematic errors involved.

Our analyses can certainly be improved. Our estimate of the detection times acceptance efficiency was borrowed from the estimate for a W' signal from [156]. Obviously a detector simulation of the signal will provide a better estimate of this factor. The theoretical error on the signal rate will be further reduced once the next-leading-order QCD contributions are known.

Finally, the interaction Lagrangian (5.39) can be generalized to include interactions of the electron with neutrinos of all flavors, with a corresponding generalization of $\epsilon_{S,T} \to \epsilon^{\alpha}_{S,T}$ where $\alpha \in \{e, \mu, \tau\}$. Because the final states with different neutrino flavors do not interfere and neither do the scalar and tensor interactions after integrating over the rapidity distributions, the derived and projected bounds shown in Figures 5.6 and 5.7 now apply to the quantities $\sqrt{\sum_\alpha (\epsilon^{\alpha}_{S,T})^2}$.

5.6.2. Scalar resonance

A larger signal rate is obtained if the particle that generates the scalar interaction is kinematically accessible at the LHC. In this case there can be a direct relationship between ϵ_S and the production cross-section and mass of the resonance, as we now demonstrate.

We assume that after electroweak symmetry breaking there is a charged scalar ϕ^+ of mass m, with the following couplings to first-generation quarks and leptons:

$$\mathcal{L} = \lambda_S V_{ud} \phi^+ \overline{u} d + \lambda_P V_{ud} \phi^+ \overline{u} \gamma_5 d + \lambda_l \phi^- \overline{e} P_L \nu_e + \text{h.c.} \,, \tag{5.46}$$

where $\phi^- \equiv (\phi^+)^*$. At low energies the exchange of ϕ^+ generates a scalar operator with

$$\epsilon_S = 2 \lambda_S \lambda_l \frac{v^2}{m^2} \,, \tag{5.47}$$

and a pseudoscalar operator with

$$\epsilon_P = 2 \lambda_P \lambda_l \frac{v^2}{m^2} \,. \tag{5.48}$$

To proceed, at leading order the cross-section for the on-shell production of ϕ, which then decays to $l\nu$ (of a given sign), is given in the narrow-width approxima-

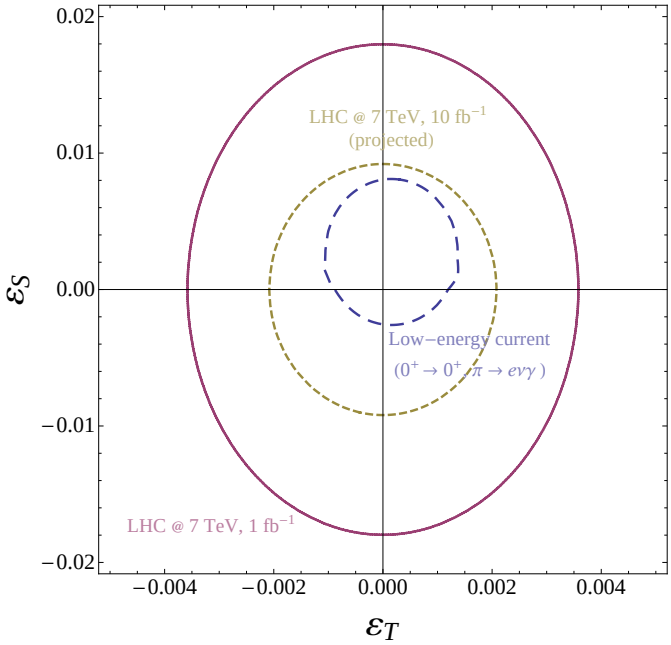

Figure 5.6: Joint 90% CL limit on ϵ_S and ϵ_T implied by: (i) current bounds from nuclear β decay $0^+ \to 0^+$ and radiative pion decay (blue, dashed); (ii) CMS search [156] in the channel $pp \to e\nu + X$ at $\sqrt{s} = 7$ TeV with 1.03 fb^{-1} of data. The limit is obtained by requiring less than 3.7 $e\nu$-produced events having $m_T > 1$ TeV (red, solid). LO MSTW 2008 [158] parton distribution functions are used; (iii) projected LHC searches in the channel $pp \to e\nu + X$ at $\sqrt{s} = 7$ TeV with 10 fb^{-1} of data (gold, dotted). The limit is obtained by requiring less than 3 $e\nu$-produced signal events with $m_T > 1.5$ TeV and assuming that no events are observed. The cut is chosen to reduce the expected leading background to be below 1 event. The effective couplings $\epsilon_{S,T}$ are defined in the $\overline{\text{MS}}$ scheme at 2 GeV.

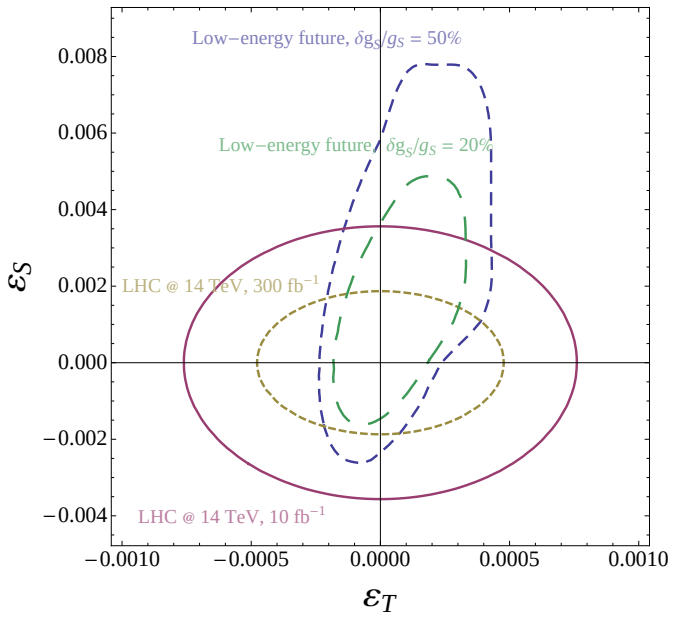

Figure 5.7: Projected joint 90% credibility level limit on ϵ_S and ϵ_T from the LHC at $\sqrt{s} = 14$ TeV, obtained from requiring less than 3 $e\nu$-produced signal events with: (i) $m_T > 2.5$ TeV and 10 fb^{-1} of integrated luminosity (solid, red ellipse); and (ii) $m_T > 4$ TeV and 300 fb^{-1} (dashed, yellow ellipse). Cuts are chosen to reduce the expected leading background to be below 1 event. To obtain the projection it is assumed no events are found. Same PDFs are used as in Figure 5.6. Note the change in scale between these two figures. Anticipated bounds from low-energy experiments and reduced LQCD uncertainties, redrawn from Figure 5.5, are shown for comparison. The effective couplings $\epsilon_{S,T}$ are defined in the $\overline{\text{MS}}$ scheme at 2 GeV.

tion by

$$\sigma \cdot \mathrm{BR} = \lambda_l^2 \left(\lambda_S^2 + \lambda_P^2\right) |V_{ud}|^2 \frac{m}{48 s \Gamma_\phi} L(\tau) \ , \tag{5.49}$$

with $\tau = m^2/s$, $L(\tau) = \int_\tau^1 dx f_q(x) f_q'(\tau/x)/x$, and where Γ_ϕ is the total decay width of ϕ. Next, note that since ϕ may decay to other particles (not just to $l\nu$ and ud) ,

$$\Gamma_\phi \geq \Gamma_l + \Gamma_q = \left(\lambda_l^2 + 2N_c(\lambda_S^2 + \lambda_P^2)|V_{ud}|^2\right) \frac{m}{16\pi} \ , \tag{5.50}$$

with $N_c = 3$. Next note that $m/\Gamma_\phi \leq 16\pi/(\lambda_l^2 + 2N_c(\lambda_S^2 + \lambda_P^2)|V_{ud}|^2)$, and then use the arithmetic-geometric inequality $\sqrt{2N_c}\lambda_\phi\lambda_l < \frac{1}{2}(\lambda_l^2 + 2N_c(\lambda_S^2 + \lambda_P^2)|V_{ud}|^2)$, where $\lambda_\phi = \sqrt{\lambda_S^2 + \lambda_P^2}|V_{ud}|$, to finally obtain our main result of this subsection,

$$\sigma \cdot \mathrm{BR} \leq \frac{|V_{ud}|}{12v^2} \frac{\pi}{\sqrt{2N_c}} \left(\sqrt{\epsilon_S^2 + \epsilon_P^2}\right) \tau L(\tau) \ . \tag{5.51}$$

Because of the severe constraint imposed by $\pi \to e\nu$, the coupling λ_P of ϕ to the pseudoscalar quark scalar density must be significantly suppressed. In the limit $\epsilon_P \ll \epsilon_S$ one then has

$$\sigma \cdot \mathrm{BR} \leq \frac{|V_{ud}|}{12v^2} \frac{\pi}{\sqrt{2N_c}} |\epsilon_S| \tau L(\tau) \tag{5.52}$$

This expression can be rearranged to obtain a lower bound on ϵ_S, that is stronger after summing in L over both charged-particle final states. The bound depends only on τ and $\sigma \cdot \mathrm{BR}$. Figure 5.8 shows the bound as a function of τ for several choices of $\sigma \cdot \mathrm{BR}$ that will be probed by the LHC. Equivalent limits are shown in Figures 5.9 and 5.10, where we show the dependence of the bound on the mass of the resonance, for several values of $\sigma \cdot \mathrm{BR}$ and at $\sqrt{s} = 7$ and 14 TeV. LO CTEQ6 [159] parton distribution functions are used for all these figures.

We have shown that if a signal is observed in $pp \to e +$missing energy (MET)$+ X$, then a lower bound on ϵ_S can be obtained, provided the signal is due to the on-shell production of a scalar, which decays to an electron and missing energy provided by an electron neutrino, and whose pseudoscalar coupling to quarks is suppressed compared to its scalar coupling. That the resonance couples to an electron neutrino is important in deriving the above relation to ϵ_S, since at linear order in the ϵ's, neutron-decay experiments do not probe couplings to other neutrino flavors $\epsilon_S^{\alpha \in \{\mu,\tau\}}$.

Further confidence that the signal is due to the production of an on-shell particle can be established by the detection of an edge in the transverse electron-neutrino mass distribution, and through the detection of a resonance in dijets. The only additional theoretical assumption used to obtain the lower limit (5.52) is that the charged resonance ϕ is interpreted as a scalar and not as a vector or a tensor.

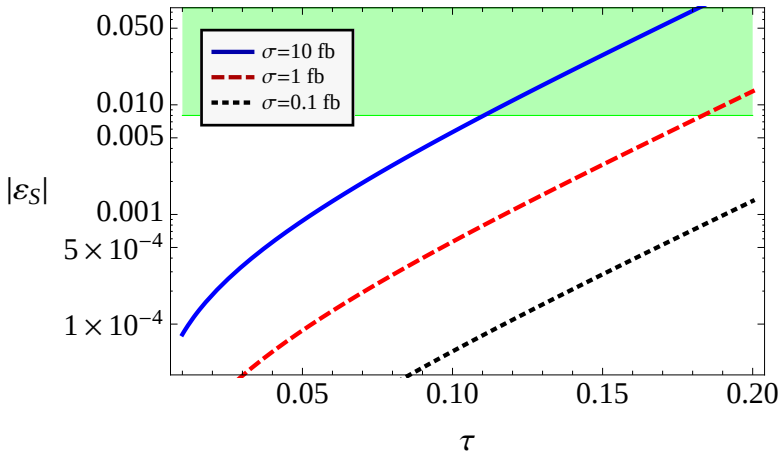

Figure 5.8: Projected lower bound on $|\epsilon_S|$ (at $\mu = 2$ GeV), for a discovery cross-section of $\sigma(pp \to e + \text{ MET} + X) = 10$ fb (blue, solid), 1 fb (red, dashed) and 0.1 fb (black, dotted), as a function of $\tau = m^2/s$. Shaded region (green) shows the current experimental exclusion on ϵ_S from $0^+ \to 0^+$ nuclear β decay.

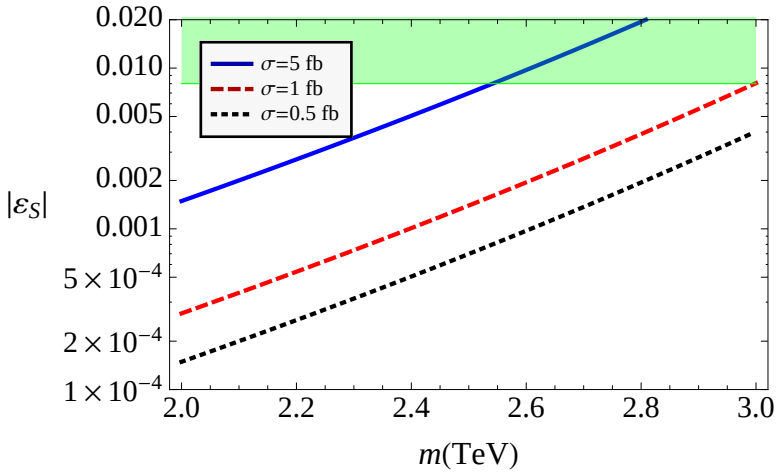

Figure 5.9: Projected lower bound on $|\epsilon_S|$ (at $\mu = 2$ GeV) for $\sqrt{s} = 7$ TeV and a discovery cross-section of $\sigma(pp \to e + \text{ MET} + X) = 5$ fb (blue, solid), 1 fb (red, dashed) and 0.5 fb (black, dotted). Shaded region (green) shows the current experimental exclusion on ϵ_S from $0^+ \to 0^+$ nuclear β decay. The bound scales linearly with $\sigma \cdot \text{BR}$.

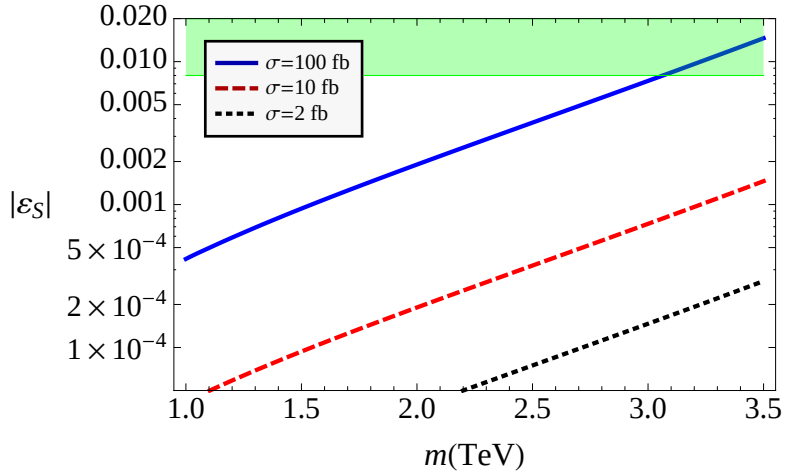

Figure 5.10: Same as Figure 5.9 but for $\sqrt{s} = 14$ TeV and $\sigma \cdot \mathrm{BR} = 100$ fb (blue, solid), 10 fb (red, dashed) and 2 fb (black, dotted).

Measurements of the rapidity distribution of the electron should determine the spin of ϕ.

If a signal is discovered in $pp \to e + \mathrm{MET} + X$ then neutron and nuclear β-experiments will be crucial in order to pin down the properties of the resonance and of the MET. As an illustration, suppose the measured cross-section and mass imply an ϵ_S in excess of existing neutron decay bounds, then either: (i) the resonance does not have spin 0; or (ii) as already described above, since the outgoing neutrino flavor is not identified, the relationship between the cross-section and ϵ_S can be undone simply if the scalar ϕ couples preferentially to muon and tau neutrinos rather than to the electron neutrino; or (iii) there are additional scalars at the TeV scale or a scalar contact interaction, such that partial cancellations occur in summing the multiple contributions to ϵ_S.

5.7. Conclusions

It is anticipated that the next generation of neutron β-decay experiments will increase their sensitivity to BSM scalar and tensor interactions by an order of magnitude, through improved measurements of the neutrino asymmetry parameter B and the Fierz interference term b (see Figures 5.2, 5.3, and 5.5). In order to assess the impact of these future experiments, we have performed a comprehensive analysis of constraints on scalar and tensor BSM interactions from a broad range of low-energy probes (neutron decay, nuclear decays, pion decays) as well as collider searches.

Extracting bounds on scalar and tensor BSM couplings from neutron and nuclear beta decays requires knowledge of the nucleon scalar and tensor form factors

at zero momentum transfer. Using the first lattice-QCD estimate of the scalar form-factor, $g_S = 0.8(4)$, and a new average of existing tensor form-factor results, $g_T = 1.05(35)$ published in [18], we find that to fully exploit the increased experimental sensitivity will require understanding the lattice-QCD estimates of the proton-to-neutron matrix elements at the level of 10–20% (see Figure 5.5). With the anticipated increase in computing power and resources, calculations should reach this precision in 2–4 years [18].

In our survey of probes of BSM scalar and tensor interactions, we have found that the currently strongest bounds arise from nuclear β decay (ϵ_S) and radiative pion decay (ϵ_T), probing effective scales $\Lambda_S > 4.7$ TeV and $\Lambda_T > 5$ TeV, respectively. We also find that within a specific model for the lepton flavor structure of the scalar and tensor interactions, significantly stronger bounds arise from $\pi \to e\nu$ decay, a conclusion in agreement with previous literature.

We have used LHC data to obtain constraints on the scalar and tensor interactions, finding bounds within sight of current limits obtained from low-energy measurements (see Figure 5.6). We have also provided a preliminary estimate of expected future bounds from the LHC, finding that an order of magnitude improvement should ultimately be achievable and that the future collider constraints (associated with effective scales $\Lambda_{S,T} \sim 7$ TeV) will compete with improved neutron-decay constraints based on experimental sensitivities $\delta b, \delta b_\nu \sim 10^{-3}$ (see Figure 5.7). Finally, if a charged resonance decaying to an electron plus missing energy is discovered at the LHC, we have shown how, with some theoretical assumptions, the production cross-section provides a lower bound on the scalar interaction probed at low energy (see Figures 5.8, 5.9, and 5.10).

Our analysis shows that in order to compete with upcoming collider bounds on scalar and tensor interactions, future neutron-decay experiments should aim at the very least to sensitivities $\delta b, \delta b_\nu \sim 10^{-3}$ in the Fierz interference term and neutrino asymmetry. Moreover, experiments aiming for $\delta b, \delta b_\nu \sim 10^{-4}$ would provide an unmatched discovery potential for new scalar and tensor interactions, and therefore should be vigorously pursued.

Chapter 6

EFT: The Higgsless scenario

We will focus now on a scenario that is in some way complementary to the one presented in Chapter 2, analyzing the possibility that the particle spectrum of the SM does not contain a light Higgs. In order to study this new picture we will need a different description of the symmetry breaking sector of the SM and, as long as we are interested in processes with a typical energy well below the Higgs mass, we can use an effective description based on the symmetry breaking pattern of the SM. Indeed, whereas the details of the SM Higgs potential are still only theoretical hypotheses, the existing phenomenological tests have already confirmed the pattern of symmetry breaking. It can be demonstrated that the most general effective theory responding to these symmetry requirements is a *non-linear* sigma model coupled in a gauge invariant manner to the SM [39]. We can understand this fact rewriting the SM Higss sector using the 2×2 matrix field defined as:

$$M(x) = \sqrt{2}\left(\tilde{h}(x)\ ,\ h(x)\right) = \sigma(x) + i\vec{\tau}\cdot\vec{\pi}(x)\ , \tag{6.1}$$

where $\vec{\tau}$ are the Pauli matrices, the Higgs field is now $\sigma(x)$ and $\vec{\pi} = (\pi_1, \pi_2, \pi_3)$ is a triplet of would-be Goldstone bosons fields that, trough the Higgs mechanism, will give masses to the gauge bosons. The most general scalar sector consistent with the requirements of renormalizability and $SU(2)_L \times U(1)_Y$ gauge invariance is then [19]:

$$\mathcal{L}_h = \frac{1}{4}\langle D_\mu M^\dagger D_\mu M\rangle - \frac{1}{4}\lambda\left[\frac{1}{2}\langle M^\dagger M\rangle + \frac{\mu^2}{\lambda}\right]^2\ . \tag{6.2}$$

Here and in the following $\langle ...\rangle$ denotes the trace in the $SU(2)$ space and the covariant derivative reads:

$$D_\mu M(x) = \partial_\mu M(x) + i\frac{g}{2}\tau^I W^I_\mu(x) M(x) - i\frac{g'}{2}B_\mu(x) M(x)\tau^3\ . \tag{6.3}$$

The Lagrangian in Eq (6.2) is exactly the one of a *linear* σ model. In the $g' = 0$ limit, it is invariant under $G = SU(2)_L \times SU(2)_R$ global transformations:

$$\Sigma \rightarrow g_L\,\Sigma\,g_R^\dagger, \qquad\qquad g_{L,R} \in SU(2)_{L,R}\,. \tag{6.4}$$

In the SM only the $SU(2)_L \times U(1)_Y$ subgroup is gauged. The Lagrangian $\mathcal{L}_h$ breaks the group G down to the $SU(2)_{L+R}$ global group, usually called the custodial symmetry group. This remaining symmetry ensures that the corrections to the ρ parameter, which measure the relative strength of the charged and neutral weak currents and that at tree level reads $\rho = M_W^2/(M_Z^2 \cos^2\theta_W)$, are small, i.e. $\rho = 1 + \mathcal{O}(g'^2)$, as required by the phenomenology.

We want now to explore the limit in which the Higgs mass is taken to infinity:

$$M_h^2 = 2\lambda v^2 \to \infty \ , \tag{6.5}$$

that is equivalent to keep v fixed, taking $\lambda \to \infty$, exploring in this way the strongly interacting range of the theory. In this limit the Higgs is effectively removed from the physical spectrum and the resulting non-renormalizable theory is a non-linear sigma model coupled to the SM. Taking to the infinity the Higgs mass formally corresponds to apply to the Lagrangian in Eq. (6.2) the constraint:

$$MM^\dagger = M^\dagger M = \sigma^2 + \vec{\pi}^2 \equiv v^2 \ . \tag{6.6}$$

The scalar part of this Lagrangian then becomes:

$$\begin{aligned} \mathcal{L}_{\text{scalar}} &= \frac{1}{2}\left(\partial_\mu \vec{\pi}\right)^2 + \frac{1}{2}\frac{\left(\vec{\pi}\cdot\partial_\mu\vec{\pi}\right)^2}{v^2 - \vec{\pi}^2} \\ &= \frac{1}{2}\left(\partial_\mu \vec{\pi}\right)^2 + \frac{1}{2v^2}\left(\vec{\pi}\cdot\partial_\mu\vec{\pi}\right)^2 \left(1 + \frac{\vec{\pi}^2}{v^2} + \mathcal{O}\left[\left(\frac{\vec{\pi}^2}{v^2}\right)^2\right]\right) \ , \end{aligned} \tag{6.7}$$

where the non-linear character of the model can be explicitly seen. At this point the symmetry breaking dynamics is described only in terms of the Goldstone bosons.

We want to stress that, even if we developed the present scenario starting from the SM Higgs sector and taking the Higgs mass to infinity, the same effective theory can describe the low-energy behavior of a theory in which the electroweak symmetry breaking is related to a strongly interacting sector, without the need of introducing an explicit scalar field. In fact in this scenario we are specifying only the Goldstone symmetry structure, independently of the specific implementation of the symmetry breaking.

Our phenomenological analysis based on the Higgsless scenario will be dealing exclusively with the gauge symmetry breaking sector of the SM. For this reason in what follows we will focus only on the Lagrangian describing this sector of the theory.

6.1. The Electroweak Chiral Lagrangian

As we saw in the introduction of this chapter, in the absence of a light Higgs, a strongly interacting sector responsible for providing masses to the electroweak gauge bosons is described by Goldstone bosons $\pi^I, I = 1, 2, 3$, associated to the

$SU(2)_L \otimes U(1)_Y \longrightarrow U(1)_{\rm em}$ spontaneous symmetry breaking (SSB), which become the longitudinal components of the electroweak gauge bosons. The corresponding Higgsless electroweak chiral effective theory (EChET) Lagrangian is then described by a non-linear sigma model based on the coset:

$$SU(2)_L \otimes SU(2)_R / SU(2)_{L+R} \,, \tag{6.8}$$

where $SU(2)_L \otimes U(1)_Y$ is gauged. Interestingly enough the Lagrangian that describes it is the one of two-flavor Chiral Perturbation Theory (ChPT) [160, 161] with pions substituted by the Goldstone bosons associated to the SSB of the electroweak symmetry. ChPT is an effective field theory of Quantum Chromodynamics (QCD) at very low-energy, driven by the chiral symmetry of massless QCD, perturbative in momenta and valid for $p^2 \ll (4\pi F_\pi)^2$ (being F_π the decay constant of the pion), and renormalizable order by order in its perturbative expansion. In the same way EChET is valid for $p^2 \ll (4\sqrt{2}\pi v)^2 \sim (3\,\text{TeV})^2$ [20, 19, 21] (note that the $\sqrt{2}$ factor depends on the convention used for the vev v). It is worth to stress that, as in the ChPT case, $\mathcal{L}_{\rm EChET}$ involves a perturbative derivative expansion, driven by the scale $\Lambda_{\rm EW} = 4\sqrt{2}\pi v$, *i.e.* an expansion in powers of $(p^2, M_V^2)/\Lambda_{\rm EW}^2$, where M_V is the mass of a SM gauge boson.

A convenient parametrization of the Goldstone fields is given by:

$$U(x) = \exp\left(\frac{i}{v}\,\pi^I \tau^I\right) \,, \tag{6.9}$$

with τ^I the Pauli matrices. This transforms as $LUR^\dagger$, with $L \in SU(2)_L$ and $R \in U(1)_Y$, under the gauge group. Up to dimension four operators, the most general $SU(2)_L \otimes U(1)_Y$ gauge invariant and CP-invariant Lagrangian which implements the global symmetry breaking $SU(2)_L \otimes SU(2)_R$ into $SU(2)_{L+R}$ in the limit when g' vanishes is given by the terms [19, 20, 21]:

$$\mathcal{L}_{\rm EChET} = \frac{v^2}{4}\langle (D_\mu U)^\dagger\, D^\mu U\rangle + \sum_{i=0,\ldots 5} a_i\, \mathcal{O}_i \,. \tag{6.10}$$

Due to the non-renormalizable character of the theory, at each order in the perturbative expansion we need to add at the tree level non-linear Lagrangian (the first term in Eq. (6.10)) a sufficient number of counterterms. At $\mathcal{O}(p^4)$ the needed counterterms are the operators $\mathcal{O}_i$ of Eq. (6.10). They explicitly read:

$$\begin{aligned}
\mathcal{O}_0 &= g'^2\,\frac{v^2}{4}\langle T\, V_\mu\rangle^2 \,, \\
\mathcal{O}_1 &= \frac{igg'}{2}\, B^{\mu\nu}\langle T\, W_{\mu\nu}\rangle \,, \\
\mathcal{O}_2 &= \frac{ig'}{2}\, B^{\mu\nu}\langle T\,[V^\mu, V^\nu]\rangle \,, \\
\mathcal{O}_3 &= i\, g\, \langle W_{\mu\nu}\,[V^\mu, V^\nu]\rangle \,, \\
\mathcal{O}_4 &= \langle V_\mu V_\nu\rangle^2 \,, \\
\mathcal{O}_5 &= \langle V_\mu V^\mu\rangle^2 \,,
\end{aligned} \tag{6.11}$$

where $V_\mu = (D_\mu U)\, U^\dagger$, $T = U\,\tau^3\, U^\dagger$. The covariant derivative takes the form:

$$D_\mu U = \partial_\mu U + \frac{i}{2}\, g\, \tau^I\, W_\mu^I U - \frac{i}{2}\, g'\, \tau^3\, U B_\mu\,, \tag{6.12}$$

with $W_{\mu\nu} = \tau^I\, W^I_{\mu\nu}/2$, and being $W^I_{\mu\nu}$ and $B_{\mu\nu}$ the gauge field strength tensors. The first term in the Lagrangian (6.10) has dimension two, and provides the SM mass terms for the gauge bosons. The rest of terms are dimension 4 operators, and only $\mathcal{O}_{3-5}$ are relevant for the purposes of the work presented in the next chapter. $\mathcal{O}_3$ represents an anomalous triple gauge-boson coupling while $\mathcal{O}_4$ and $\mathcal{O}_5$ give anomalous quartic gauge-boson interactions. The corresponding low-energy couplings a_3, a_4 and a_5 encode the information of the heavier spectrum that has been integrated out in order to get $\mathcal{L}_{\text{EChET}}$.

There are other eight operators that respect gauge and CP symmetry, namely:

$$\begin{aligned}
\mathcal{O}_6 &= \langle V_\mu V_\nu\rangle\langle TV^\mu\rangle\langle TV^\nu\rangle \\
\mathcal{O}_7 &= \langle V_\mu V^\mu\rangle\langle TV^\nu\rangle^2 \\
\mathcal{O}_8 &= \frac{g^2}{4}\langle TW_{\mu\nu}\rangle^2 \\
\mathcal{O}_9 &= \frac{g}{2}\langle TW_{\mu\nu}\rangle\langle T[V^\mu, V^\nu]\rangle \\
\mathcal{O}_{10} &= [\langle TV_\mu\rangle\langle TV_\nu\rangle]^2 \\
\mathcal{O}_{12} &= \langle TD_\mu D_\nu V^\nu\rangle\langle TV^\mu\rangle \\
\mathcal{O}_{13} &= \frac{1}{2}\langle TD_\mu V_\nu\rangle^2\ .
\end{aligned} \tag{6.13}$$

It can be easily proven that every operator containing the T factor actually violates custodial symmetry. As the operators in Eq. (6.13) do not vanish when $g' \to 0$ they would introduce an explicit violation of this symmetry and then we will neglect them in the analysis presented in this thesis. We need to consider one last gauge invariant operator:

$$\mathcal{O}_{11} = \langle (D_\mu V^\mu)^2\rangle \tag{6.14}$$

As we are in practice only interest in calculating on-shell S matrix elements obtained from the first term of $\mathcal{L}_{\text{EChET}}$ at one loop, plus the counterterms considered at tree level, we can neglect this operator, that vanishes on-shell [39].

Chapter 7

$W_L Z_L \to W_L Z_L$ scattering: where vector resonances stand

The search for the dynamics of the spontaneous breaking of the electroweak gauge symmetry is certainly a crucial goal of the high-energy physics research. On July 4th 2012, ATLAS and CMS experiments at CERN announced the discovery of a new boson with a mass around 125 GeV that could eventually be identified with the SM Higgs boson. If this would be the case, we would have a hint on the mechanism that Nature has chosen to break spontaneously the gauge symmetry of the SM. On the other hand, ignoring for now the nature of the boson recently discovered, there is no reason to exclude different possibilities.

A Higgsless world or a scenario that includes a light composite Higgs would be most probably characterized by the presence of a new physics scale associated to a strong interacting sector lying around $E \sim 1\,\text{TeV}$ and related with the spontaneous breaking of the electroweak symmetry [162, 163]. A reasonable assumption, based on our knowledge of low-energy hadron physics, is that such a non-perturbative dynamics would lead to resonances that can be at the reach of future runs at the LHC or at an envisaged Linear Collider. It has also been argued that without a light Higgs the violation of perturbative partial-wave unitarity in the elastic scattering of the longitudinal components of those W or Z gauge bosons could be prevented by those spin-1 resonances [164] though this is by no means compulsory [163]. In this chapter we plan to investigate the possible existence of those vector resonances contributing to the $W_L Z_L \to W_L Z_L$ scattering process.

The symmetry breaking sector of the Standard Model without a Higgs becomes a non-linear sigma model and it is described by the effective Lagrangian in Eq. (6.10), that, as we already noted, resembles the one of the two-flavor ChPT. Let us recall some interesting features of ChPT that will be extremely useful also in the electroweak case. As in any effective field theory the low-energy coupling constants (LECs) of ChPT carry the information of the heavier spectra that has been left out in the procedure of constructing the low-energy theory. Indeed it

has been shown that, at $\mathcal{O}(p^4)$, the LECs are saturated by the lightest hadron resonances [165]. In particular the two relevant LECs that appear in the two-flavor amplitude of the elastic pion-pion scattering are given by the contribution of the $\rho(770)$. Hence one can wonder if it would be possible to obtain the mass of this resonance from the values of those LECs. Of course it is not possible to establish the existence and properties of resonances using a perturbative framework. However one can provide procedures to resummate the perturbative contributions to the amplitude. We will translate one of these methods from the well studied QCD framework to the electroweak sector.

The procedure that we devise in order to explore the occurrence of spin-1 resonances in the $E \sim 1\,\text{TeV}$ region is based on the information about the spin-J resonances ($J \geq 1$) provided by the zeros of the scattering amplitude. This method goes back to the study of the zeros in $\pi\pi \to \pi\pi$ [166]. In Ref. [22] it was shown in the framework of ChPT that the zeros of the $\mathcal{O}(p^4)$ $I = 1$ $\pi\pi \to \pi\pi$ amplitude (I is short for the isospin quantum number) predict the mass of the $\rho(770)$ resonance when the chiral LECs are supposed to be saturated by the resonance contributions. This shows that, though the ChPT amplitude is only valid for $p^2 \ll M_\rho^2$, the extrapolation provided by its zeros is to be trusted up to $E \sim M_\rho$.

The method can be applied to the electroweak sector employing the two following ingredients. First, the fact that the elastic scattering amplitude of the longitudinal components of the gauge bosons is given, at $E \gg M_W$, by the amplitude of the elastic scattering of the Goldstone bosons associated to the spontaneous electroweak symmetry breaking. This is known as the *equivalence theorem* and was devised originally to study those processes with a very heavy Higgs [167, 168, 163]. The equivalence theorem thus allow us to trade the dynamics of the longitudinally polarized gauge bosons by the one of the corresponding Goldstone modes. And the second ingredient, already commented above, is the fact that the interactions among Goldstone bosons in the Higgsless electroweak theory is described, at least at leading order, by the two-flavor ChPT Lagrangian where now the multiplet of pions is substituted by the Goldstone fields that provide masses to the gauge bosons. The obvious difference is the relevant scale that rules the perturbative expansion of the amplitude. Taking into account the equivalence theorem, the perturbative expansion and the EChET discussed in Chapter 6, our working region is determined by $M_W \ll E \ll 4\sqrt{2}\pi v$.

We therefore exploit in this work the analogies between ChPT and Higgsless EChET and study the elastic scattering of the longitudinal components of the electroweak gauge bosons as described by the latter. Then, assuming that the LECs of the effective theory are saturated by the lightest vector resonances (if these exist) we determine the zeros of the amplitude and we explore the parameter space of the two only LECs that appear in the two-flavor scattering amplitude, obtaining important information on the possible resonances.

The contents of this chapter are the following. In Section 7.1 we revisit the role of the zeros of an amplitude and its relation with the resonances of the theory. We

will focus on the well known case of $\pi\pi \to \pi\pi$ scattering and the $\rho(770)$. In Section 7.2 we briefly review the $W_LZ_L \to W_LZ_L$ scattering amplitude in the framework of the Higgsless electroweak effective theory reviewed in Chapter 6. Section 7.3 will be devoted to the analysis of the zeros of that amplitude and their interpretation as vector resonances. We will also discuss our results and the possibility left for LHC to disentangle the presence of these vector resonances in Section 7.4. Our conclusions will be given in Section 7.5.

7.1. The role of the zeros of the scattering amplitude

We will now develop our method using QCD as the reference framework, taking advantage of the precise experimental data available and the good knowledge of the LEC values of $\mathcal{O}(p^4)$ ChPT used to describe the low-energy processes like $\pi\pi$ scattering. No conceptual changes will be needed to apply the method to the electroweak case.

The low-energy dynamics of elastic $\pi\pi$ scattering is determined by the existence of the lightest meson resonances contributing to that amplitude, $\sigma(600)$ and $\rho(770)$. Though the $\sigma(600)$ is mainly related with the chiral logs (it appears at next-to-leading order in the large number of colours (N_C) expansion), the information of the $\rho(770)$, leading in $1/N_C$, is encoded in the low-energy couplings at $\mathcal{O}(p^4)$ in the chiral expansion [165]. Within a quantum field theory approach, one can determine the resonance contributions to the chiral LECs starting from a Lagrangian with explicit resonance fields and then integrating them out. Typically those LECs are given in terms of the resonance couplings to the pions and inverse powers of the resonance masses.

One can wonder if the opposite procedure is viable. That is, if it would be possible to determine the mass of the resonances from the phenomenological determination of the LECs. As the ChPT amplitudes provide a perturbative expansion in momenta it is clear that the poles of resonances are not a feature of chiral symmetry. However a link between chiral dynamics and resonance contributions can be provided employing some ad-hoc resummation techniques like Padé approximants, the inverse amplitude method or the N/D construction [39, 169, 170]. We will propose an alternative procedure based on the zeros of the scattering amplitude [22, 166, 171, 172, 173] as given by ChPT at $\mathcal{O}(p^4)$ (we will also comment on the next $\mathcal{O}(p^6)$ contribution).

Consider the amplitude $F(s,t)$ for $\pi^-(p_1)\pi^0(p_2) \to \pi^-\pi^0$ in the s-channel:

$$s = (p_1 + p_2)^2, \qquad t = \frac{1}{2}(s - 4M_\pi^2)(\cos\theta - 1). \tag{7.1}$$

This amplitude has no $I = 0$ component, and from the phenomenology we know that the isovector P-wave is large whereas the $I = 2$ (exotic) S-wave is small. We

can anticipate that these features are essential for our method. The P-wave is dominated by the $\rho(770)$ resonance and therefore around this energy region we can write the partial-wave expansion of the amplitude as:

$$F(s,t) = 16\pi f_0^2(s) + \frac{48\pi}{\sigma} \frac{M_\rho \Gamma_\rho(s)}{M_\rho^2 - s - iM_\rho \Gamma_\rho(s)} \cos\theta + \ldots , \tag{7.2}$$

where $\sigma = \sqrt{1 - 4M_\pi^2/s}$ and $f_\ell^I(s)$ is the partial-wave with isospin I and angular momentum ℓ, defined through the partial-wave expansion of the s-channel amplitude with defined isospin:

$$F^I(s,t) = 32\pi \sum_{\ell=0}^{\infty} (2\ell+1) f_\ell^I(s) P_\ell(\cos\theta) , \tag{7.3}$$

with $P_\ell(z)$ the Legendre polynomial of degree ℓ. Unitarity imposes severe constraints on the structure of the partial-waves $f_\ell^I(s)$. A description consistent with unitarity is given by

$$f_\ell^I(s) = \frac{1}{\sigma} e^{i\delta_\ell^I} \sin\delta_\ell^I , \tag{7.4}$$

with δ_ℓ^I the phase shift of isospin I and angular momentum ℓ, that is real for elastic scattering.

The remaining terms not quoted in Eq. (7.2) amount to numerically suppressed higher partial waves. Taking into account the small size of the S-wave component, the angular distribution associated to $F(s,t)$ would have a marked dip at $\cos\theta = 0$, where also $F(s,t) \simeq 0$. This reflects the spin-1 nature of the $\rho(770)$. Due to the properties of the Legendre polynomials these dips in the angular distribution (or zeros of the amplitude) will appear for $\ell > 0$ and their number in the physical region, $\cos\theta \in [-1,1]$, will be given by the angular momentum of the partial-wave. These zeros can be considered as dynamical features which give the spin to the resonance.

This observation gives us a possible path to analyze the spectrum of $J \geq 1$ resonances integrated out and hidden in the couplings of the effective field theory. Let us specify several features of the zeros of the amplitude and give precise definitions that will help to fix our procedure.

Being analytical functions of more than one variable the zeros of the amplitude are not isolated but continuous, defining a one-dimensional manifold for real s and complex t. Using Eq. (7.1) the $F(s,t)$ amplitude in the s-channel may be expressed as $F(s,z)$ with $z \equiv \cos\theta$. Then the solution of $F(s,z_0) = 0$ for physical values of the s variable is defined by $z = z_0(s)$. Though the zeros of the function happen at complex values of the z variable, we define the *zero contour* as the real part of the zeros ($\mathrm{Re}\, z_0(s)$). It is also phenomenologically observed [174, 175] that this contour continues smoothly from one region to another in the Mandelstam plane[1].

[1]There is one known situation where this is not the case and the contours wiggle. This

Using Eqs. (7.2,7.4) we get:

$$z_0(s) = -\frac{e^{i\delta_0^2}\sin\delta_0^2}{3\,M_\rho\,\Gamma_\rho(s)}\left(M_\rho^2 - s - iM_\rho\Gamma_\rho(s)\right)\,, \tag{7.5}$$

and we have:

$$\mathrm{Re}\, z_0(s) = -\frac{\sin 2\delta_0^2}{6\,M_\rho\,\Gamma_\rho(s)}\left(M_\rho^2 - s\right) - \frac{1}{3}\sin^2\delta_0^2\,, \tag{7.6}$$

that satisfies $\left|\mathrm{Re}\, z(M_\rho^2)\right| \leq \frac{1}{3}$. In fact, and due to the exotic character of the S-wave $I = 2$ background $\left(\mathrm{Im} f_0^2(s) \ll \mathrm{Re} f_0^2(s)\right)$ and to the absence of the S-wave $I = 0$ channel, we know that $\left|\mathrm{Re}\, z(M_\rho^2)\right| \ll \frac{1}{3}$.

Hence, for a generic amplitude where the P-wave contribution dominates and is saturated by a vector resonance, the resonance mass M_R should be found as the solution of:

$$\mathrm{Re}\, z_0(M_R^2) \simeq 0\,, \tag{7.7}$$

where $z_0(s)$ is the zero contour obtained from that amplitude. We will take this condition as our source of information on the resonances given by $F(s,t)$. It is clear, from Eq. (7.2), that how deep is the dip of the angular distribution will also depend on the size of the imaginary part of the zeros. We will comment further on this point in Section 7.3.

The zero contours provide also an alternative unitarization procedure for the ChPT amplitude. Indeed assuming that the amplitude satisfies the partial-wave expansion (7.3) and neglecting $\ell \geq 2$ partial waves one obtains:

$$\tan\delta_1^1(s) = \frac{-\frac{1}{2}\sin 2\delta_0^2(s)}{3\,\mathrm{Re}\, z_0(s) + \sin^2\delta_0^2(s)}\,. \tag{7.8}$$

Note that, if the S-wave $I = 2$ phase-shift is small, the P-wave phase shift δ_1^1 will pass through $\pi/2$ when $\mathrm{Re}\, z_0(s) \to 0$, thus indicating the presence of a resonance. The zero contour provided by the $\mathcal{O}(p^4)$ ChPT amplitude could then be employed to obtain the contribution of the lightest vector resonance (the $\rho(770)$ in the QCD case) to the $\delta_1^1(s)$ phase shift. This is by no means evident. The chiral expansion provides an accurate description at very low energies only, namely for $E \ll M_\rho$. Hence the fact that the zero contour is able to unitarize the theory at $E \sim M_\rho$ has to rely on the properties of those zero contours.

7.1.1. Applying the zero contour method to the $\rho(770)$ case

Let us repeat (and update) now the procedure in Ref. [22], showing how the method developed works in a real case. The $\mathcal{O}(p^4)$ amplitude of $\pi^-\pi^0 \to \pi^-\pi^0$,

happens when they pass a threshold that opens strongly in the S-wave. One such example is the $K\overline{K}$ threshold in $I = 0$ $\pi\pi$ scattering [176]. As we consider here the $\pi^-\pi^0$ channel, which has no isoscalar component, we expect the zero contour to be quite smooth well beyond the $\rho(770)$ mass.

with the variables defined in Eq. (7.1), is given by [161]:

$$A(t,s,u) = \frac{t-M^2}{F^2} + \frac{1}{6\,F^4}\Big[3(t^2-M^2)\,\bar{J}(t) + [s(s-u) - 2\,M^2\,s + 4\,M^2\,u - 2\,M^4]\,\bar{J}(s) + [u(u-s) - 2\,M^2\,u + 4\,M^2\,s - 2\,M^4]\,\bar{J}(u)\Big] + \frac{1}{96\pi^2\,F^4}\left[2\left(\bar{\ell}_1 - \frac{4}{3}\right)(t-2\,M^2)^2 + \left(\bar{\ell}_2 - \frac{5}{6}\right)(t^2+(s-u)^2) - 12\,M^2\,t + 15\,M^4\right], \tag{7.9}$$

where F is the decay constant of the pion in the chiral limit, $F \simeq F_\pi \simeq 92.4\,\mathrm{MeV}$ and $M \simeq M_\pi \simeq 138\,\mathrm{MeV}$. In Eq. (7.9), $\bar{J}(x) = \{\sigma \ln[(\sigma-1)/(\sigma+1)] + 2\}/(16\pi^2)$, with $\sigma = \sqrt{1-4M^2/x}$, is the two-point one-loop integral for equal masses. $\bar{\ell}_1$ and $\bar{\ell}_2$ are a priori unknown low-energy couplings related with those of the $\mathcal{O}(p^4)$ ChPT Lagrangian with two flavors, $\ell_i^r(\mu)\,(i=1,2)$, through:

$$\ell_1^r(\mu) = \frac{1}{96\pi^2}\left(\bar{\ell}_1 + \ln\frac{M_\pi^2}{\mu^2}\right),$$
$$\ell_2^r(\mu) = \frac{1}{48\pi^2}\left(\bar{\ell}_2 + \ln\frac{M_\pi^2}{\mu^2}\right). \tag{7.10}$$

Here μ is the renormalization scale. With these definitions the $\bar{\ell}_i$ couplings are, but for a factor, equal to $\ell_i^r(M_\pi^2)$ and thus scale independent. It is well known [165] that the $\mathcal{O}(p^4)$ chiral LECs are saturated by the contribution of the lightest resonances that have been integrated out. In fact, $\ell_1^r(\mu)$ and $\ell_2^r(\mu)$ are saturated by the lightest multiplet of vector resonances. Upon resonance integration at tree level one gets the three-flavor LECs $L_i^r(\mu)$. Using the $\mathcal{O}(p^4)$ matching with the two-flavor $\ell_i^r(\mu)$ [177], the resonance contributions to the latter read $\ell_1^r(\mu) = -G_V^2/M_V^2 - \nu_K/24$ and $\ell_2^r(\mu) = G_V^2/M_V^2 - \nu_K/12$. Here $M_V \simeq M_\rho$ is the mass of the lightest nonet of vector resonances, and G_V is a coupling of the Resonance Chiral Theory phenomenological Lagrangian [165].

Its value is estimated as $G_V \in [40,50]\,\mathrm{MeV}$ [178, 179] and we take $G_V \simeq 45\,\mathrm{MeV}$ for the numerical evaluation. In addition $\nu_K = \left(\ln\left(M_K^2/\mu^2\right) + 1\right)/(32\pi^2)$. The constants $\bar{\ell}_i$ become $\mu-$dependent if we substitute the $\ell_i^r(\mu)$ in Eq. (7.10) by the tree-level estimates above. It is generally assumed that vector resonance saturation of the low-energy constants implies that the resonance contributions determine the LECs quite well for a scale μ of the order of the mass of the resonance. Within the interval $\mu \in [0.6, 0.9]$ GeV, the couplings $\bar{\ell}_1$ and $\bar{\ell}_2$ take the values shown in Table 7.1; for the central value, $\mu = M_\rho$, one gets $\bar{\ell}_1 = 0.25$, $\bar{\ell}_2 = 5.03$. With these estimates, we can readily evaluate the zero contour from the $\mathcal{O}(p^4)$ ChPT, and

μ(GeV)	0.6	0.77	0.9
$\overline{\ell}_1$	-0.33	0.25	0.58
$\overline{\ell}_2$	4.46	5.03	5.37
$10^5 r_5^V$	5.55	4.96	4.78
$10^5 r_6^V$	0.67	0.86	0.94

Table 7.1: Renormalization scale dependence of the LECs determinations relevant for the evaluation of the zero contours at $\mathcal{O}(p^4)$ and $\mathcal{O}(p^6)$ in ChPT.

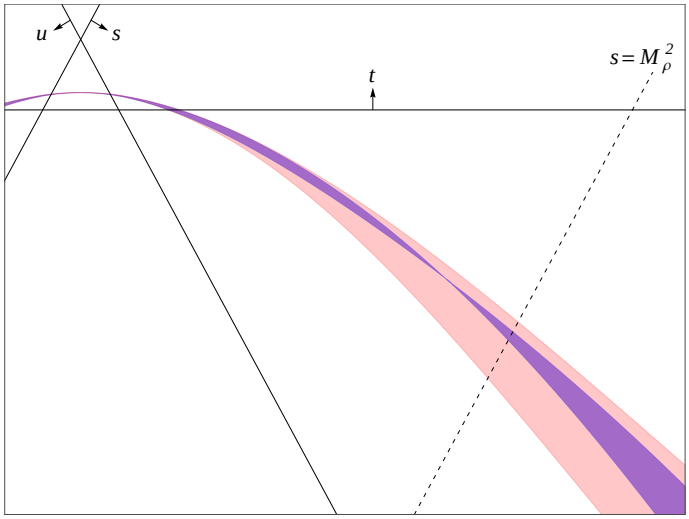

Figure 7.1: Zero contours of $\pi^-\pi^0 \to \pi^-\pi^0$ at $\mathcal{O}(p^4)$ (light colour) and $\mathcal{O}(p^6)$ (dark colour) in the Mandelstam plane. The bands correspond to the range of LECs for $\mu = 0.6\,\text{GeV}$ and $\mu = 0.9\,\text{GeV}$ as given in Table 7.1. The zero contours connect with the Weinberg's projection of the Adler zero inside the Mandelstam triangle [180].

obtain the $\rho(770)$ mass through Eq. (7.7). In the Mandelstam plane the outcome for the zero contours takes the form of the lighter band in Figure 7.1, whose limits are given by the extreme values of $\overline{\ell}_1$ and $\overline{\ell}_2$ in Table 7.1. These zero contours intersect the Re z-axis for $M_R \in [0.69, 0.91]$ GeV. The estimate is particularly good for the central value $\mu = M_\rho$, which yields $M_R = 0.75$ GeV. Let us note that the μ-dependence of the zero contour prediction for the $\rho(770)$ mass does not reflect any uncertainty intrinsic to the method, but is just a consequence of the incomplete knowledge of the resonance estimates of the LECs.

Zero contours at $\mathcal{O}(p^6)$

We would like next to show how the zero contour in Figure 7.1 changes when the next chiral order is considered. The $\pi^-\pi^0 \to \pi^-\pi^0$ amplitude up to $\mathcal{O}(p^6)$

has been computed in Ref. [181]. At this order the result depends on 6 low-energy couplings $r_i^r(\mu)$, $i = 1, \ldots 6$. Assuming that the values of the latter are saturated by vector resonance contributions, one can get estimates for $r_i^r(\mu) \simeq r_i^V$ [181] in the same way as for the $\ell_i^r(\mu)$. We took the formulas for $r_i^V, i = 1, 2, 3, 4$, as given in [181], updating the values of the dimensionless coupling constants g_V and f_χ. Using the present experimental values for the widths of the processes $\rho \to \pi\pi$ and $K^* \to K\pi$ [38], we found $g_V = 0.0892$ and $f_\chi = -0.0238$. The resulting values for $r_i^V, i = 1, 2, 3, 4$, are summarized in Table 7.2. For r_i^V with $i = 5, 6$ we have an updated evaluation, obtained as follows:

1. We use the definition of r_5^V and r_6^V in terms of the $\mathcal{O}(p^6)$ two-flavor LECs $c_i^r(\mu)$ [182],

2. Then we employ the relation of the two-flavor LECs with the three-flavor ones $C_i^r(\mu)$ [183],

3. And finally we determine the latter by integrating the resonance fields at tree-level [184].

Incidentally only vector resonances contribute to r_5^V and r_6^V. The numerical values of r_5^V and r_6^V that we get, shown in Table 7.1, are typically a factor of 2 to 4 smaller than the ones quoted in Ref. [181]. This procedure cannot be applied, at the moment, for r_i^V, $i = 1, 2, 3, 4$, because the conversion between the corresponding LECs with two and three flavors has not been made available yet. However we have updated the numerical values of these constants given in Ref. [181].

The obtained $\mathcal{O}(p^6)$ zero contours are displayed by the darker band of Figure 7.1, that is defined by the μ-dependent values of the LECs given in Table 7.1. The $\rho(770)$ mass estimates from these $\mathcal{O}(p^6)$ zero contours read $M_R \in [0.80, 0.86]$ GeV, and significantly decrease the renormalization-scale ambiguity seen in the $\mathcal{O}(p^4)$ contours. These determinations depend mostly on the values of $r_5^r(\mu)$ and $r_6^r(\mu)$, which are the coefficients of $\mathcal{O}(p^6)$ polynomial terms in $s/(4\pi F_\pi)^2$ that become thus of order $M_\rho^2/(4\pi F_\pi)^2$ close to the resonance. They depend somewhat less on $r_4^r(\mu)$, since the latter multiplies a polynomial term suppressed by a power of $M_\pi^2/(4\pi F_\pi)^2$, and very little on $r_i^r(\mu)$ for $i = 1, 2, 3$. We notice that the resonance estimate of $r_4^r(\mu)$ from Ref. [181] involves a cancellation of two different

LEC	Value
r_1^V	-1.09×10^{-4}
r_2^V	3.03×10^{-4}
r_3^V	-2.79×10^{-4}
r_4^V	-5.75×10^{-5}

Table 7.2: Numerical values for the Low Energy Constants r_i^V $i = 1, 2, 3, 4$ as given by the update of those in Ref. [181].

contributions of similar size. If we, for instance, change the sign of r_4^V, the $\rho(770)$ mass estimates at $\mathcal{O}(p^6)$ are shifted down to $M_R \in [0.78, 0.82]$ GeV. An updated evaluation of the latter would be required before assessing the accuracy of the zero contour approach at $\mathcal{O}(p^6)$ for the case of the $\rho(770)$.

Results for the $\rho(770)$ case

In Figure 7.2 we compare the experimental data on the $\delta_1^1(s)$ phase-shift from elastic $\pi\pi$ scattering with different theoretical predictions. As expected the prediction given by the ChPT amplitude does not provide the right description for $E \sim M_\rho$, as can be seen looking at the dot dashed line that represents the ChPT result for the P-wave phase-shift, namely $\delta_1^1(s) = \sigma\, \mathrm{Re} f_1^1(s)$ [188]. On the other hand the $\delta_1^1(s)$ phase-shift as given by (7.8) is in much better agreement with experimental data. We plotted the theoretical results for two different $I = 2$ S-wave phase-shift representations, the one coming from the $\mathcal{O}(p^4)$ ChPT result (dashed line) and the one given by the Schenk parameterization [189] (continuous line). As

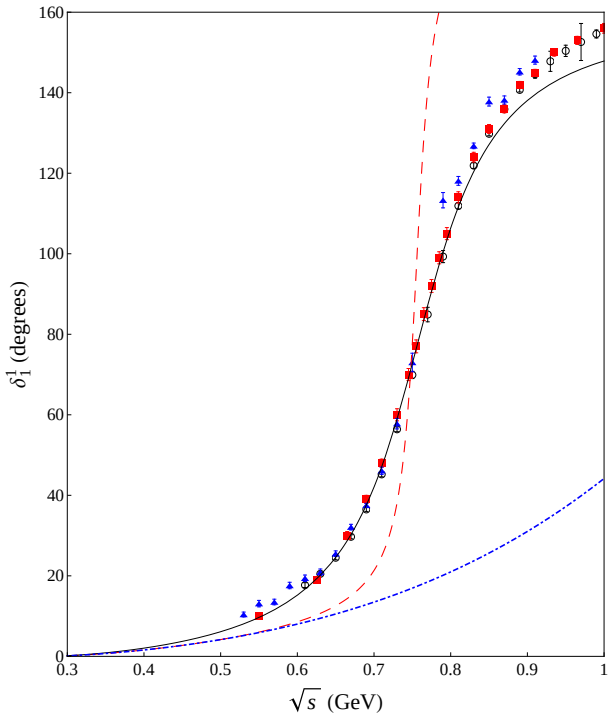

Figure 7.2: $\delta_1^1(s)$ phase-shift in elastic $\pi\pi$ scattering. Comparison of experimental data [185, 186, 187] with the prediction given by Eq. (7.8) for the S-wave given by the Schenk parameterization (continuous line) and by $\mathcal{O}(p^4)$ ChPT (dashed line) with $\bar{\ell}_1 = 0.25$ and $\bar{\ell}_2 = 5.03$. The $\mathcal{O}(p^4)$ ChPT result for the P-wave phase-shift, namely $\delta_1^1(s) = \sigma \mathrm{Re} f_1^1(s)$, is also shown (dot-dashed line).

it can be seen the latter provides a much better agreement to the data in the low-energy region, however the pass through $\pi/2$ depends little on the parameterization used for $\delta_0^2(s)$.

In summary, we have seen that the zeros of the amplitude of elastic $\pi\pi$ scattering carry important dynamical information on the structure of the interaction, in particular the role of vector resonances. This information, encoded in the low-energy couplings of $\mathcal{O}(p^4)$ ChPT, emerges through the zero contour definition and the condition in Eq. (7.7). Alternatively the unitarization in Eq. (7.8) is able to show the mark of the $\rho(770)$ in the $\delta_1^1(s)$ phase-shift, as we demonstrated in Figure 7.2. This is not a trivial exercise because the results of ChPT are only valid for $E \ll M_\rho$, however the smoothness of the zero contour and its stability under unitarization procedures [173, 190], collaborate to disentangle the information of the LECs, at least in the channel we are considering.

7.2. Longitudinally polarized gauge boson scattering

In this work we are interested in the scattering of vector bosons with longitudinal polarization because is the one linked, through the Higgs mechanism, with the Goldstone bosons of the electroweak symmetry breaking sector. The exact relation is provided by the *equivalence theorem* [163, 168]:

$$A\left(V_L^a V_L^b \to V_L^c V_L^d\right) = A\left(\pi^a\pi^b \to \pi^c\pi^d\right) + \mathcal{O}\left(\frac{M_V}{E}\right), \tag{7.11}$$

which states that, at center of mass energies $E \gg M_V$, the amplitude for the elastic scattering of longitudinally polarized vector bosons (V_L^a) equals the amplitude where the gauge fields have been replaced by their corresponding Goldstone bosons (π^a). Now, we can use the electroweak effective Lagrangian (6.10) to calculate the amplitude of Goldstone boson scattering of Eq. (7.11). Since the effective Lagrangian formalism is a low-energy expansion, some care is needed to apply the equivalence theorem, which is valid in the high-energy limit. The restricted version of the theorem which applies to the gauge boson scattering amplitude calculated at $\mathcal{O}(p^4)$ reads [191]:

$$\begin{aligned} A\left(V_L^a V_L^b \to V_L^c V_L^d\right) = A^{(4)}\left(\pi^a\pi^b \to \pi^c\pi^d\right) + \mathcal{O}\left(\frac{M_V}{E}\right) \\ + \mathcal{O}(g, g') + \mathcal{O}\left(\frac{E^5}{\Lambda_{\text{EW}}^5}\right), \end{aligned} \tag{7.12}$$

where $A^{(4)}$ is the amplitude of Goldstone boson scattering at lowest order in the electroweak couplings (g and g') as obtained from the effective Lagrangian $\mathcal{L}_{\text{EChET}}$. Therefore only the operators $\mathcal{O}_4$ and $\mathcal{O}_5$ in Eq. (6.11) contribute to

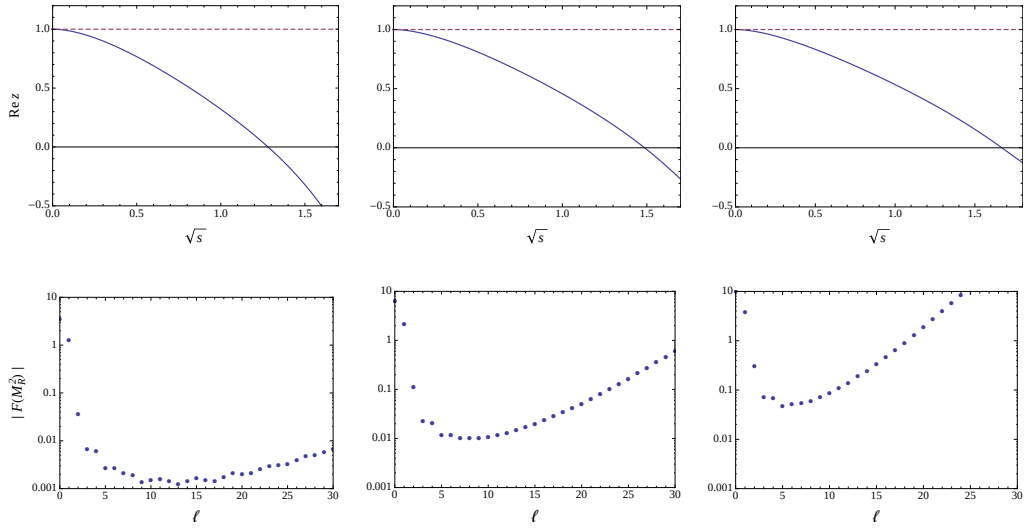

Figure 7.3: Upper panels: Zero contours from the $\mathcal{O}(p^4)$ amplitude for, from left to right, $(\bar{a}_4, \bar{a}_5) = (10, 10)$, $(\bar{a}_4, \bar{a}_5) = (8.5, 10)$ and $(\bar{a}_4, \bar{a}_5) = (7.7, 10)$. The dashed line are the amplitude zeros obtained from the lowest order chiral amplitude. Lower panels: Corresponding $\mathcal{O}(p^4)$ amplitudes $|F(M_R^2)| \equiv |A^{(4)}(M_R^2, z_0(M_R^2))|$ (in logarithmic scale) for the upper panel cases, using the partial-wave expansion up to order ℓ.

that amplitude, which is linear in the a_4 and a_5 couplings. Let us remark that at $\mathcal{O}(g^0, g'^0)$ the masses of the gauge bosons vanish and the equivalence theorem, as given by Eq. (7.12), indicates that the Goldstone boson scattering amplitude has to be calculated in the zero mass limit. Mass corrections appear in the neglected terms.

Notice that the restricted version given by Eq. (7.12) is valid in the energy range given by $M_V \ll E \ll \Lambda_{\rm EW}$. Since the EChET framework is analogous to ChPT, and the latter works reasonably well up to 500 MeV $\simeq 2\pi F_\pi$, we can assume that the effective formalism for the electroweak theory is limited at about $2\sqrt{2}\pi v \simeq 1.5$ TeV. Given the success of the zero-contour method for the case of the $\rho(770)$ resonance, whose mass is larger than the limit of validity of the theory, the range above may be extended up to $E \lesssim 2$ TeV, at least for what concerns the determination of the resonance mass through the zero contours.

7.3. Analysis of the zeros of the $W_LZ_L \to W_LZ_L$ amplitude

The equivalence theorem pointed out in the last section can be used to relate, at leading order, the amplitude of $W_LZ_L \to W_LZ_L$ with the one of the corresponding Goldstone bosons, which is analogous to the $\pi^-\pi^0 \to \pi^-\pi^0$ amplitude described in

Section 7.1. Notice that the physical system provided by the Higgsless Lagrangian in Eq. (6.10) is, but for the change of scale ($F_\pi \to v$), the same than the one of the ChPT. Therefore one would expect a similar dynamics if the P-wave contribution is saturated by a vector resonance. Consequently we could apply the same procedure and study the occurrence of $I = 1$ vector resonances [2] in the scattering $W_L Z_L \to W_L Z_L$ through the analysis of the zero contours of the EChET amplitude. As explained in Section 7.1, zero contours cross the resonance location close to where the Legendre polynomial vanishes, which for vector resonances amounts to the condition (7.7).

By virtue of the equivalence theorem, the amplitude for $W_L Z_L \to W_L Z_L$ is equal, up to $\mathcal{O}(p^4)$ terms, to $A^{(4)}\left(\pi^-\pi^0 \to \pi^-\pi^0\right) = A(t,s,u)$ in Eq. (7.9), with the trivial replacements:

$$F \to v \quad , \quad (\bar{\ell}_1, \bar{\ell}_2) \to (\bar{a}_5, \bar{a}_4)\,.$$

In addition, the limit $M \to 0$ has to be performed, according to the restricted form of the theorem. This amounts to writing $M = 0$ in the polynomial contributions in $A(t,s,u)$. Care has to be taken in the one-loop functions, where keeping the leading order in that limit leaves a mass dependence in the logarithms. The scale-independent $\bar{a}_i$ couplings are related to their renormalized counterparts in the $\overline{\text{MS}}$ scheme as:

$$\begin{aligned} a_4^r(\mu) &= \frac{1}{4}\frac{1}{48\pi^2}\left(\bar{a}_4 - 1 + \ln\frac{M_W^2}{\mu^2}\right), \\ a_5^r(\mu) &= \frac{1}{4}\frac{1}{96\pi^2}\left(\bar{a}_5 - 1 + \ln\frac{M_W^2}{\mu^2}\right). \end{aligned} \tag{7.13}$$

This definition for $a_4^r(\mu)$ and $a_5^r(\mu)$ differs from that of Eq. (7.10) that relates the $\ell_i^r(\mu)$ to the $\bar{\ell}_i$; it matches though the definition used in recent literature [192, 193] for these couplings, so it is adopted here to make contact with those results. The natural order of magnitude of the couplings is $\bar{a}_{4,5} \sim \mathcal{O}(1)$, so we can expect that $a_i^r \sim \mathcal{O}(10^{-3})$.

Recalling the procedure that we used in Section 7.1, we will look for the zero contours of the amplitude, $A^{(4)}(s, z_0) = 0$, and identify the vector resonances with solutions of $\text{Re}\, z_0(M_R^2) = 0$. However we still need to impose another constraint on this result to ensure that the assumptions leading to condition (7.7) are fulfilled. As it was seen in Section 7.1, our procedure depends crucially, after neglecting higher partial waves, on having a dominant resonance-saturated P-wave and a small, non-vanishing, S-wave contribution. We can translate this requirement to a numerical bound in the following way. Writing the equation $A^{(4)}(s, z_0) = 0$ in terms of its partial-wave series, one gets:

$$f_0^2(s) + 3\, f_1^1(s)\, z_0(s) \simeq 0\,, \tag{7.14}$$

[2] Isospin, in the context of the Lagrangian (6.10), indicates the quantum number associated to the unbroken $SU(2)_{L+R}$ custodial symmetry.

if higher-order partial waves are neglected. At the resonance location, $s = M_R^2$, the latter equation relates the size of the imaginary part of the zero with the ratio between the S- and the P-wave contributions:

$$\left|z_0(M_R^2)\right| = \left|\mathrm{Im}\, z_0(M_R^2)\right| = \left|\frac{f_0^2(M_R^2)}{3\, f_1^1(M_R^2)}\right| < \lambda\,. \tag{7.15}$$

The bound λ then defines the range of applicability of our method: zeros of the amplitude with imaginary part smaller than λ can be considered positive results in the search for vector resonances. The zeros which pass this condition bear a similarity to the near-by zeros introduced in the pioneering works on zero contours, characterized by small imaginary parts. A reference value for λ can be inferred from the $\rho(770)$ case studied in Section 7.1, where one gets $|\mathrm{Im}\, z_0(M_\rho^2)| \simeq 0.36$ (for $\mu = 0.77$ GeV; see Table 7.1). For values of λ larger than $1/2$ we cannot consider the S-wave to be significantly smaller than the P-wave, and we therefore choose $\lambda = 1/2$ as a limiting value for the identification of resonances in the zero contours. The dependence of our results on this cut is discussed later.

The λ-cut in Eq. (7.15) is also related with the convergence of the partial-wave expansion of the amplitude. For the zero mass case the partial-wave expansion is convergent only in the physical region, i.e. for $z \equiv \cos\theta \in [-1, 1]$ (see Appendix B). The partial-wave series continued to complex values of z is at best asymptotically convergent. Hence smaller imaginary parts of the zeros imply a better behaviour of the series. In the lower panels of Figure 7.3 we show the convergence of the partial-wave series at $s = M_R^2$ for three representative examples, corresponding (from left to right) to $(\bar{a}_4, \bar{a}_5) = (10, 10), (8.5, 10), (7.7, 10)$, with non-zero imaginary parts given by $|\mathrm{Im}\, z_0(M_R^2)| \simeq 0.26, 0.39$ and 0.56, respectively. As can be seen there is a direct correlation between the size of the imaginary part of $z_0(M_R^2)$ and the convergence of the expansion. Note also that the minimal value of the amplitude at the resonance location gets closer to zero for smaller $|\mathrm{Im}\, z_0(M_R^2)|$. The corresponding zero contours, obtained from the amplitude (7.9) (now keeping only the leading order in the $M \to 0$ limit), are smooth lines in the $(\mathrm{Re}\, z, s)$ plane, as shown in the upper panels of Figure 7.3. The dashed line are the amplitude zeros obtained from the lowest order chiral amplitude, which are simply given by $t = 0$ and thus lie on a straight line in the Mandelstam plane. In terms of z the $\mathcal{O}(p^2)$ zeros are given by $z_0(s) = 1$ and have no imaginary part because the $\mathcal{O}(p^2)$ amplitude is real. The $\mathcal{O}(p^4)$ corrections induce an imaginary part in the zero trajectories, and are essential to bend down the zero contour towards $\mathrm{Re}\, z = 0$. The crossing, from left to right in Figure 7.3, takes place at $M_R \simeq 1.28, 1.49$ and 1.67 TeV.

A final note is needed to interpret correctly the results we will discuss in the next section. Although the ChPT and EChPT cases seem to be identical and related by a simple rescaling ($F \to v$), in evaluating the zeros of the amplitude there are some details we need to take into account. Let us rewrite the $\pi^-\pi^0 \to \pi^-\pi^0$ amplitude $A(t, s, u)$ (7.9), in the limit $M \to 0$, in terms of the dimensionless variables $\hat{s} \equiv s/F^2$

and z. It is immediate to see that it can be split into two terms,

$$A(t,s,u) = A_1(\hat{s},z) + A_2(\hat{s},z)\,, \tag{7.16}$$

with:

$$\begin{aligned} A_1(\hat{s},z) = -\frac{\hat{s}}{2}(1-z) + \frac{\hat{s}^2}{192\pi^2}\Bigg\{ & \frac{13}{2} + z + \frac{11}{6}z^2 + \bar{\ell}_1\,(1-z)^2 + \bar{\ell}_2\,(5+2z+z^2) \\ & -(3+z)\ln(-\hat{s}) - \frac{3}{2}(1-z)^2 \ln\left[\frac{\hat{s}}{2}(1-z)\right] \\ & -\frac{1}{2}(1+z)(3+z)\ln\left[\frac{\hat{s}}{2}(1+z)\right]\Bigg\}\,, \end{aligned} \tag{7.17}$$

$$A_2(\hat{s},z) = \frac{\hat{s}^2}{48\pi^2}\,(3+z^2)\,\ln\left(\frac{M}{F}\right)\,. \tag{7.18}$$

Note that the dependence of the second term on the Goldstone boson mass is just a consequence of having written the amplitude in terms of the "bar" LECs, $\bar{\ell}_1, \bar{\ell}_2$, which correspond to the renormalized ones with $\mu = M$. The zero contours obtained from $A_1(\hat{s},z)$ alone depend only on the values of the LECs, and the corresponding resonance masses are located at $M_R = F\sqrt{\hat{s}_R}$; in order to switch from QCD to the electroweak case we would only need to rescale the value of the resonance masses obtained from the zero contour method, making the substitution $F \to v$. However, the second term in the amplitude, $A_2(\hat{s},z)$, gives a contribution to the zero contour that depends on the ratio M/F, which is very different in the QCD ($M_\pi/F_\pi \simeq 1.5$) and the EW ($M_W/v \simeq 0.33$) cases. In conclusion, the values of the resonance masses found using the zero contour method in the QCD and electroweak can be in general not related by a simple rescaling, giving rise to possibly very different patterns.

7.4. Results and discussion

Figure 7.4 is the central result of our work. The shaded areas show where resonances, defined by the conditions (7.7) and (7.15) with $\lambda = 1/3$, are found in the $(\bar{a}_4, \bar{a}_5)$-plane. The contour lines drawn correspond to pairs of $(\bar{a}_4, \bar{a}_5)$ which yield the same resonance mass. Though the validity of the approach cannot be trusted beyond $E \simeq 2$ TeV, we have displayed in the plot resonances found with masses up to 2.5 TeV. In order to show how dependent are the solutions from Eq. (7.7) to the cut (7.15) on the imaginary part of the zeros, we have also drawn in Figure 7.4 (outer dashed line) the boundary of the region yielding resonances when $\lambda = 1/2$. The hatched region in the left and lower parts of the plot corresponds to values of $\bar{a}_4$ and $\bar{a}_5$ forbidden by positivity conditions on the $\pi\pi$ scattering

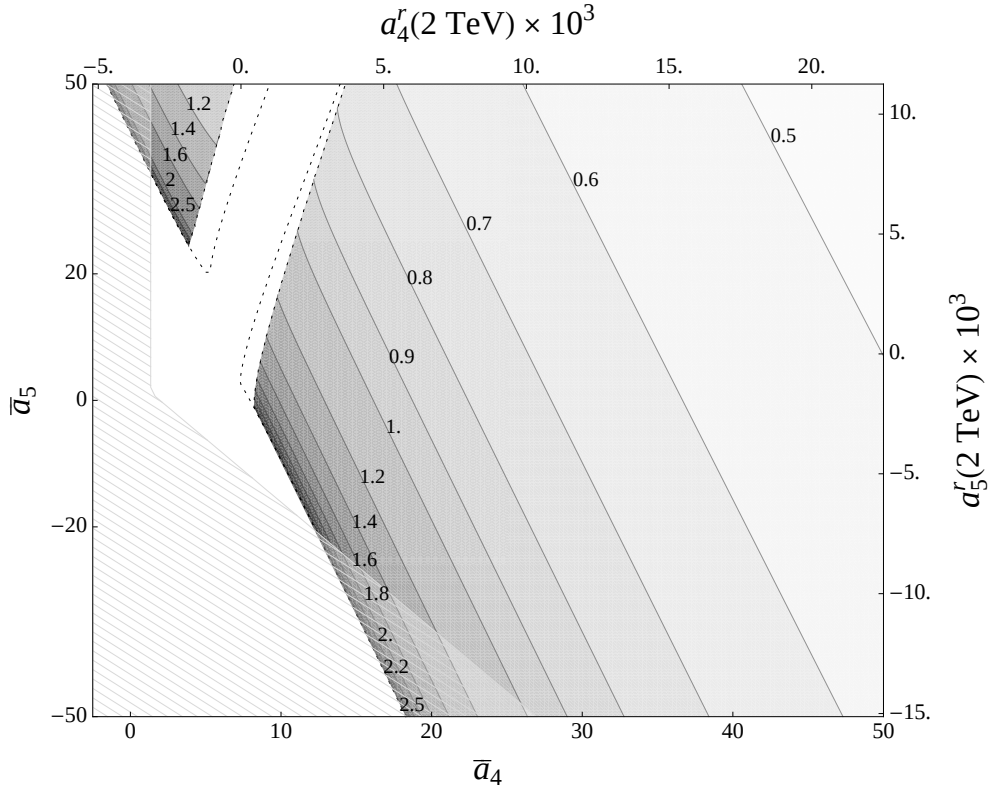

Figure 7.4: Resonance masses as a function of the low-energy couplings $\bar{a}_4$ and $\bar{a}_5$. The scales in terms of the renormalized couplings $a_4^r(\mu)$ and $a_5^r(\mu)$ at $\mu = 2$ TeV are also drawn. The shaded areas show where resonances defined by the conditions (7.7) and (7.15) with $\lambda = 1/3$ are found in the $(\bar{a}_4, \bar{a}_5)$-plane. The contour lines drawn correspond to pairs of $(\bar{a}_4, \bar{a}_5)$ which yield the same resonance mass. The hatched region in the left and lower parts of the plot, given by Eq. (7.19), corresponds to values of $\bar{a}_4$ and $\bar{a}_5$ forbidden by positivity conditions on the $\pi\pi$ scattering amplitudes. The outermost dashed lines mark the boundary of the resonance region corresponding to $\lambda = 1/2$.

amplitudes. These bounds were obtained in Ref. [22], and slightly improved in Ref. [194]. Translated to $\bar{a}_4$ and $\bar{a}_5$ they read:

$$\bar{a}_5 + 2\,\bar{a}_4 \geq \frac{157}{40} \quad , \quad \bar{a}_4 \geq \frac{27}{20}\,. \tag{7.19}$$

Let us comment the most relevant features of the results of Figure 7.4:

i/ No vector resonances are found for $\bar{a}_4 \lesssim 8$ and $\bar{a}_5 \lesssim 25$. This would exclude to a large extent Higgsless models with vector resonances which saturate the low-energy couplings to the expected natural order of magnitude ($\bar{a}_{4,5} \sim 1$). Since in QCD one does find the ρ meson for natural values of the LECs (namely $\bar{\ell}_1^\rho \sim 0$ and $\bar{\ell}_2^\rho \sim 5$), one could naively expect an EW "ρ-like" resonance to be found for $(\bar{a}_4, \bar{a}_5) = (\bar{\ell}_2^\rho\,, \bar{\ell}_1^\rho)$ with a mass $M_\rho^{\rm EW} = (v/F_\pi)\,M_\rho$.

The $\pi\pi$ scattering amplitudes obtained from ChPT and EChPT are however not simply related by a rescaling of the energy variables, but depend also on the (unequal) ratios F_π/M_π and v/M_W through logarithmic terms, as we have seen at the end of Section 7.3.

ii/ Masses above 1.8 TeV are confined to a thin slice in the lower-left and upper-left parts of the shaded regions and are mostly excluded by the positivity constraints. Conversely, light resonances ($\lesssim 0.8$ TeV) require values of either $\bar{a}_4$ or $\bar{a}_5$ larger than 20. The validity of the EChET Lagrangian for such large values of the LECs is nevertheless questionable and could indicate that additional degrees of freedom linked to the Goldstone boson dynamics are missing in the effective description.

iii/ The dependence on the λ-cut is visible in the upper part ($\bar{a}_5 \gtrsim 0$) of the boundary of the allowed region for resonances, where the $\lambda = 1/2$ contour departs from the $\lambda = 1/3$ one, which defines the shaded region. Making the cut smaller would further constrain the region where resonances are found. We nevertheless think that the value $\lambda = 1/3$ is a realistic one, since it provides a reasonable suppression of S-waves and it is also found in the QCD case for the $\rho(770)$ resonance.

iv/ For resonance masses $M_R \lesssim 0.8\,\text{TeV}$, where either $\bar{a}_4$ or $\bar{a}_5$ are large, the formula:

$$M_R = v\left(\frac{192\,\pi^2}{-11 + 10\,\bar{a}_4 + 2\,\bar{a}_5}\right)^{1/2}, \tag{7.20}$$

provides an approximation to the resonance masses in Figure 7.4 with an accuracy better than 10%. The formula (7.20) corresponds to the zero contours obtained by setting the loop functions $\bar{J}(x)$ in $A(t,s,u)$ to zero, and further neglecting the mass M.

v/ A final consistency check for our method is provided by the Eq. (7.8) for the $I = 1$ P-wave phase-shift δ_1^1. We evaluated the energy at which $\delta_1^1 = \pi/2$ for each value of the parameters $\bar{a}_4$, $\bar{a}_5$ in the shaded region of Figure 7.4 and we found that the result is basically the same we obtained from the condition in Eq. (7.7). Indeed, if we allow for at most a 10% deviation between both mass determinations, only the points in a tiny slice lying exactly on the boundary of the lower-half part of the big shaded region (in fact mostly excluded already by the positivity constraints) fail to pass the test. This result confirms that the S-wave background is indeed small, and therefore that the condition Re $z_0(M_R^2) \simeq 0$ is a characteristic signature for vector resonances. As it was commented in relation with Figure 7.2, this result does not depend, essentially, on our knowledge of the $\delta_0^2(s)$ phase shift. It is enough that this is small with respect to the $\delta_1^1(s)$ phase shift at $E \simeq M_R$.

The LHC sensitivity to explore the values of the coefficients a_4 and a_5 has been investigated in Ref. [192]. The reported limits imply that in the combined region $\bar{a}_4 \lesssim 35$ and $-38 < \bar{a}_5 < 45$ no deviation from the SM prediction could be observed at the LHC. The prospects of measuring these parameters with improved accuracy in a high-luminosity e^+e^- collider operating at 1 TeV are slightly better [195]. On the other hand, present limits on new vector resonances could be used in combination with our results in Figure 7.4 to constrain the allowed regions of $\bar{a}_4$ and $\bar{a}_5$ which can accommodate a vector-saturated model. Using ATLAS and CMS data, the most recent bounds on the mass of new charged vector resonances have been obtained analyzing $\ell\nu_\ell$ ($\ell = \mu, e$) [196] or WZ [197, 198] final states. Depending on the model assumed to interpret the data, it is possible to exclude resonances with a mass as heavy as 1.14 and 2.5 TeV, in the WZ and leptonic case respectively. The present bounds on new neutral vector resonances obtained recently [199] exclude masses up to 1-2.3 TeV depending on their couplings and widths.

A systematic study of resonance masses in the parametric space spanned by $a_4^r(\mu)$ and $a_5^r(\mu)$ using the Inverse Amplitude Method (IAM) has also been performed [200, 201]. Their results, compared with our Figure 7.4, look rather different. From the pole of the Padé-improved P-wave they find for the vector resonance masses the result:

$$M_R^{\rm IAM} = v\left(\frac{144\,\pi^2}{3\,\bar{a}_4 - 3\,\bar{a}_5 + 1}\right)^{1/2}, \tag{7.21}$$

that can be compared with our Eq. (7.20), though the latter is only valid for large values of $\bar{a}_4, \bar{a}_5$, i.e. for $M_R \lesssim 0.8\,\text{TeV}$. The slope of the lines of equal mass do not agree. Moreover, formula (7.21) forbids vector resonances in the region defined by $\bar{a}_5 > \bar{a}_4 + 1/3$, where their existence is consistent with our conditions. Also we note that the results of [200, 201] predict resonances in the region of $\bar{a}_{4,5} \sim 1$, that contradicts our findings. As emphasized in the IAM works (see for instance Ref. [39], p. 159) the LEC constants in the IAM amplitude are not to be identified with the chiral LECs of ChPT. Therefore the $\bar{a}_4$ and $\bar{a}_5$ in Eq. (7.21) do not correspond to our $\bar{a}_4$, $\bar{a}_5$ defined in Eq. (7.13). However this mishap alone cannot explain the very different results obtained from both procedures. A detailed comparative analysis between both methods in order to trace the origin of the discrepancies shall be carried out elsewhere.

7.5. Conclusions

In this work we have investigated a method to identify vector resonances originated from a strong electroweak symmetry-breaking sector in the 1 TeV energy region. These resonances could be a possible alternative to the SM Higgs in preventing the seeming loss of perturbative partial-wave unitarity in the elastic scattering of the longitudinal components of W and Z gauge bosons. More important is that those resonances would provide a clear signal that a strong interacting dynamics

is responsible for the spontaneous breaking of the electroweak symmetry.

We have focused, in particular, on the resonances that could contribute to the $W_L Z_L \to W_L Z_L$ scattering. This channel has the appropriate characteristics to implement our approach, that searches for vector resonances dominating the amplitude. Assuming resonance saturation of the LECs of the effective chiral Lagrangian describing the interaction among Goldstone bosons, we could extract relevant information on the lightest vector resonances from the zeros of the elastic scattering amplitude. We first applied our method to the well known case of the $\rho(770)$ resonance and the $\mathcal{O}(p^4)$ chiral $\pi^-\pi^0 \to \pi^-\pi^0$ amplitude and considered the impact of introducing the next order in the chiral expansion.

Turning to the electroweak case we exploited the fact that, at leading order in the expansion provided by the equivalence theorem, the dynamics of the longitudinally polarized gauge boson scattering is described by the electroweak chiral Lagrangian (6.10), which is identical to the one that generates the $\rho(770)$ in elastic $\pi\pi$ scattering upon the obvious change of scale $F_\pi \to v$. Within this approach we have explored the parameter space of the two low-energy couplings $\bar{a}_4$ and $\bar{a}_5$ needed to describe the $W_L Z_L \to W_L Z_L$ scattering amplitude, in order to identify the region where a vector resonance can dominate the amplitude, and provide an estimate of its mass. The outcome has been shown in Figure 7.4 as a contour plot in the ($\bar{a}_4$,$\bar{a}_5$)-plane. Our main conclusion is that no vector resonances are found for $\bar{a}_4 \lesssim 8$ and $\bar{a}_5 \lesssim 25$, indicating that Higgsless models with vector resonances which saturate the low-energy couplings to the expected natural order of magnitude ($\bar{a}_{4,5} \sim 1$) would be excluded to a large extent. If we consider the neighborhood outside that natural order of magnitude, we see that the first resonances, appearing for $\bar{a}_4 \gtrsim 8$, have masses above 1 TeV. Lighter vector resonance masses appear for rather unnatural values of the parameters.

The improvement of our method by the inclusion of the $\mathcal{O}(p^6)$ contributions will entail a few technical difficulties, since it carries many new couplings (as it was seen in the QCD case in Section 7.1) that make an analogous treatment to the one proposed here rather cumbersome. Nevertheless, if LHC confirms that there is no light Higgs, the study of the zeros of the gauge boson scattering amplitudes with the use of effective field theories driven by the spontaneous symmetry breaking pattern could provide a model-independent tool to explore the role of the resonances emerging from the new strong dynamics and shall therefore be pursued, for instance, through the search for higher spin states.

Conclusions

The LHC made a big step ahead in the search for the SM Higgs boson with the discovery of a new boson announced on July 4^{th}, 2012. It is in fact the first strong indication that the symmetry breaking picture of SM could be actually realized in Nature through a Higgs mechanism. Awaiting further confirmations, from a theoretical point of view it is interesting to consider both the SM scenario and the possibility that a strongly interacting sector would be responsible for the electroweak symmerry breaking. In this second case, as we have seen in Chapter 7, it is possible to include the boson discovered by LHC as a light pseudo-Goldstone boson related to the strong sector.

In this thesis we developed analyses based on both Higgs and Higgsless scenarios, analyzing the present phenomenology and the possible role of upcoming experimental tests, with the aim of extracting valuable information to build a coherent description of beyond SM physics. Throughout the thesis we used an effective field theory approach that allowed us to deliver results valid for a broad range of models and to treat very different issues in a unified and simple language.

The first part of the thesis has been dedicated to the light Higgs scenario, in which we assumed that the electroweak symmetry breaking is associated to a non-zero vacuum expectation value of a Higgs boson with a mass well below the TeV scale. The possibility of uncovering NP effects involving flavor violation using leptonic decays of pseudoscalar mesons has been analyzed in Chapter 3. These processes are a perfect test-bench due to their strong helicity suppression and the extreme precision of the current experimental data, in particular on π and K decays. Taking advantage of the high accuracy within which it is possible to predict the lepton-flavor universality ratios $R_P^{\ell\ell'} = \mathcal{B}(P \to \ell\nu)/\mathcal{B}(P \to \ell'\nu)$, in this work we have analyzed the deviations from the SM in these ratios using a general effective theory approach and employing different ansätze about the flavor-symmetry breaking structures of physics beyond the SM. We found that, assuming a minimal breaking of the lepton flavor symmetry, the effects are too small to be observed in the next generations of experiments in all relevant meson systems ($P = \pi, K, B$). On the other hand, if we take into account a Grand Unified framework, large violations of lepton-flavor universality are possible in the B system (see Table 3.3). These are possible mainly because of the enhancement of the flavor-violating $B \to e\nu_\tau$ rate. This result can be extremely interesting in view of the

future precision improvement of heavy-meson decay data expected at the Super-B factories.

The apparent discrepancy between the SM predictions and the latest results from the LEP2 experiment about the universality of the coupling of leptons to the gauge bosons was the subject of Chapter 4. In fact the most recent data showed a deviation from universality in the $W\ell\nu_\ell$ coupling of more than two sigmas when comparing the third leptonic family with the two light ones, as shown in Eq. (4.1). We then tested the possibility that this deviation represents a real NP effect, performing an Effective Field Theory analysis in which we assumed different flavor symmetries where the third family plays a special role. Within this framework we have found that EW precision observables (EWPO) represent such a strong constraint that not even in a global analysis where all the effective dimension-six operators affecting the third family are present one can accommodate the anomaly (see Eq. 4.37). So, if this departure from universality would be confirmed by new data, our analysis inevitably points toward a different description of NP that could involve new light degrees of freedom, like a charged Higgs, or a strongly interacting sector with flavor dependent couplings to leptons.

In Chapter 5 we analyzed the impact of the next generation of neutron β-decay experiments in constraining beyond SM scalar and tensor interactions. We performed a comprehensive analysis of the constraints coming from a broad range of low-energy probes (neutron decay, nuclear decays, pion decays) as well as collider searches. Using the last lattice-QCD estimates of the scalar and tensor form-factors, we found that to fully exploit the increased experimental sensitivity will require understanding the lattice-QCD estimates of the proton-to-neutron matrix elements at the level of 10–20% (see Figure 5.5). We have then provided a preliminary estimate of expected future bounds from the LHC, finding that the future collider constraints (associated with effective scales $\Lambda_{S,T} \sim 7$ TeV, for scalar (S) and tensor (T) interactions) will compete with improved neutron-decay constraints based on experimental sensitivities $\delta b, \delta b_\nu \sim 10^{-3}$ in the Fierz interference term and neutrino asymmetry (see Figure 5.7). On the other hand experiments aiming for $\delta b, \delta b_\nu \sim 10^{-4}$ would provide an unmatched discovery potential for new scalar and tensor interactions. Finally, if a charged resonance decaying to an electron plus missing energy is discovered at the LHC, we have shown how, with some theoretical assumptions, the production cross-section provides a lower bound on the scalar interaction probed at low energy (see Figures 5.8, 5.9, and 5.10).

In the second part of the thesis we considered a Higgsless scenario, in which the electroweak symmetry breaking sector was described through a non-linear sigma model. Some details on the construction of the $\mathcal{O}(p^4)$ electroweak chiral Lagrangian has been given in Chapter 6. In this framework we could exploit the similarities between the Higgsless electroweak effective theory and Chiral Perturbation Theory to investigate a method to identify vector resonances originated from a strong electroweak symmetry-breaking sector standing in the 1 TeV energy region. We

focused, in particular, on the $W_L Z_L \to W_L Z_L$ scattering channel, appropriate to implement our approach, that searches for vector resonances dominating the amplitude and assumes resonance saturation of the LECs of the effective chiral Lagrangian.

In order to demonstrate how the method worked, we applied it to the well known case of the $\rho(770)$ resonance and the $\mathcal{O}(p^4)$ chiral $\pi^-\pi^0 \to \pi^-\pi^0$ amplitude and we considered also the impact of introducing the next order in the chiral expansion. In the electroweak case we explored the parameter space of the two low-energy couplings $\bar{a}_4$ and $\bar{a}_5$ needed to describe the $W_L Z_L \to W_L Z_L$ scattering amplitude, in order to identify the region where a vector resonance can dominate the amplitude, and provide an estimate of its mass. The outcome has been shown in Figure 7.4 as a contour plot in the ($\bar{a}_4$,$\bar{a}_5$)-plane. Our main conclusion is that no vector resonances are found for $\bar{a}_4 \lesssim 8$ and $\bar{a}_5 \lesssim 25$, indicating that Higgsless models with vector resonances which saturate the low-energy couplings to the expected natural order of magnitude ($\bar{a}_{4,5} \sim 1$) would be excluded to a large extent. On the other hand lighter vector resonance masses appear for rather unnatural values of the parameters. If LHC would hint for the presence of a strongly interacting sector at the TeV scale, the study of the zeros of the gauge boson scattering amplitudes with the use of effective field theories driven by the spontaneous symmetry breaking pattern could provide a model-independent tool to explore the role of the resonances emerging from the new strong dynamics.

Appendix A

Details of neutron decay distribution

The effective Fierz interference term $\bar{b}$ and effective energy-dependent correlation coefficients $\bar{a}(E_e)$, $\bar{A}(E_e)$, $\bar{B}(E_e)$ and $\bar{C}_{(aa,aA,aB)}(E_e)$ introduced in Eq. 5.9 are [115, 116]:

$$\bar{b} = b^{\rm SM} + b^{\rm BSM} \tag{A.1a}$$

$$\bar{a}(E_e) = \left(a_{\rm LO}(\tilde{\lambda}) + c_0^{(a)} + c_1^{(a)}\frac{E_e}{M_N}\right)\left(1 + \frac{\alpha}{2\pi}\delta_\alpha^{(2)}(E_e)\right) \tag{A.1b}$$

$$\bar{A}(E_e) = \left(A_{\rm LO}(\tilde{\lambda}) + c_0^{(A)} + c_1^{(A)}\frac{E_e}{M_N}\right)\left(1 + \frac{\alpha}{2\pi}\delta_\alpha^{(2)}(E_e)\right) \tag{A.1c}$$

$$\bar{B}(E_e) = B_{\rm LO}(\tilde{\lambda}) + c_0^{(B)} + c_1^{(B)}\frac{E_e}{M_N} + \frac{m_e}{E_e}\left(b_\nu^{\rm SM} + b_\nu^{\rm BSM}\right) \tag{A.1d}$$

$$\bar{C}_{(aa)}(E_e) = c_1^{(aa)}\frac{E_e}{M_N} \tag{A.1e}$$

$$\bar{C}_{(aA)}(E_e) = c_1^{(aA)}\frac{E_e}{M_N} \tag{A.1f}$$

$$\bar{C}_{(aB)}(E_e) = \left(c_0^{(aB)} + c_1^{(aB)}\frac{E_e}{M_N}\right) \ . \tag{A.1g}$$

In these expressions the subscript LO indicates the well-known leading-order contributions that survive if we neglect the radiative corrections, recoil effects and new-physics contributions[1]

$$a_{\rm LO}(\lambda) = \frac{1-\lambda^2}{1+3\lambda^2} \ , \quad A_{\rm LO}(\lambda) = \frac{2\lambda(1-\lambda)}{1+3\lambda^2} \ , \quad B_{\rm LO}(\lambda) = \frac{2\lambda(1+\lambda)}{1+3\lambda^2} \ . \tag{A.2}$$

As discussed in the main text, the linear new-physics effect due to the ϵ_R coupling has been included in the replacement $\lambda \to \tilde{\lambda} = \lambda(1-2\epsilon_R)$. The only other linear

[1] In that limit, of course $\tilde{\lambda} \to \lambda$ in $a_{\rm LO}, A_{\rm LO}$ and $B_{\rm LO}$.

BSM effects in the differential distribution are $b^{\rm BSM}$ and $b_\nu^{\rm BSM}$, whose expressions are shown in the main text, Eqs. (5.11).

Radiative corrections are encoded in the function $\delta_\alpha^{(2)}(E_e)$ [115], while recoil corrections are encoded in the coefficients $c_{0,1}^{a,A,B,aa,aA,aB}$, $b^{\rm SM}$ and $b_\nu^{\rm SM}$, whose explicit expressions are [116]

$$c_0 = -\frac{2\lambda(\lambda+\mu_V)}{1+3\lambda^2}\,\frac{E_0}{M_N} \tag{A.3}$$

$$c_1 = \frac{3+4\lambda\mu_V+9\lambda^2}{1+3\lambda^2} \tag{A.4}$$

$$c_0^{(a)} = \frac{2\lambda(\lambda+\mu_V)}{1+3\lambda^2}\,\frac{E_0}{M_N} \tag{A.5}$$

$$c_1^{(a)} = -\frac{4\lambda(3\lambda+\mu_V)}{1+3\lambda^2} \tag{A.6}$$

$$c_0^{(A)} = \frac{(\lambda-1)(\lambda+\mu_V)}{1+3\lambda^2}\,\frac{E_0}{M_N} \tag{A.7}$$

$$c_1^{(A)} = \frac{\mu_V(1-3\lambda)+\lambda(7-5\lambda)}{1+3\lambda^2} \tag{A.8}$$

$$c_0^{(B)} = -\frac{2\lambda(\lambda+\mu_V)}{1+3\lambda^2}\,\frac{E_0}{M_N} \tag{A.9}$$

$$c_1^{(B)} = \frac{\mu_V(1+3\lambda)+\lambda(5+7\lambda)}{1+3\lambda^2} \tag{A.10}$$

$$c_0^{(aB)} = \frac{(1+\lambda)(\lambda+\mu_V)}{1+3\lambda^2}\,\frac{E_0}{M_N} \tag{A.11}$$

$$c_1^{(aB)} = -\frac{(\mu_V+7\lambda)(1+\lambda)}{1+3\lambda^2} \tag{A.12}$$

$$c_1^{(aa)} = -\frac{3(1-\lambda^2)}{1+3\lambda^2} \tag{A.13}$$

$$c_1^{(aA)} = \frac{(\lambda-1)(\mu_V+5\lambda)}{1+3\lambda^2} \tag{A.14}$$

$$b^{\rm SM} = -\frac{m_e}{M_N}\,\frac{1+2\,\mu_V\lambda+\lambda^2}{1+3\lambda^2} \tag{A.15}$$

$$b_\nu^{\rm SM} = -\frac{m_e}{M_N}\,\frac{(1+\lambda)(\mu_V+\lambda)}{1+3\lambda^2} \tag{A.16}$$

In the above relations μ_V represents the difference between the proton and neutron magnetic moments. Numerically, one has $b^{\rm SM} = -1.35(1)\times 10^{-3}$ and $b_\nu^{\rm SM} = -1.27(1)\times 10^{-3}$.

Appendix B

Convergence of the partial-wave expansion in $\pi\pi$ scattering

The partial-wave expansion of the elastic $\pi\pi$ scattering amplitude for a fixed s is defined in the real interval $z = [-1, 1]$, but it can be analytically continued to a larger region in the complex z-plane, according to a well-known theorem by K. Neumann (see *e.g.* Ref. [202]). The theorem states that the expansion of a function $f(z)$ in a series of Legendre polynomials is absolutely convergent in the interior of the largest ellipse with foci at $z = \pm 1$ in which $f(z)$ is analytic, and divergent in the exterior of the ellipse. In our case $f(z)$ is the $\mathcal{O}(p^4)$ chiral amplitude $A(t(s,z), s, u(s,z))$, Eq. (7.9), which for a fixed s has branch discontinuities at the t-channel and u-channel thresholds, *i.e.* at $t = 4M^2$ and $u = 4M^2$. In the complex z-plane this translates to branch cuts extending from $z_+ = 1 + 8M^2/(s - 4M^2)$

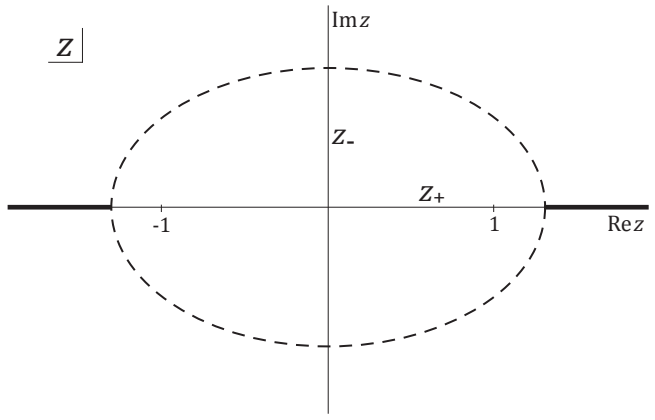

Figure B.1: Ellipse of convergence of the partial-wave expansion in Eq. (7.3). See text for a detailed explanation.

to $+\infty$ and from $(-z_+)$ to $-\infty$. The region of convergence of the partial-wave expansion for $A(t(s,z),s,u(s,z))$ is thus an ellipse with foci at $z=\pm 1$ and semi-major axis z_+ and is sketched graphically in Figure B.1. The semi-minor axis of the ellipse of convergence is equal to

$$z_- = \sqrt{z_+^2 - 1} = \frac{4\,M\,\sqrt{s}}{s-4M^2}\,, \tag{B.1}$$

and limits the size of the imaginary part of z for which the partial-wave series converges. Incidentally, for $M=0$ the ellipses contracts to the interval $z=[-1,1]$ and, hence, the partial-wave expansion is not convergent for $\mathrm{Im}\,z \neq 0$.

Bibliography

[1] A. Pich, "The Standard Model of Electroweak Interactions," arXiv:1201.0537 [hep-ph].

[2] W. Buchmuller and D. Wyler, "Effective Lagrangian Analysis of New Interactions and Flavor Conservation," *Nucl. Phys.* **B268** (1986) 621.

[3] C. N. Leung, S. T. Love, and S. Rao, "Low-Energy Manifestations of a New Interaction Scale: Operator Analysis," *Z. Phys.* **C31** (1986) 433.

[4] V. Cirigliano, B. Grinstein, G. Isidori, and M. B. Wise, "Minimal flavor violation in the lepton sector," *Nucl. Phys.* **B728** (2005) 121–134, arXiv:hep-ph/0507001.

[5] A. Filipuzzi and G. Isidori, "Violations of lepton-flavour universality in $P \to \ell\nu$ decays: A Model-independent analysis," *Eur.Phys.J.* **C64** (2009) 55–62, arXiv:0906.3024 [hep-ph].

[6] B. Grinstein, V. Cirigliano, G. Isidori, and M. B. Wise, "Grand unification and the principle of minimal flavor violation," *Nucl. Phys.* **B763** (2007) 35–48, arXiv:hep-ph/0608123.

[7] **ALEPH** Collaboration, A. Heister *et al.*, "Measurement of W-pair production in e^+e^- collisions at centre-of-mass energies from 183 GeV to 209 GeV," *Eur.Phys.J.* **C38** (2004) 147–160.

[8] **L3** Collaboration, P. Achard *et al.*, "Measurement of the cross section of W-boson pair production at LEP," *Phys.Lett.* **B600** (2004) 22–40, arXiv:hep-ex/0409016 [hep-ex].

[9] **DELPHI** Collaboration, J. Abdallah *et al.*, "Measurement of the W pair production cross-section and W branching ratios in e^+e^- collisions at $\sqrt{s} = 161$ GeV to 209 GeV," *Eur.Phys.J.* **C34** (2004) 127–144, arXiv:hep-ex/0403042 [hep-ex].

[10] **OPAL** Collaboration, G. Abbiendi *et al.*, "Measurement of the $e^+e^- \to W^+W^-$ cross section and W decay branching fractions at LEP," *Eur.Phys.J.* **C52** (2007) 767–785, arXiv:0708.1311 [hep-ex].

[11] **LEP Electroweak Working Group, ALEPH, DELPHI, L3, OPAL** Collaboration, J. Alcaraz *et al.*, "A Combination of preliminary electroweak measurements and constraints on the standard model," arXiv:hep-ex/0612034 [hep-ex].

[12] A. Filipuzzi, J. Portolés, and M. González-Alonso, "$U(2)^5$ flavor symmetry and lepton universality violation in $W \to \tau\nu_\tau$," *Phys. Rev. D* **85** (2012) 116010, arXiv:1203.2092 [hep-ph].

[13] R. Dermisek, "Light Charged Higgs and Lepton Universality in W boson Decays," arXiv:0807.2135 [hep-ph].

[14] J. hyeon Park, "Lepton non-universality at LEP and charged Higgs," *JHEP* **0610** (2006) 077, arXiv:hep-ph/0607280 [hep-ph].

[15] **BaBar** Collaboration, J. Lees *et al.*, "Evidence for an excess of $\bar{B} \to D^{(*)}\tau^-\bar{\nu}_\tau$ decays," arXiv:1205.5442 [hep-ex].

[16] H. Abele, "The neutron. Its properties and basic interactions," *Prog.Part.Nucl.Phys.* **60** (2008) 1–81.

[17] D. Dubbers and M. G. Schmidt, "The neutron and its role in cosmology and particle physics," *Rev.Mod.Phys.* **83** (2011) 1111–1171, arXiv:1105.3694 [hep-ph].

[18] T. Bhattacharya, V. Cirigliano, S. D. Cohen, A. Filipuzzi, M. González-Alonso, *et al.*, "Probing Novel Scalar and Tensor Interactions from (Ultra)Cold Neutrons to the LHC," *Phys.Rev.* **D85** (2012) 054512, arXiv:1110.6448 [hep-ph].

[19] A. C. Longhitano, "Low-Energy Impact of a Heavy Higgs Boson Sector," *Nucl.Phys.* **B188** (1981) 118.

[20] A. C. Longhitano, "Heavy Higgs Bosons in the Weinberg-Salam Model," *Phys.Rev.* **D22** (1980) 1166.

[21] T. Appelquist and G.-H. Wu, "The Electroweak chiral Lagrangian and new precision measurements," *Phys.Rev.* **D48** (1993) 3235–3241, arXiv:hep-ph/9304240 [hep-ph].

[22] M. Pennington and J. Portolés, "The Chiral Lagrangian parameters, ℓ_1, ℓ_2, are determined by the ρ resonance," *Phys.Lett.* **B344** (1995) 399–406, arXiv:hep-ph/9409426 [hep-ph].

[23] A. Filipuzzi, J. Portolés, and P. Ruiz-Femenía, "Zeros of the $W_L Z_L \to W_L Z_L$ amplitude: where vector resonances stand," arXiv:1205.4682 [hep-ph].

[24] D. Gross and F. Wilczek, "Ultraviolet Behavior of Nonabelian Gauge Theories," *Phys.Rev.Lett.* **30** (1973) 1343–1346.

[25] S. Weinberg, "Nonabelian Gauge Theories of the Strong Interactions," *Phys.Rev.Lett.* **31** (1973) 494–497.

[26] H. Fritzsch, M. Gell-Mann, and H. Leutwyler, "Advantages of the Color Octet Gluon Picture," *Phys.Lett.* **B47** (1973) 365–368.

[27] S. Glashow, "Partial Symmetries of Weak Interactions," *Nucl.Phys.* **22** (1961) 579–588.

[28] S. Weinberg, "A Model of Leptons," *Phys.Rev.Lett.* **19** (1967) 1264–1266.

[29] A. Salam, *Elementary particle physics*. N. Svartholm, 1969.

[30] A. Pich, "Aspects of quantum chromodynamics," `arXiv:hep-ph/0001118 [hep-ph]`.

[31] P. W. Higgs, "Broken symmetries, massless particles and gauge fields," *Phys.Lett.* **12** (1964) 132–133.

[32] P. W. Higgs, "Spontaneous Symmetry Breakdown without Massless Bosons," *Phys.Rev.* **145** (1966) 1156–1163.

[33] N. Cabibbo, "Unitary Symmetry and Leptonic Decays," *Phys.Rev.Lett.* **10** (1963) 531–533.

[34] M. Kobayashi and T. Maskawa, "CP Violation in the Renormalizable Theory of Weak Interaction," *Prog.Theor.Phys.* **49** (1973) 652–657.

[35] L. Wolfenstein, "Parametrization of the Kobayashi-Maskawa Matrix," *Phys.Rev.Lett.* **51** (1983) 1945.

[36] B. Pontecorvo, "Mesonium and anti-mesonium," *Sov.Phys.JETP* **6** (1957) 429.

[37] Z. Maki, M. Nakagawa, and S. Sakata, "Remarks on the unified model of elementary particles," *Prog.Theor.Phys.* **28** (1962) 870–880.

[38] **Particle Data Group** Collaboration, J. Beringer *et al.*, "2012 Review of Particle Physics," *Phys. Rev.* **D86** (2012) 010001. `http://pdg.lbl.gov/`.

[39] A. Dobado, A. Gómez-Nicola, A. L. Maroto, and J. R. Peláez, *Effective Lagrangians for the Standard Model*. Springer, Heidelberg, 1997.

[40] B. Grzadkowski, M. Iskrzynski, M. Misiak, and J. Rosiek, "Dimension-Six Terms in the Standard Model Lagrangian," *JHEP* **1010** (2010) 085, `arXiv:1008.4884 [hep-ph]`.

[41] J. D. Bjorken and S. D. Drell, *Relativistic Quantum Mechanics*. McGraw-Hill Inc., New York, USA, 1964.

[42] G. D'Ambrosio, G. F. Giudice, G. Isidori, and A. Strumia, "Minimal flavour violation: An effective field theory approach," *Nucl. Phys.* **B645** (2002) 155–187, arXiv:hep-ph/0207036.

[43] P. Paradisi, M. Ratz, R. Schieren, and C. Simonetto, "Running minimal flavor violation," *Phys.Lett.* **B668** (2008) 202–209, arXiv:0805.3989 [hep-ph].

[44] G. Cacciapaglia, C. Csaki, J. Galloway, G. Marandella, J. Terning, *et al.*, "A GIM Mechanism from Extra Dimensions," *JHEP* **0804** (2008) 006, arXiv:0709.1714 [hep-ph].

[45] A. L. Kagan, G. Perez, T. Volansky, and J. Zupan, "General Minimal Flavor Violation," *Phys.Rev.* **D80** (2009) 076002, arXiv:0903.1794 [hep-ph].

[46] M. Raidal *et al.*, "Flavour physics of leptons and dipole moments," *Eur. Phys. J.* **C57** (2008) 13–182, arXiv:0801.1826 [hep-ph].

[47] **NA48/2 and NA62** Collaboration, E. Goudzovski, "Kaon programme at CERN: recent results," arXiv:1111.2818 [hep-ex].

[48] **KLOE** Collaboration, B. Sciascia, "Test of lepton flavor universality with Ke2 decay at KLOE and KLOE-2," *PoS* **HQL2010** (2011) 027. http://pos.sissa.it//archive/conferences/128/027/HQL%202010_027.pdf.

[49] E. Goudzovski, "Prospects for lepton universality test with k_{e2} $k_{\mu 2}$," in *NA62 Physics Handbook Workshop*. 2009. http://indico.cern.ch/contributionDisplay.py?contribId=28&confId=65927.

[50] A. Sher, M. Aoki, M. Blecher, D. Bryman, J. Comfort, *et al.*, "PIENU experiment at TRIUMF: Measurement of $\pi \to e\nu/\pi \to \mu\nu$ branching ratio," *AIP Conf.Proc.* **1182** (2009) 702–705.

[51] **BaBar** Collaboration, B. Aubert *et al.*, "A Search for $B^+ \to \ell^+\nu_\ell$ Recoiling Against $B^- \to D^0\ell^-\bar{\nu}X$," *Phys.Rev.* **D81** (2010) 051101, arXiv:0912.2453 [hep-ex].

[52] **Belle** Collaboration, K. Hara *et al.*, "Evidence for $B^- \to \tau^-\bar{\nu}$ with a Semileptonic Tagging Method," *Phys.Rev.* **D82** (2010) 071101, arXiv:1006.4201 [hep-ex].

[53] **CLEO** Collaboration, B. Eisenstein *et al.*, "Precision Measurement of $B(D^+ \to \mu^+\nu)$ and the Pseudoscalar Decay Constant f_{D^+}," *Phys.Rev.* **D78** (2008) 052003, arXiv:0806.2112 [hep-ex].

[54] **BaBar** Collaboration, P. del Amo Sanchez *et al.*, "Measurement of the Absolute Branching Fractions for $D_s^- \to \ell^- \bar{\nu}_\ell$ and Extraction of the Decay Constant f_{D_s}," *Phys.Rev.* **D82** (2010) 091103, arXiv:1008.4080 [hep-ex].

[55] **CLEO** Collaboration, J. Alexander *et al.*, "Measurement of $B(D_s^+ \to \ell^+ \nu)$ and the Decay Constant $f_{D_s^+}$ From 600 pb^{-1} of $e^\pm$ Annihilation Data Near 4170 MeV," *Phys.Rev.* **D79** (2009) 052001, arXiv:0901.1216 [hep-ex].

[56] G. Isidori and P. Paradisi, "Hints of large $\tan\beta$ in flavour physics," *Phys. Lett.* **B639** (2006) 499–507, arXiv:hep-ph/0605012.

[57] R. S. Chivukula and H. Georgi, "Composite Technicolor Standard Model," *Phys.Lett.* **B188** (1987) 99.

[58] A. Buras, P. Gambino, M. Gorbahn, S. Jager, and L. Silvestrini, "Universal unitarity triangle and physics beyond the standard model," *Phys.Lett.* **B500** (2001) 161–167, arXiv:hep-ph/0007085 [hep-ph].

[59] R. Chivukula, "Composite Technicolor Standard Models,". Ph.D. Thesis.

[60] R. Peccei and H. R. Quinn, "Constraints Imposed by CP Conservation in the Presence of Instantons," *Phys.Rev.* **D16** (1977) 1791–1797.

[61] V. Cirigliano and B. Grinstein, "Phenomenology of minimal lepton flavor violation," *Nucl. Phys.* **B752** (2006) 18–39, arXiv:hep-ph/0601111.

[62] A. Masiero, P. Paradisi, and R. Petronzio, "Probing new physics through $\mu - e$ universality in $K \to \ell\nu$," *Phys. Rev.* **D74** (2006) 011701, arXiv:hep-ph/0511289.

[63] R. Kitano, M. Koike, and Y. Okada, "Detailed calculation of lepton flavor violating $\mu - e$ conversion rate for various nuclei," *Phys. Rev.* **D66** (2002) 096002, arXiv:hep-ph/0203110.

[64] V. Cirigliano and I. Rosell, "The Standard Model prediction for $R_{e/mu}^{(pi,K)}$," *Phys. Rev. Lett.* **99** (2007) 231801, arXiv:0707.3439 [hep-ph].

[65] **LEP Electroweak Working Group, ALEPH, DELPHI, L3, OPAL** Collaboration. Unpublished note, 2005. http://lepewwg.web.cern.ch/LEPEWWG/lepww/4f/PDG05/.

[66] B. A. Kniehl, F. Madricardo, and M. Steinhauser, "Gauge independent W boson partial decay widths," *Phys.Rev.* **D62** (2000) 073010, arXiv:hep-ph/0005060 [hep-ph].

[67] A. Pich, "Tau Physics: Theory Overview," *Nucl.Phys.Proc.Suppl.* **181-182** (2008) 300–305, arXiv:0806.2793 [hep-ph].

[68] A. Pich, I. Boyko, D. Dedovich, and I. Bigi, "Tau decays," *Int.J.Mod.Phys.* **A24S1** (2009) 715–737.

[69] Z. Han, "Electroweak constraints on effective theories with $U(2) \times U(1)$ flavor symmetry," *Phys.Rev.* **D73** (2006) 015005, arXiv:hep-ph/0510125 [hep-ph].

[70] Z. Han and W. Skiba, "Effective theory analysis of precision electroweak data," *Phys.Rev.* **D71** (2005) 075009, arXiv:hep-ph/0412166 [hep-ph].

[71] V. Cirigliano, M. Gonzalez-Alonso, and J. Jenkins, "Semileptonic decays of light quarks beyond the Standard Model," *Nucl.Phys.* **B830** (2009) 95–115, arXiv:0908.1754 [hep-ph].

[72] R. Barbieri, G. Isidori, J. Jones-Perez, P. Lodone, and D. M. Straub, "$U(2)$ and Minimal Flavour Violation in Supersymmetry," *Eur.Phys.J.* **C71** (2011) 1725, arXiv:1105.2296 [hep-ph].

[73] W. Buchmuller and D. Wyler, "Effective Lagrangian Analysis of New Interactions and Flavor Conservation," *Nucl. Phys.* **B268** (1986) 621.

[74] J. Bernabeu, G. González-Sprinberg, M. Tung, and J. Vidal, "The Tau weak magnetic dipole moment," *Nucl.Phys.* **B436** (1995) 474–486, arXiv:hep-ph/9411289 [hep-ph].

[75] T. G. Rizzo, "Searching for anomalous tau-neutrino W couplings," *Phys.Rev.* **D56** (1997) 3074–3080, arXiv:hep-ph/9704337 [hep-ph].

[76] G. A. González-Sprinberg, A. Santamaria, and J. Vidal, "Model independent bounds on the tau lepton electromagnetic and weak magnetic moments," *Nucl.Phys.* **B582** (2000) 3–18, arXiv:hep-ph/0002203 [hep-ph].

[77] **DELPHI** Collaboration, J. Abdallah *et al.*, "Study of tau-pair production in photon-photon collisions at LEP and limits on the anomalous electromagnetic moments of the tau lepton," *Eur.Phys.J.* **C35** (2004) 159–170, arXiv:hep-ex/0406010 [hep-ex].

[78] S. Eidelman and M. Passera, "Theory of the tau lepton anomalous magnetic moment," *Mod.Phys.Lett.* **A22** (2007) 159–179, arXiv:hep-ph/0701260 [hep-ph].

[79] V. Cirigliano, M. González-Alonso, and M. L. Graesser, "Work in progress,".

[80] A. Pak and A. Czarnecki, "Mass effects in muon and semileptonic $b \to c$ decays," *Phys.Rev.Lett.* **100** (2008) 241807, arXiv:0803.0960 [hep-ph].

[81] Z.-H. Guo and P. Roig, "One meson radiative tau decays," *Phys.Rev.* **D82** (2010) 113016, arXiv:1009.2542 [hep-ph].

[82] R. Decker and M. Finkemeier, "Radiative corrections to the decay $\tau \to \pi(K)\nu_\tau$. 2.," *Phys.Lett.* **B334** (1994) 199–202.

[83] **ALEPH** Collaboration, S. Schael *et al.*, "Branching ratios and spectral functions of tau decays: Final ALEPH measurements and physics implications," *Phys.Rept.* **421** (2005) 191–284, arXiv:hep-ex/0506072 [hep-ex].

[84] J.-h. Park, "Lepton non-universality at LEP and charged Higgs," *JHEP* **10** (2006) 077, arXiv:hep-ph/0607280.

[85] X.-Y. Li and E. Ma, "Puzzle of W leptonic decay branching fractions and gauge model of generation nonuniversality," arXiv:hep-ph/0507017 [hep-ph].

[86] S. Weinberg, "V-A was the key," *J.Phys.Conf.Ser.* **196** (2009) 012002.

[87] N. Severijns, M. Beck, and O. Naviliat-Cuncic, "Tests of the standard electroweak model in beta decay," *Rev. Mod. Phys.* **78** (2006) 991–1040, arXiv:nucl-ex/0605029.

[88] M. Dewey, K. Coakley, D. Gilliam, G. Greene, A. Laptev, J. Nico, W. Snow, F. Wietfeldt, and A. Yue, "Prospects for a new cold neutron beam measurement of the neutron lifetime," *Nucl.Instr.Meth.* **A611** (2009) no. 2-3, 189 – 192.

[89] S. Arzumanov, L. Bondarenko, P. Geltenbort, V. Morozov, V. Nesvizhevsky, Y. Panin, and A. Strepetov, "A new project to measure the neutron lifetime using storage of ultracold neutrons and detection of inelastically scattered neutrons," *Nucl.Instr.Meth.* **A611** (2009) no. 2-3, 186 – 188.

[90] P. Walstrom, J. Bowman, S. Penttila, C. Morris, and A. Saunders, "A magneto-gravitational trap for absolute measurement of the ultra-cold neutron lifetime," *Nucl.Instr.Meth.* **A599** (2009) no. 1, 82 – 92.

[91] S. Materne, R. Picker, I. Altarev, H. Angerer, B. Franke, E. Gutsmiedl, F. Hartmann, A. Müller, S. Paul, and R. Stoepler, "PENeLOPE—on the way towards a new neutron lifetime experiment with magnetic storage of ultra-cold neutrons and proton extraction," *Nucl.Instr.Meth.* **A611** (2009) no. 2-3, 176 – 180.

[92] K. Leung and O. Zimmer, "Proposed neutron lifetime measurement using a hybrid magnetic trap for ultra-cold neutrons," *Nucl.Instr.Meth.* **A611** (2009) no. 2-3, 181 – 185.

[93] B. Markisch *et al.*, "The new neutron decay spectrometer PERKEO III," *Nucl.Instrum.Meth.* **A611** (2009) 216–218.

[94] B. Plaster, R. Carr, B. Filippone, D. Harrison, J. Hsiao, *et al.*, "A Solenoidal electron spectrometer for a precision measurement of the neutron β-asymmetry with ultracold neutrons," *Nucl.Instrum.Meth.* **A595** (2008) 587–598, arXiv:0806.2097 [nucl-ex].

[95] R. Alarcon *et al.*, "Precise Measurement of Neutron Decay Parameters,". http://nab.phys.virginia.edu/abba_proposal_2007.pdf.

[96] D. Dubbers, H. Abele, S. Baessler, B. Maerkisch, M. Schumann, *et al.*, "A Clean, bright, and versatile source of neutron decay products," *Nucl.Instrum.Meth.* **A596** (2008) 238–247, arXiv:0709.4440 [nucl-ex].

[97] W. Wilburn *et al.*, "Measurement of the neutrino-spin correlation Parameter b in neutron decay using ultracold neutrons," *Rev. Mex. Fis.* **Suppl. 55** (2009) no. 2, 119.

[98] **Nab Collaboration** Collaboration, D. Pocanic *et al.*, "Nab: Measurement Principles, Apparatus and Uncertainties," *Nucl.Instrum.Meth.* **A611** (2009) 211–215, arXiv:0810.0251 [nucl-ex].

[99] S. S. Baeßler *et al.*, "First measurements with the neutron decay spectrometer aSPECT," *Eur.Phys.J.* **A38** (2008) 17–26.

[100] F. Wietfeldt, B. Fisher, C. Trull, G. Jones, B. Collet, *et al.*, "A method for an improved measurement of the electron–antineutrino correlation in free neutron beta decay," *Nucl.Instrum.Meth.* **A545** (2005) 181–193.

[101] K. P. Hickerson, "The Fierz Interference Term in Beta-Decay Spectrum of UCN." -, 2009. http://neutron.physics.ncsu.edu/UCN_Workshop_09/Hickerson_SantaFe_2009.pdf. UCN Workshop, November 6–7 2009, Santa Fe, New Mexico.

[102] P. Herczeg, "Beta decay beyond the standard model," *Prog. Part. Nucl. Phys.* **46** (2001) 413–457.

[103] M. Carpentier and S. Davidson, "Constraints on two-lepton, two quark operators," *Eur.Phys.J.* **C70** (2010) 1071–1090, arXiv:1008.0280 [hep-ph].

[104] M. Voloshin, "Upper bound on tensor interaction in the decay $\pi \to e\nu\gamma$," *Phys.Lett.* **B283** (1992) 120–122.

[105] P. Herczeg, "On the question of a tensor interaction in $\pi \to e\nu\gamma$ decay," *Phys.Rev.* **D49** (1994) 247–253.

[106] B. A. Campbell and D. W. Maybury, "Constraints on scalar couplings from $\pi \to e\nu$," *Nucl.Phys.* **B709** (2005) 419–439, arXiv:hep-ph/0303046 [hep-ph].

[107] S. Weinberg, "Charge symmetry of weak interactions," *Phys.Rev.* **112** (1958) 1375–1379.

[108] B. R. Holstein, "Recoil Effects in Allowed beta Decay: The Elementary Particle Approach," *Rev. Mod. Phys.* **46** (1974) 789.

[109] M. Ademollo and R. Gatto, "Nonrenormalization Theorem for the Strangeness Violating Vector Currents," *Phys.Rev.Lett.* **13** (1964) 264–265.

[110] J. F. Donoghue and D. Wyler, "Isospin breaking and the precise determination of V_{ud}," *Phys.Lett.* **B241** (1990) 243.

[111] T. Lee and C.-N. Yang, "Question of Parity Conservation in Weak Interactions," *Phys.Rev.* **104** (1956) 254–258.

[112] J. D. Jackson, S. B. Treiman, and H. W. Wyld, "Possible tests of time reversal invariance in Beta decay," *Phys. Rev.* **106** (1957) 517–521.

[113] D. H. Wilkinson, "Analysis of neutron beta decay," *Nucl.Phys.* **A377** (1982) 474–504.

[114] F. Gluck, I. Joo, and J. Last, "Measurable parameters of neutron decay," *Nucl.Phys.* **A593** (1995) 125–150.

[115] S. Ando *et al.*, "Neutron beta decay in effective field theory," *Phys. Lett.* **B595** (2004) 250–259, arXiv:nucl-th/0402100.

[116] V. P. Gudkov, G. Greene, and J. Calarco, "General classification and analysis of neutron β-decay experiments," *Phys.Rev.* **C73** (2006) 035501, arXiv:nucl-th/0510012 [nucl-th].

[117] A. Czarnecki, W. J. Marciano, and A. Sirlin, "Precision measurements and CKM unitarity," *Phys.Rev.* **D70** (2004) 093006, arXiv:hep-ph/0406324 [hep-ph].

[118] S. Gardner and C. Zhang, "Sharpening low-energy, standard model tests via correlation coefficients in neutron beta decay," *Phys.Rev.Lett.* **86** (2001) 5666–5669, arXiv:hep-ph/0012098 [hep-ph].

[119] H. Abele, M. Astruc Hoffmann, S. Baessler, D. Dubbers, F. Gluck, *et al.*, "Is the unitarity of the quark mixing CKM matrix violated in neutron β-decay?," *Phys.Rev.Lett.* **88** (2002) 211801, arXiv:hep-ex/0206058 [hep-ex].

[120] **UCNA Collaboration** Collaboration, J. Liu *et al.*, "Determination of the Axial-Vector Weak Coupling Constant with Ultracold Neutrons," *Phys.Rev.Lett.* **105** (2010) 181803, arXiv:1007.3790 [nucl-ex].

[121] M. Schumann, T. Soldner, M. Deissenroth, F. Gluck, J. Krempel, *et al.*, "Measurement of the neutrino asymmetry parameter B in neutron decay," *Phys.Rev.Lett.* **99** (2007) 191803, arXiv:0706.3788 [hep-ph].

[122] J. Byrne, P. Dawber, M. van der Grinten, C. Habeck, F. Shaikh, *et al.*, "Determination of the electron anti-neutrino angular correlation coefficient a_0 and the parameter $|\lambda| = |G_A/G_V|$ in free neutron β-decay from measurements of the integrated energy spectrum of recoil protons stored in an ion trap," *J.Phys.* **G28** (2002) 1325–1349.

[123] G. Konrad, W. Heil, S. Baessler, D. Pocanic, and F. Gluck, "Impact of Neutron Decay Experiments on non-Standard Model Physics," arXiv:1007.3027 [nucl-ex].

[124] A. Serebrov, V. Varlamov, A. Kharitonov, A. Fomin, Y. Pokotilovski, *et al.*, "Measurement of the neutron lifetime using a gravitational trap and a low-temperature Fomblin coating," *Phys.Lett.* **B605** (2005) 72–78, arXiv:nucl-ex/0408009 [nucl-ex].

[125] A. Pichlmaier, V. Varlamov, K. Schreckenbach, and P. Geltenbort, "Neutron lifetime measurement with the UCN trap-in-trap MAMBO II," *Phys.Lett.* **B693** (2010) 221–226.

[126] W. J. Marciano and A. Sirlin, "Improved calculation of electroweak radiative corrections and the value of V_{ud}," *Phys.Rev.Lett.* **96** (2006) 032002, arXiv:hep-ph/0510099 [hep-ph].

[127] J. Hardy and I. Towner, "Superallowed $0^+ \to 0^+$ nuclear β decays: A New survey with precision tests of the conserved vector current hypothesis and the standard model," *Phys.Rev.* **C79** (2009) 055502, arXiv:0812.1202 [nucl-ex].

[128] M. Bychkov, D. Pocanic, B. VanDevender, V. Baranov, W. H. Bertl, *et al.*, "New Precise Measurement of the Pion Weak Form Factors in $\pi \to e\nu\gamma$ Decay," *Phys.Rev.Lett.* **103** (2009) 051802, arXiv:0804.1815 [hep-ex].

[129] V. Mateu and J. Portoles, "Form-factors in radiative pion decay," *Eur.Phys.J.* **C52** (2007) 325–338, arXiv:0706.1039 [hep-ph].

[130] F. Wauters, I. Kraev, D. Zakoucky, M. Beck, M. Breitenfeldt, *et al.*, "Precision measurements of the ^{60}Co β-asymmetry parameter in search for tensor currents in weak interactions," *Phys.Rev.* **C82** (2010) 055502, arXiv:1005.5034 [nucl-ex].

[131] F. Wauters, I. Kraev, M. Tandecki, E. Traykov, S. Van Gorp, *et al.*, "β asymmetry parameter in the decay of ^{114}In," *Phys.Rev.* **C80** (2009) 062501, arXiv:0901.0081 [nucl-ex].

[132] A. Carnoy, J. Deutsch, T. Girard, and R. Prieels, "Limits on nonstandard weak currents from the polarization of ^{14}O and ^{10}C decay positrons," *Phys.Rev.* **C43** (1991) 2825–2834.

[133] V. Wichers, T. Hageman, J. Van Klinken, H. Wilschut, and D. Atkinson, "Bounds on Right-handed Currents from Nuclear Beta Decay," *Phys.Rev.Lett.* **58** (1987) 1821–1824.

[134] N. Severijns *et al.*, "Fundamental Weak Interaction Studies using Polarised Nuclei and Ion Traps," *Hyperfine Interactions* **129** (2000) 223–236.

[135] P. Vetter, J. Abo-Shaeer, S. Freedman, and R. Maruyama, "Measurement of the β-ν correlation of ^{21}Na using shakeoff electrons," *Phys.Rev.* **C77** (2008) 035502, arXiv:0805.1212 [nucl-ex].

[136] A. Gorelov, D. Melconian, W. Alford, D. Ashery, G. Ball, *et al.*, "Scalar interaction limits from the β-ν correlation of trapped radioactive atoms," *Phys.Rev.Lett.* **94** (2005) 142501, arXiv:nucl-ex/0412032 [nucl-ex].

[137] **ISOLDE** Collaboration, E. Adelberger *et al.*, "Positron neutrino correlation in the $0^+ \to 0^+$ decay of ^{32}Ar," *Phys.Rev.Lett.* **83** (1999) 1299–1302, arXiv:nucl-ex/9903002 [nucl-ex].

[138] C. Johnson, F. Pleasonton, and T. Carlson, "Precision Measurement of the Recoil Energy Spectrum from the Decay of ^{6}He," *Phys.Rev.* **132** (1963) 1149–1165.

[139] D. Britton, S. Ahmad, D. Bryman, R. Burnbam, E. Clifford, *et al.*, "Measurement of the $\pi^+ \to e^+\nu$ branching ratio," *Phys.Rev.Lett.* **68** (1992) 3000–3003.

[140] G. Czapek, A. Federspiel, A. Fluckiger, D. Frei, B. Hahn, *et al.*, "Branching ratio for the rare pion decay into positron and neutrino," *Phys.Rev.Lett.* **70** (1993) 17–20.

[141] V. Cirigliano and I. Rosell, "$\pi/K \to e\bar{\nu}_e$ branching ratios to $O(e^2p^4)$ in Chiral Perturbation Theory," *JHEP* **0710** (2007) 005, arXiv:0707.4464 [hep-ph].

[142] V. Cirigliano and I. Rosell, "Two-loop effective theory analysis of $\pi(K) \to e\bar{\nu}_e[\gamma]$ branching ratios," *Phys.Rev.Lett.* **99** (2007) 231801, arXiv:0707.3439 [hep-ph].

[143] A. Young. Private communication.

[144] J. Laiho, E. Lunghi, and R. S. Van de Water, "Lattice QCD inputs to the CKM unitarity triangle analysis," *Phys. Rev.* **D81** (2010) 034503, arXiv:0910.2928 [hep-ph].

[145] C. Sachrajda, "Phenomenology from the Lattice," *PoS Lattice 2010* (2010) 018, arXiv:1103.5959 [hep-lat]. http://pos.sissa.it/archive/conferences/105/018/Lattice%202010_018.pdf.

[146] G. Colangelo, S. Durr, A. Juttner, L. Lellouch, H. Leutwyler, *et al.*, "Review of lattice results concerning low energy particle physics," *Eur.Phys.J.* **C71** (2011) 1695, arXiv:1011.4408 [hep-lat].

[147] **CKMfitter Group** Collaboration, J. Charles *et al.*, "CP violation and the CKM matrix: Assessing the impact of the asymmetric B factories," *Eur. Phys. J.* **C41** (2005) 1–131, arXiv:hep-ph/0406184.

[148] **CDF** Collaboration, F. Abe *et al.*, "Limits on quark-lepton compositeness scales from dileptons produced in 1.8 TeV $p\bar{p}$ collisions," *Phys.Rev.Lett.* **79** (1997) 2198–2203.

[149] **CMS** Collaboration, V. Khachatryan *et al.*, "Search for Quark Compositeness with the Dijet Centrality Ratio in pp Collisions at $\sqrt{s} = 7$ TeV," *Phys. Rev. Lett.* **105** (2010) 262001, arXiv:1010.4439 [hep-ex].

[150] **ATLAS** Collaboration, G. Aad *et al.*, "Search for New Physics in Dijet Mass and Angular Distributions in pp Collisions at $\sqrt{s} = 7$ TeV Measured with the ATLAS Detector," *New J. Phys.* **13** (2011) 053044, arXiv:1103.3864 [hep-ex].

[151] **CMS** Collaboration, V. Khachatryan *et al.*, "Measurement of Dijet Angular Distributions and Search for Quark Compositeness in pp Collisions at 7 TeV," *Phys. Rev. Lett.* **106** (2011) 201804, arXiv:1102.2020 [hep-ex].

[152] **ATLAS** Collaboration, G. Aad *et al.*, "Search for Contact Interactions in Dimuon Events from pp Collisions at $\sqrt{s} = 7$ TeV with the ATLAS Detector," *Phys.Rev.* **D84** (2011) 011101, arXiv:1104.4398 [hep-ex].

[153] D. J. Broadhurst and A. Grozin, "Matching QCD and HQET heavy - light currents at two loops and beyond," *Phys.Rev.* **D52** (1995) 4082–4098, arXiv:hep-ph/9410240 [hep-ph].

[154] R. Ellis, W. Stirling, and B. Webber, *QCD and Collider Physics*. Cambridge Monographs on Particle Physics, Nuclear Physics and Cosmology. Cambridge University Press, 2003.

[155] **ATLAS** Collaboration, G. Aad *et al.*, "Search for a heavy gauge boson decaying to a charged lepton and a neutrino in 1 fb^{-1} of pp collisions at

$\sqrt{s} = 7$ TeV using the ATLAS detector," *Phys.Lett.* **B705** (2011) 28–46, arXiv:1108.1316 [hep-ex].

[156] **CMS** Collaboration, V. Khachatryan *et al.*, "Search for W' in the leptonic channels in pp Collisions at $\sqrt{s} = 7$ TeV,". http://cdsweb.cern.ch/record/1369201. CERN Report number CMS-PAS-EXO-11-024.

[157] **CMS** Collaboration, V. Khachatryan *et al.*, "Search for a heavy gauge boson W' in the final state with an electron and large missing transverse energy in pp collisions at $\sqrt{s} = 7$ TeV," *Phys.Lett.* **B698** (2011) 21–39, arXiv:1012.5945 [hep-ex].

[158] A. D. Martin, W. J. Stirling, R. S. Thorne, and G. Watt, "Parton distributions for the LHC," *Eur. Phys. J.* **C63** (2009) 189–285, arXiv:0901.0002 [hep-ph].

[159] J. Pumplin, D. Stump, J. Huston, H. Lai, P. M. Nadolsky, *et al.*, "New generation of parton distributions with uncertainties from global QCD analysis," *JHEP* **0207** (2002) 012, arXiv:hep-ph/0201195 [hep-ph].

[160] S. Weinberg, "Phenomenological Lagrangians," *Physica* **A96** (1979) 327.

[161] J. Gasser and H. Leutwyler, "Chiral Perturbation Theory to One Loop," *Annals Phys.* **158** (1984) 142.

[162] M. Veltman, "Second Threshold in Weak Interactions," *Acta Phys.Polon.* **B8** (1977) 475.

[163] B. W. Lee, C. Quigg, and H. Thacker, "The Strength of Weak Interactions at Very High-Energies and the Higgs Boson Mass," *Phys.Rev.Lett.* **38** (1977) 883–885.

[164] H. G. Veltman and M. Veltman, "On the possibility of resonances in longitudinally polarized vector boson scattering," *Acta Phys.Polon.* **B22** (1991) 669–696.

[165] G. Ecker, J. Gasser, A. Pich, and E. de Rafael, "The Role of Resonances in Chiral Perturbation Theory," *Nucl.Phys.* **B321** (1989) 311.

[166] M. Pennington, "Zeros in $\pi\pi$ scattering (talk)," *AIP Conf.Proc.* **13** (1973) 89–116.

[167] C. E. Vayonakis, "Born helicity amplitudes and cross-sections in nonabelian gauge theories," *Lett. Nuovo Cim.* **17** (1976) 383.

[168] J. M. Cornwall, D. N. Levin, and G. Tiktopoulos, "Derivation of Gauge Invariance from High-Energy Unitarity Bounds on the s Matrix," *Phys.Rev.* **D10** (1974) 1145.

[169] A. Martin and T. Spearman, *Elementary Particle Theory*. North-Holland Pub. Co., Amsterdam, 1970.

[170] B. Martin, D. Morgan, and G. Shaw, *Pion-Pion Interactions in Particle Physics*. Academic Press, London, 1976.

[171] M. Pennington and P. Pond, "Zeros in $\pi\pi$ amplitudes," *Nuovo Cim.* **A3** (1971) 548–560.

[172] M. Pennington and S. Protopopescu, "$\pi\pi$ scattering amplitude in the low-energy region," *Phys.Rev.* **D7** (1973) 1429–1441.

[173] M. Pennington and C. Schmid, "Continuation of zero contours from Weinberg's low-energy $\pi\pi$ model to the ρ region," *Phys.Rev.* **D7** (1973) 2213–2219.

[174] R. Odorico, "About the anomaly at 980 MeV in the pi+ pi- system," *Phys.Lett.* **B38** (1972) 411–414.

[175] E. Barrelet, "A new point of view in the analysis of two-body reactions," *Nuovo Cim.* **A8** (1972) 331–371.

[176] M. Pennington and S. Protopopescu, "Odorico zeros and low energy $\pi\pi$ scattering data," *Phys.Lett.* **B40** (1972) 105–108.

[177] J. Gasser and H. Leutwyler, "Chiral Perturbation Theory: Expansions in the Mass of the Strange Quark," *Nucl.Phys.* **B250** (1985) 465.

[178] A. Pich, I. Rosell, and J. J. Sanz-Cillero, "The vector form factor at the next-to-leading order in $1/N_C$: chiral couplings $L_9(\mu)$ and $C_{88}(\mu) - C_{90}(\mu)$," *JHEP* **1102** (2011) 109, `arXiv:1011.5771 [hep-ph]`.

[179] D. Gómez Dumm, P. Roig, A. Pich, and J. Portolés, "$\tau \to \pi\pi\pi\nu_\tau$ decays and the $a_1(1260)$ off-shell width revisited," *Phys.Lett.* **B685** (2010) 158–164, `arXiv:0911.4436 [hep-ph]`.

[180] S. Weinberg, "Pion scattering lengths," *Phys.Rev.Lett.* **17** (1966) 616–621.

[181] J. Bijnens, G. Colangelo, G. Ecker, J. Gasser, and M. Sainio, "Pion pion scattering at low-energy," *Nucl.Phys.* **B508** (1997) 263–310, `arXiv:hep-ph/9707291 [hep-ph]`.

[182] J. Bijnens, G. Colangelo, and G. Ecker, "Renormalization of chiral perturbation theory to order p^6," *Annals Phys.* **280** (2000) 100–139, `arXiv:hep-ph/9907333 [hep-ph]`.

[183] J. Gasser, C. Haefeli, M. A. Ivanov, and M. Schmid, "Integrating out strange quarks in ChPT: Terms at order p^6," *Phys.Lett.* **B675** (2009) 49–53, `arXiv:0903.0801 [hep-ph]`.

[184] V. Cirigliano, G. Ecker, M. Eidemuller, R. Kaiser, A. Pich, and J. Portolés, "Towards a consistent estimate of the chiral low-energy constants," *Nucl.Phys.* **B753** (2006) 139–177, arXiv:hep-ph/0603205 [hep-ph].

[185] S. Protopopescu, M. Alston-Garnjost, A. Barbaro-Galtieri, S. M. Flatte, J. Friedman, *et al.*, "$\pi\pi$ Partial Wave Analysis from Reactions $\pi^+ p \to \pi^+\pi^-\Delta^{++}$ and $\pi^+ p \to K^+K^-\Delta^{++}$ at 7.1 GeV/c," *Phys.Rev.* **D7** (1973) 1279.

[186] W. Ochs. PhD thesis, University of Munich, 1973.

[187] P. Estabrooks and A. D. Martin, "$\pi\pi$ Phase Shift Analysis Below the K anti-K Threshold," *Nucl.Phys.* **B79** (1974) 301.

[188] J. Gasser and U. G. Meissner, "On the phase of ϵ'," *Phys.Lett.* **B258** (1991) 219–224.

[189] A. Schenk, "Absorption and dispersion of pions at finite temperature," *Nucl.Phys.* **B363** (1991) 97–116.

[190] A. Arneodo, F. Guerin, and J. Donohue, "Zero contours and ρ dominance in low-energy $\pi\pi$ scattering," *Nuovo Cim.* **A17** (1973) 329–342.

[191] A. Dobado and J. Peláez, "On The Equivalence theorem in the chiral perturbation theory description of the symmetry breaking sector of the standard model," *Nucl.Phys.* **B425** (1994) 110–136, arXiv:hep-ph/9401202 [hep-ph].

[192] O. Éboli, M. González-García, and J. Mizukoshi, "$pp \to jje^\pm\mu^\pm\nu\nu$ and $jje^\pm\mu^\pm\nu\nu$ at $O(\alpha_{em}^6)$ and $O(\alpha_{em}^4\alpha_s^2)$ for the study of the quartic electroweak gauge boson vertex at CERN LHC," *Phys.Rev.* **D74** (2006) 073005, arXiv:hep-ph/0606118 [hep-ph].

[193] M. Fabbrichesi and L. Vecchi, "Possible experimental signatures at the CERN LHC of strongly interacting electro-weak symmetry breaking," *Phys.Rev.* **D76** (2007) 056002, arXiv:hep-ph/0703236 [hep-ph].

[194] A. V. Manohar and V. Mateu, "Dispersion Relation Bounds for pi pi Scattering," *Phys.Rev.* **D77** (2008) 094019, arXiv:0801.3222 [hep-ph].

[195] E. Boos, H. He, W. Kilian, A. Pukhov, C. Yuan, *et al.*, "Strongly interacting vector bosons at TeV $e^\pm e^-$ linear colliders: Addendum," *Phys.Rev.* **D61** (2000) 077901, arXiv:hep-ph/9908409 [hep-ph].

[196] **CMS Collaboration** Collaboration, S. Chatrchyan *et al.*, "Search for leptonic decays of W' bosons in pp collisions at $\sqrt{s} = 7$ TeV," arXiv:1204.4764 [hep-ex].

[197] **CMS Collaboration** Collaboration, S. Chatrchyan *et al.*, "Search for exotic particles decaying to WZ in pp collisions at $\sqrt{s} = 7$ TeV," arXiv:1206.0433 [hep-ex].

[198] **ATLAS Collaboration** Collaboration, G. Aad *et al.*, "Search for resonant WZ production in the $WZ \to \ell\nu\ell^{p}rime\ell'$ channel in $\sqrt{s} = 7$ TeV pp collisions with the ATLAS detector," *Phys. Rev.* **D85** (2012) 112012, arXiv:1204.1648 [hep-ex].

[199] O. Éboli, J. González-Fraile, and M. González-García, "Present Bounds on New Neutral Vector Resonances from Electroweak Gauge Boson Pair Production at the LHC," *Phys.Rev.* **D85** (2012) 055019, arXiv:1112.0316 [hep-ph].

[200] A. Dobado, M. Herrero, J. Peláez, and E. Ruiz Morales, "CERN LHC sensitivity to the resonance spectrum of a minimal strongly interacting electroweak symmetry breaking sector," *Phys.Rev.* **D62** (2000) 055011, arXiv:hep-ph/9912224 [hep-ph].

[201] J. Peláez, "Resonance spectrum of the strongly interacting symmetry breaking sector," *Phys.Rev.* **D55** (1997) 4193–4202, arXiv:hep-ph/9609427 [hep-ph].

[202] P. J. Davis, *Interpolation and Approximation*. Dover Publications, New York, 1975.